FEDERAL UNIVERSITY OF UBERLÂNDIA
FACULTY OF ELECTRICAL ENGINEERING

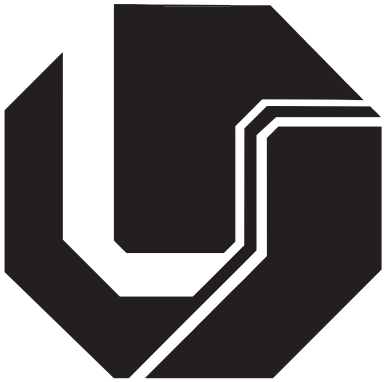

Objective assessment of motor symptoms of Parkinson's disease through non-contact sensors

FÁBIO HENRIQUE MONTEIRO OLIVEIRA

Uberlândia - 2020

FÁBIO HENRIQUE MONTEIRO OLIVEIRA

Objective assessment of motor symptoms of Parkinson's disease through non-contact sensors

Thesis submitted in partial fulfillment of the requirements for the degree of Doctor of Sciences to the Post-Graduate Program of the Faculty of Electrical Engineering at the Federal University of Uberlândia.

Members of the Committee:

Prof. Dr. Adriano de Oliveira Andrade (Supervisor) - UFU
Prof. Dr. Igor Santos Peretta - UFU
Prof. Dr. Adriano Alves Pereira - UFU
Prof. Dr. André Salles Cunha Peres - ISD
Prof. Dr. Marcus Fraga Vieira - UFG

Uberlândia - 2020

Ficha Catalográfica Online do Sistema de Bibliotecas da UFU
com dados informados pelo(a) próprio(a) autor(a).

O48
2020

Oliveira, Fábio Henrique Monteiro, 1990-
Objective assessment of motor symptoms of Parkinson's disease through non-contact sensors [recurso eletrônico] / Fábio Henrique Monteiro Oliveira. - 2020.

Orientador: Adriano de Oliveira Andrade.
Tese (Doutorado) - Universidade Federal de Uberlândia, Pós-graduação em Engenharia Elétrica.
Modo de acesso: Internet.
Disponível em: http://doi.org/10.14393/ufu.te.2020.393
Inclui bibliografia.

1. Engenharia elétrica. I. Andrade, Adriano de Oliveira,1975-, (Orient.). II. Universidade Federal de Uberlândia. Pós-graduação em Engenharia Elétrica. III. Título.

CDU: 621.3

Bibliotecários responsáveis pela estrutura de acordo com o AACR2:
Gizele Cristine Nunes do Couto - CRB6/2091
Nelson Marcos Ferreira - CRB6/3074

UNIVERSIDADE FEDERAL DE UBERLÂNDIA
Coordenação do Programa de Pós-Graduação em Engenharia Elétrica
Av. João Naves de Ávila, 2121, Bloco 3N - Bairro Santa Mônica, Uberlândia-MG, CEP 38400-902
Telefone: (34) 3239-4707 - www.posgrad.feelt.ufu.br - copel@ufu.br

ATA DE DEFESA - PÓS-GRADUAÇÃO

Programa de Pós-Graduação em:	Engenharia Elétrica				
Defesa de:	Tese de Doutorado, 261, PGEELT.				
Data:	Três de abril de dois mil e vinte	Hora de início:	08:30	Hora de encerramento:	13:00
Matrícula do Discente:	11423EEL003				
Nome do Discente:	Fábio Henrique Monteiro Oliveira				
Título do Trabalho:	Objective assessment of motor symptoms of Parkinson's disease through non-contact sensors				
Área de concentração:	Processamento da informação				
Linha de pesquisa:	Engenharia biomédica				
Projeto de Pesquisa de vinculação:	Título: Caracterização de sinais motores da doença de Parkinson por meio de sensores capacitivos sem contato DOUTORADO Agência Financiadora: FAPEMIG Início 01/08/2017 Término 06/12/2020 No. do Projeto na agência: APQ-00942-17 Professor Coordenador: Adriano de Oliveira Andrade				

Reuniu-se por videoconferência, a Banca Examinadora, designada pelo Colegiado do Programa de Pós-graduação em Engenharia Elétrica, assim composta: Professores Doutores: Igor Santos Peretta - FEELT/UFU; Adriano Alves Pereira - FEELT/UFU; André Salles Cunha Peres - FPCE/Universidade de Coimbra; Marcus Fraga Vieira - UFG; Adriano de Oliveira Andrade - FEELT/UFU, orientador(a) do(a) candidato(a).

Iniciando os trabalhos o(a) presidente da mesa, Dr. Adriano de Oliveira Andrade, apresentou a Comissão Examinadora e o candidato, agradeceu a presença do público, e concedeu ao Discente a palavra para a exposição do seu trabalho. A duração da apresentação do Discente e o tempo de arguição e resposta foram conforme as normas do Programa.

A seguir o senhor(a) presidente concedeu a palavra, pela ordem sucessivamente, aos(às) examinadores(as), que passaram a arguir o(a) candidato(a). Ultimada a arguição, que se desenvolveu dentro dos termos regimentais, a Banca, em sessão secreta, atribuiu o resultado final, considerando o(a) candidato(a):

Aprovado(a).

Esta defesa faz parte dos requisitos necessários à obtenção do título de Doutor.

O competente diploma será expedido após cumprimento dos demais requisitos, conforme as normas do Programa, a legislação pertinente e a regulamentação interna da UFU.

Nada mais havendo a tratar foram encerrados os trabalhos. Foi lavrada a presente ata que após lida e achada conforme foi assinada pela Banca Examinadora.

Documento assinado eletronicamente por **Adriano de Oliveira Andrade**, **Professor(a) do Magistério Superior**, em 03/04/2020, às 13:04, conforme horário oficial de Brasília, com fundamento no art. 6º, § 1º, do Decreto nº 8.539, de 8 de outubro de 2015.

Documento assinado eletronicamente por **Marcus Fraga Vieira**, **Usuário Externo**, em 03/04/2020, às 13:04, conforme horário oficial de Brasília, com fundamento no art. 6º, § 1º, do Decreto nº 8.539, de 8 de outubro de 2015.

Documento assinado eletronicamente por **Adriano Alves Pereira**, **Professor(a) do Magistério Superior**, em 03/04/2020, às 13:05, conforme horário oficial de Brasília, com fundamento no art. 6º, § 1º, do Decreto nº 8.539, de 8 de outubro de 2015.

Documento assinado eletronicamente por **Andre Salles Cunha Peres**, **Usuário Externo**, em 03/04/2020, às 13:05, conforme horário oficial de Brasília, com fundamento no art. 6º, § 1º, do Decreto nº 8.539, de 8 de outubro de 2015.

Documento assinado eletronicamente por **Igor Santos Peretta**, **Professor(a) do Magistério Superior**, em 03/04/2020, às 13:05, conforme horário oficial de Brasília, com fundamento no art. 6º, § 1º, do Decreto nº 8.539, de 8 de outubro de 2015.

A autenticidade deste documento pode ser conferida no site https://www.sei.ufu.br/sei/controlador_externo.php?acao=documento_conferir&id_orgao_acesso_externo=0, informando o código verificador **1872206** e o código CRC **8C704245**.

Referência: Processo nº 23117.010456/2020-28 SEI nº 1872206

Acknowledgements

It took years to complete this work and a lot of things happened during this period. It is hard to remember every single time. The completion of this study and my training as a researcher required the involvement of several people. I would like to express my gratitude for those who have crossed my path during this journey. To be sure, several tools have been used to write this page today, it's an equation of mysterious deduction. Still, this trajectory has been marked by some people, situations and places.

I thank God for nurturing me in many ways.

Thanks in particular to my supervisor "Adriano de Oliveira Andrade" for his masterful guidance, encouragement and support.

To my colleagues and lab friends for sharing knowledge and support in daily activities.

To the professors who were in this journey.

To the examination board who agreed to participate and collaborate in the evaluation and enrichment of this work.

To my wife "Rafaela Gonçalves", for her patience, support and encouragement. Her contribution was essential.

To my parents and siblings for their love and support in many situations.

To my friends, with whom I have shared various moments of my life, they are responsible for much of the brightness of each day.

The present work was carried out with the support of the National Council for Scientific and Technological Development (CNPq), Coordination for the Improvement of Higher Education Personnel (CAPES), the Foundation for Research Support of the State of Minas Gerais (FAPEMIG-APQ-00942-17) and Foundation for Research Support of the Federal District (FAPDF). I am thankful to the volunteers and to the patients of the Parkinson's disease Association of Triângulo (Associação de Parkinson do Triângulo, Uberlândia, Brazil) for their participation in this study.

"So slight and nearly imperceptible are the first inroads of this malady, and so extremely slow its progress, that it rarely happens, that the patient can form any recollection of the precise period of its commencement."

James Parkinson

Abstract

Oliveira, F. H. M., *Objective assessment of motor symptoms of Parkinson's disease through non-contact sensors* , UFU, Uberlândia, Brazil, 2020, 88p.

The diagnosis and evaluation of the severity of Parkinson's disease (PD) is a task that has been performed through clinical evaluation and use of subjective scales. Over the years several studies have reported results and technologies with the purpose of making the characterization of PD more objective. In this perspective, we have identified the possibility of using non-contact capacitive sensors to record the motor activity of the hand and wrist. Another identified challenge is related to the quantification of the severity of motor symptoms of PD. In this study, we present the use of an innovative tool, t-Distributed Stochastic Neighbor Embedding (t-SNE), for the reduction and visualization of information. The use of this tool allowed the visualization of data in a two-dimensional space and an improvement of the performance of classifiers responsible for estimating the severity of the disease. In order to evaluate the use of capacitive sensors and signal processing tools, data from neurologically healthy individuals and people with PD were collected. In the end, our contributions are the following: (i) development and evaluation of a technology for recording motor signals of hand and wrist activities, based on capacitive contactless sensors; (ii) comparative evaluation among several tools for signal processing, in order to objectively evaluate the motor symptoms of PD.

Index-terms: Parkinson's disease, Non-contact capacitive sensor, Inertial sensor, Hand motor task.

Contents

Contents **vi**

List of Figures **vii**

List of Tables **ix**

List of Abbreviations **x**

1 Introduction **1**
1.1 Problem formulation 1
1.2 Relevance of the thesis 2
1.3 The object of the research 3
1.4 The aim of the thesis 4
1.5 The objectives of the thesis 4
1.6 Research methodology 5
1.7 Scientific novelty of the thesis 5
1.8 Practical value of the research findings 6
1.9 Approval of the research findings 6
1.10 Structure of the dissertation 7

2 Parkinson's disease **8**

3 Non-contact sensors for Parkinson's disease **11**
3.1 Leap Motion controller 12
3.2 Non-contact capacitive sensor 15
3.3 Conclusions and hypothesis 19

4 Visualization and classification of motor symptoms **20**
4.1 Dimensionality reduction 21
4.2 Conclusions and hypothesis 23

5 Experimental research using Leap Motion controller **24**

5.1 Hand tremor quantification 25
5.2 Preliminary sensor evaluation 30
5.3 Conclusions 33

6 Experimental research for data visualization and classification 35
6.1 Methods 35
6.2 Results 42
6.3 Discussion 51
6.4 Conclusions 55

7 Experimental research on non-contact capacitive sensor 56
7.1 Materials 57
7.2 Methods 59
7.3 Results 64
7.4 Discussion 68
7.5 Conclusions 70

8 General conclusions 72

References 74

Appendix A List of scientific publications 84

Appendix B Supplementary materials 87

List of Figures

1.1 Approximated annual cost per capita with Parkinson's disease. 3
1.2 Conceptual idea of the proposed system. 4

2.1 Some of the common PD motor signs. 9

3.1 Commonly used sensors for quantification of PD motor signs. 12
3.2 The cartesian coordinate system of LMC. 14
3.3 PS25454 EPIC sensor. 17
3.4 Interaction with ambient ac field - NCC EPIC sensor behavior. 18

5.1 Graphical user interface of developed computer software. 25
5.2 Data collection setup of induced hand tremor. 27
5.3 Typical electric pulse generated by hand tremor stimulator. 27
5.4 Norm of left palm velocity vector (stimulated at 2.5 Hz). 28
5.5 Estimated instantaneous mean frequency. 28
5.6 Norm of left palm velocity vector (stimulated at 10 Hz). 29
5.7 Estimated instantaneous mean frequency. 29
5.8 Boxplot of IMNF distributions. 29
5.9 Setup of the experimental environment. 31
5.10 Deviation between each measured position and the mean value. 32
5.11 Box-and-whisker plot of x-, y- and z-axis deviations for each set. 32
5.12 Standard deviations of x-, y- and z-axis for each set. 33

6.1 Basic sequence of executed tasks. 36
6.2 Typical example of preprocessed signals. 37
6.3 Diagram depicting the main steps. 38
6.4 Parameter settings of the experiments. 40
6.5 Visualization of projected data onto a lower dimensional space. 43
6.6 Visualization of projected data onto a lower dimensional space. 44
6.7 Visualization of projected data onto a lower dimensional space. 45
6.8 Visualization of projected data onto a lower dimensional space. 46

6.9 Boxplots of training set performance. 48
6.10 Boxplots of test set performance. 49
6.11 ROC curves of SVM classifier for S_H group. 50
6.12 ROC curves of SVM classifier for S_{PD} group. 50
6.13 ROC curves of SVM classifier for S_{DBS} group. 51

7.1 Graphical user interface of developed computer software. 58
7.2 2-D array of PS25454 sensors. 59
7.3 Simplified circuit diagram. 59
7.4 Experimental setup for NCC system calibration. 60
7.5 Experimental setup. 62
7.6 Set of tasks executed. 62
7.7 NCC model result. 64
7.8 Typical signals collected. 65
7.9 Typical IMNFs. 66

List of Tables

3.1 Information about sensors for PD. 13
3.2 NCC electric potential sensing technology timeline. 16

5.1 Induced hand tremor experiment configuration. 28
5.2 Median difference test among the four IMNF distributions. 30
5.3 Predefined experimental conditions sets. 31

6.1 Overall mean coefficient of variation. 37
6.2 Parameters and performance values. 47
6.3 P-value of success ratios. 47
6.4 Grand average confusion matrix. 48

7.1 Participants information. 61
7.2 Comparison of descriptive statistics. 67

List of Abbreviations

t-SNE	t-distributed stochastic neighbor embedding
ADC	Analog-to-digital conversion
ADL	Activities of daily living
AM	Amplitude modulation
ANN	Artificial Neural Network
API	Application Programming Interface
AUC	Area under the curve
CNS	Central nervous system
CV	Coefficient of variation
DBS	Deep brain stimulation
DR	Dimensionality reduction
E-field	Electric field
ECG	Electrocardiography
EEG	Electroencephalography
EMG	Electromyography
EOG	Electrooculography
EPIC	Electric potential integrated circuit
EPS	Electric potential sensing
HS	Hilbert Spectrum
IMNF	Instantaneous mean frequency

IMU	Inertial measurement unit
IR	Infrared
KL	Kullback-Leibler
LED	Light-emitting diode
LMC	Leap Motion controller
LOO	Leave-one-out
MEMS	Microelectromechanical systems
NCC	Non-contact capacitive
OOS	Out-of-sample
PCA	Principal component analysis
PD	Parkinson's disease
ROC	Receiver operating characteristic
SDK	Software development kit
SNE	Stochastic neighbor embedding
SVM	Support Vector Machine
UPDRS	Unified Parkinson's Disease Rating Scale

"Que a força do medo que tenho não me impeça de ver o que anseio."

- Oswaldo Montenegro

1 Introduction

1.1 Problem formulation

This thesis is focusing on the problem of quantitative evaluation of Parkinson's disease (PD) motor symptoms by using non-contact sensors.

The fact that PD has yet to have cure defies science and this is not the only challenge. The diagnosis and follow-up of PD is another one, and over the years several researches have been focused on the detection of motor and non-motor PD symptoms. PD was originally considered a pure movement disorder characterized by its main motor symptoms, also known as cardinal signs, i.e., bradykinesia, rigidity, tremor and postural instability [1] and these motor symptoms worsen over time.

In this sense, many sensors and techniques are employed to quantify the cardinal signs of PD. Most studies [2, 3, 4] address this challenge by using contact sensors (e.g., inertial sensors), and this approach has limitations. Although a number of studies using these sensors show relevant outcomes and high correlation with severity scales [2], there are challenges intrinsic to the use of contact sensors [5]. These sensors limit natural movement and can be uncomfortable. Besides requiring skin preparation, they can cause irritation, thus, may not be indicated to be used in environments with high risk of contamination by contact [5, 6].

Although there exist many studies in the PD field, especially with the aim to quantify its motor signs, little has been investigated about the use of non-contact sensors, as well as the employment of modern tools for data visualization. As discussed in [7], the gap between the "big data" acquired with sensitive measurement technologies and their limited clinical application is still a challenge that limits the progress in this field of study.

In order to solve these problems, a series of experiments were conducted to shed light on the investigation of the use of non-contact sensors to quantify the motor symptoms of PD and the employment of machine learning tools to improve the understanding of big data frequently acquired across the many experiments with PD patients. It was expected that by means of the use of non-contact sensors, it is possible to quantify the main motor patterns of PD, similarly to one of the most used inertial sensors, i.e., the gyroscope.

1.2 Relevance of the thesis

Chronic diseases, eldery health and innovation in health were fields declared as research priorities from the Ministry of Health of Brazil [8].

PD is a neurodegenerative disease that affects about 6.1 millions of people globally [9]. Over the past generation, the global burden of PD has more than doubled as a result of increasing number of older people [9, 10]. As worldwide life expectancy has increased it will likely continue to grow. The projected number of individuals with PD in the five most populous nations of Western Europe and in the ten most populous nations of the world for 2030 is 8.67 million, considering individuals over 50 years old [11].

The economy burden of PD in the United States in 2010 was approximately $22,800 USD per patient [12]. The population with PD incurred medical expenses of approximately $14 billion USD in 2010, $8.1 billion USD higher ($12,800 USD per capita) than expected for a similar population without PD [12]. Indirect costs (e.g., reduced employment) are conservatively estimated at $6.3 billion USD (close to $10,000 USD per person with PD) [12]. In Europe, the costs per subject with PD in 2010 was estimated in €PPP 11,153 [13]. In Australia, the mean annual cost per person to the health care system in 2012 was $32,556 AUD [14]. The burden to society was an additional $45,000 AUD per annum per person with PD. In Brazil, the second most prevalent neurodegenerative disease worldwide cost in 2015 an average of $5,853.50 USD per person, including $3,172.00 USD in direct costs (medical and nonmedical) and $2,681.50 USD in indirect costs [15]. Figure 1.1 summarizes the estimated annual cost per capita with PD in some countries around the world.

The burden of chronic conditions such as PD is projected to grow and this give impetus

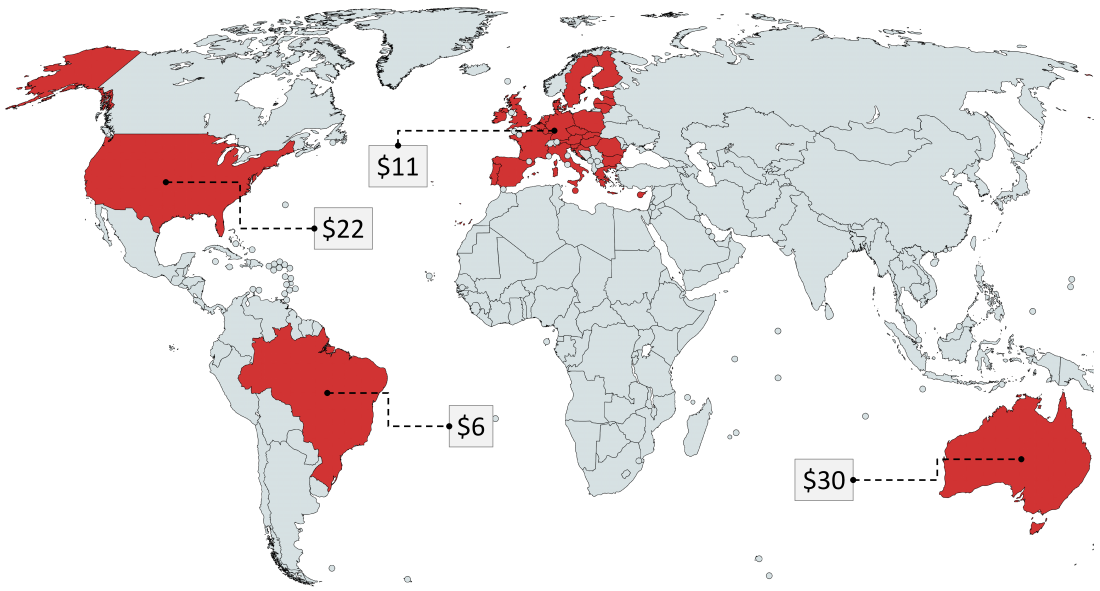

Figure 1.1: Approximated annual cost per capita with Parkinson's disease in some countries. All values are in thousands of USD.

to the need for innovative new treatments to delay onset, or alleviate symptoms.

PD is a very complicated condition for physicians to optimally manage, with multiple motor and nonmotor manifestations that evolve over time. Its diagnosis is purely clinical and relies on medical history and neurological evaluation [16]. Recently, the clinical diagnostic criteria for PD have been revised [17]. Bradykinesia (slowness of movement), rigidity (increased muscular tone) and rest tremor are still highlighted as cardinal signs of the disease. However, now, bradykinesia must occur in combination with rest tremor, rigidity or both. Over the past 10-20 years, non-motor symptoms of PD have been given considerable attention [18]. Nevertheless, the motor signs still represent the hallmarks of the disease and are the most important characteristics for the diagnosis of PD.

1.3 The object of the research

The research object of this doctoral thesis is quantitative parameters, obtained using gyroscope sensor and non-contact capacitive (NCC) system, being the latter a system designed during the doctoral research.

Obtained parameters were analyzed to quantify motor patterns and applied to discriminate PD patients from those without PD.

1.4 The aim of the thesis

The aim of the thesis is to develop a non-contact system to quantify the motor symptoms of PD and employ machine learning tools to improve the understanding of big data frequently acquired across the many data collections with PD patients. Figure 1.2 illustrates the conceptual idea of the proposed system.

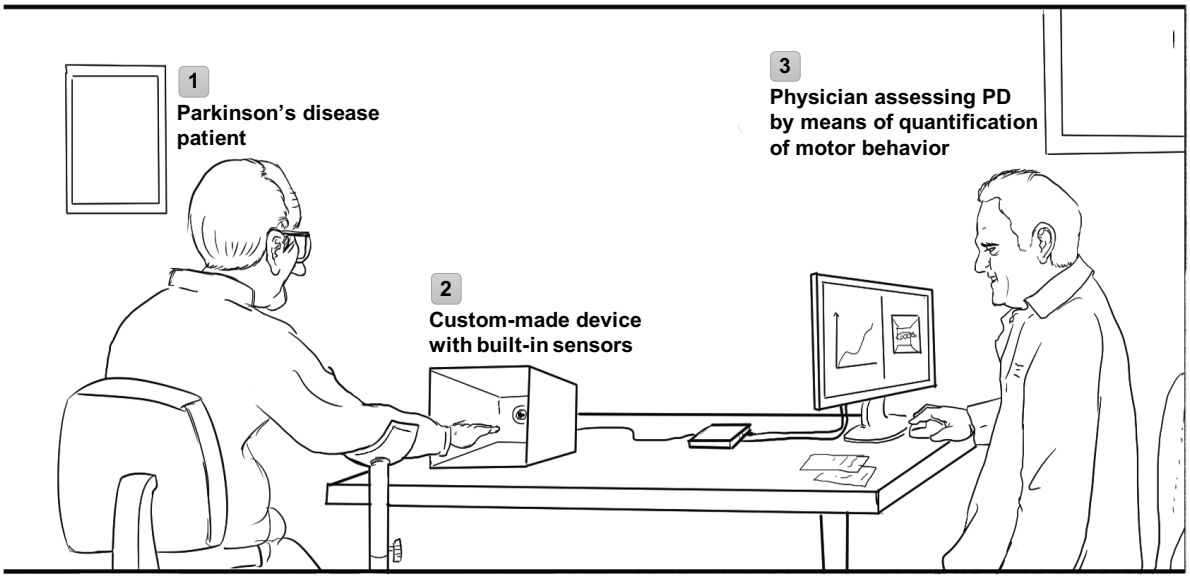

Figure 1.2: Conceptual idea of the proposed system. During the exam the patient will execute standardized motor tasks with the hand in the cube while the health professional will be able to view the results of the exam on the computer screen.

1.5 The objectives of the thesis

In order to solve the stated problem and reach the aim of the thesis, the following objectives were formulated:

1. To investigate non-contact sensors capable to quantify the PD motor signs.
2. To investigate if data acquired with NCC system allow discrimination among different hand movements and propose features to discriminate hand movements.
3. To investigate if data acquired with NCC system allow discrimination between subjects with and without the PD and propose features and clustering techniques to discriminate groups of subjects.
4. To investigate techniques to visualize and classify the huge amount of data that can be estimated from signals of a set of movements commonly evaluated for PD diagnosis.

1.6 Research methodology

Investigation in this dissertation is divided into three parts. In the first part, two non-contact sensors were experimentally evaluated. Leap Motion controller (LMC) was the first sensor analyzed and considered to be used for the quantification of PD motor signs. During the experiment with LMC a static plaster hand was used as a reference to analyze the sensor behavior and its accuracy. The second analyzed sensor was the NCC sensor based on electric potential technology, for this sensor a deeper evaluation was conducted. In this sense, a custom-made device with built-in NCC sensors was designed and validated by means of a micro-machine reference system.

In the second part of the investigation, parallel with the first part, features were extracted to evaluate techniques for visualization and classification of data from inertial and physiological signals of a set of movements commonly used for PD diagnosis. Signals used in this part of the research were acquired by Machado *et al.* [19].

The third part of the investigation comprised a series of experiments using NCC system. First, an experiment with a healthy subject was conducted to validate the data collection protocol. Secondly, an experiment with two subjects, being one with PD and other without PD, was done with aim to discriminate motor tasks between both groups. Thirdly, using NCC system and gyroscope sensor, signals from both sensors were collected at the same time for correlation analysis in time and frequency domains. Three healthy subjects participated in this part of the study doing eight hand motor tasks. Finally, in the fourth experiment, 57 subjects were recruited, being 30 with PD and 27 controls without PD. The subjects from each group were paired in terms of age and sex, and subjects with PD were evaluated using the Unified Parkinson's Disease Rating Scale (UPDRS) by three skilled raters. Signals from NCC system and gyroscope sensor were collected during the execution of nine hand motor tasks. A frequency analysis was performed (i) to compare the systems based on both sensors; (ii) for discrimination of motor patterns from both groups of subjects.

1.7 Scientific novelty of the thesis

1. Model of the relationship between hand displacement and electric potential integrated circuit (EPIC) sensor response.

2. Exhaustive analysis of three dimensionality reduction (DR) techniques for data visualization and classification of motor patterns analysis in PD. t-distributed stochastic neighbor embedding (t-SNE) is highlighted by the best achievements in terms of vi-

sual discrimination of the groups and the overall classification accuracy.

3. Design, development, employment and validation of a proposed NCC system for the assessment of people with PD.

1.8 Practical value of the research findings

Results of the research are to be used for the development of portable systems for human motion quantification. Features extracted from the signals of hand movements can be used for characterization and discrimination of motor patterns.

The investigated tools for data visualization and classification can be used for the development of computer-aided diagnosis systems to allow diagnosis and follow-up of people with PD. The two-dimensional projections enhanced the visual discrimination of thousand of features that may represent the patients. By using these visualization tools, a control zone can be estimated and used as a reference for the many exams which a person with PD goes through along the life.

1.9 Approval of the research findings

The results of the research were published in eight scientific publications - one in peer-reviewed scientific paper and seven in conference proceedings (see appendix A). Additionally, a patent was filed - number BR 10 2018 069864 8 and also a software registration - number BR 51 2015 000133 7. Furthermore, the results of the research were presented in following conferences:

- XXIV Brazilian Congress on Biomedical Engineering, 2014, Uberlândia, Brazil;
- Simpósio em Engenharia Biomédica, 2014 - 2015, Uberlândia, Brazil;
- XXV Brazilian Congress on Biomedical Engineering, 2016, Foz do Iguaçu, Brazil;
- World Congress on Medical Physics & Biomedical Engineering, 2018, Prague, Czech Republic;
- XXVI Brazilian Congress on Biomedical Engineering, 2018, Armação de Búzios, Brazil;
- 41st Annual International Conference of the IEEE Engineering in Medicine and Biology Society (EMBC), 2019, Berlin, Germany.

1.10 Structure of the dissertation

The dissertation consists of an introduction, six chapters and general conclusions. The volume of the dissertation is 88 pages, in which are given: 41 figures and 11 tables. Additionally, 119 items are cited in the dissertation.

"One, remember to look up at the stars and not down at your feet. Two, never give up work. Work gives you meaning and purpose and life is empty without it. Three, if you are lucky enough to find love, remember it is there and don't throw it away."

- Stephen Hawking

2

Parkinson's disease

In this chapter, an overview of Parkinson's disease is presented.

Parkinson's disease (PD) is one of the neurodegenerative diseases that has been largely approached and benefited by many technological progress. PD is a chronic and progressive disorder that affects the central nervous system (CNS) more specifically the base nucleus, involving the progressive loss of dopaminergic neurons from substantia nigra [1].

The loss of dopaminergic neurons from pars compacta portion of the substantia nigra located in midbrain due to PD can be observed in neurological exams [20, 21]. There is a loss of axons that depart from this brain area and are designed for the striated in coordinating the brain culminating in the dopamine deficit, consequent to atrophy and degeneration of the base nuclei [22].

These pathophysiological changes produce typical neurological symptoms or cardinal signs that can be observed in patients with PD such as, bradykinesia, muscle stiffness, rest and postural tremor, and postural instability [23, 24]. In some cases, there is also cognitive, affective and autonomic impairment [23, 25]. Figure 2.1 shows some of the common PD motor signs.

It should be emphasized that with the disease progression, secondary complications

[1] Substantia nigra is a basal ganglia structure located in the midbrain that plays an important role in reward and movement.

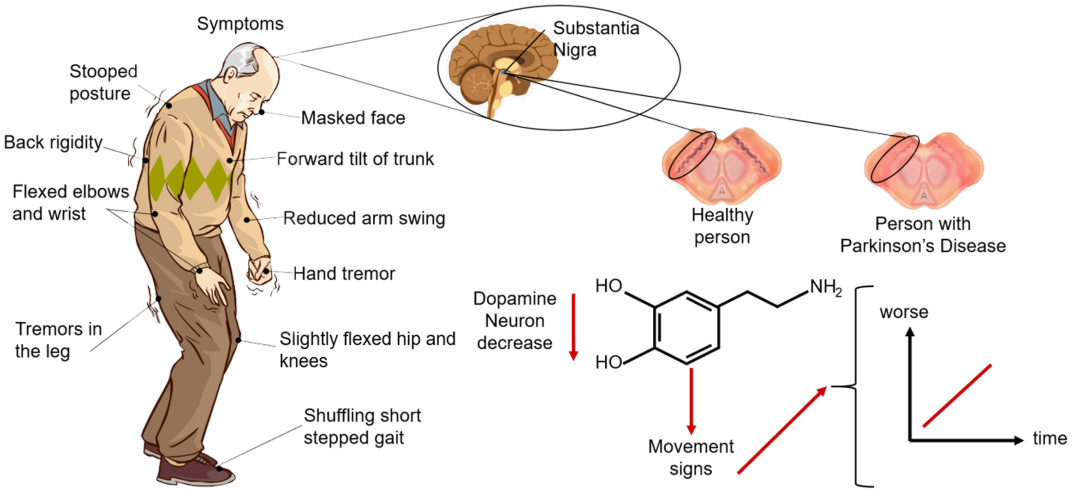

Figure 2.1: Some of the common PD motor signs.

appear. Among the complications, some are result by combination of cardinal signs, such as (i) poverty of movements; (ii) reduction in speed, range and amplitude (hypokinesia); (iii) difficulty initiating movement (akinesia); (iv) masked face; (v) musculoskeletal changes (contractures, fatigue, development of abnormal fixed postures); (vi) gait disorders (pacing pattern, festination and freezing, i.e., abrupt gait interruption); (vii) dysfunction of speech and swallowing; (viii) visual and sensorimotor disorders, in addition to cardiopulmonary alterations.

PD is among the most prevalent neurodegenerative diseases in the elderly, over 60 years old, and the prevalence increases with age [26, 27]. However, individuals younger than 40 years can be affected by the syndrome [28]. With the increase in life expectancy, the number of PD patients is expected to double by 2030 [1].

The diagnosis of PD is purely clinical, in other words, there is no examination, quantitative test or biomarker capable of indicating the diagnosis of the disease, as well as its progress, improvement or worsening of the patient condition. This assessment is performed by means of anamnesis (patient's history and symptoms related to the disease), previous medical history, observation and qualitative questionnaires [29].

Many of these signs and symptoms manifest years before diagnosing PD, meaning their onset is subtle. Due to a lack of objective tests, these signs and symptoms go unnoticed by caregivers, health professionals and even by the patient himself, sometimes resulting in late diagnosis. For the diagnosis, a thorough evaluation is necessary to rule out other possible neurological diseases that cause similar symptoms. In many cases, the clinical diagnosis should be supported by the body's response to the drug levodopa ("dopa test") [30].

In general, scales for the evaluation of neuromuscular diseases explore several compo-

nents of human experience, such as the clinical condition of the person, motor and mental functions, disabilities, limitations related to work activities and social participation, and quality of life.

The most commonly used subjective scale for assessing PD is the Unified Parkinson's Disease Rating Scale (UPDRS) [31, 29], which is composed of four parts: Part I (non-motor experiences of daily living), Part II (motor experiences of daily living), Part III (motor examination) and Part IV (motor complications).

For the quantification of the cardinal signs of PD, several sensors and algorithms have been proposed in order to make the evaluation of the disease objective. This need arises from the fact that PD still does not have a standard exam for its diagnosis, follow-up, and treatment. Unlike other pathologies that can, for example, be diagnosed and monitored by a blood test.

Usually, after diagnosis, the first attempt is always the drug with dopamine replacement, and there is an initial period ($\sim$ 5 years) when the symptoms go away. After the initial period, the drug begins to have no effect, and from time to time the dosage needs to be increased [32, 33]. Increasing the dosage may cause adverse effects (i.e., schizophrenia), and in this scenario, in some cases deep brain stimulation surgery is indicated.

"If you can't fly then run, if you can't run then walk, if you can't walk then crawl, but whatever you do you have to keep moving forward."

- Martin Luther King Jr.

3

Non-contact sensors for Parkinson's disease motor symptom quantification

In this chapter, the overview of the current research on the topic of the dissertation is presented.

Objective ways to measure the signs of PD are widely discussed [34]. Studies such as those presented in [7, 34, 35] synthesize what has been researched and indicate the perspectives and needs that involve technologies for PD. Many of the approaches use inertial sensors, such as accelerometer, gyroscope, and magnetometer.

Figure 3.1 shows some of the sensors and techniques commonly used for the quantification of the PD signs.

Table 3.1 lists the main types of sensors used to quantify the motor signs of PD, as well as some studies that have employed these sensors.

Although a number of studies using contact sensors show relevant outcomes and high correlation with the severity scales [44], there are challenges intrinsic to the use of this type of sensor [5]. These sensors can cause skin irritation, require careful skin preparation and may not be indicated to be used in environments with high risk of contamination by contact [5, 6]. On the other hand, the non-contact sensors are an alternative for the

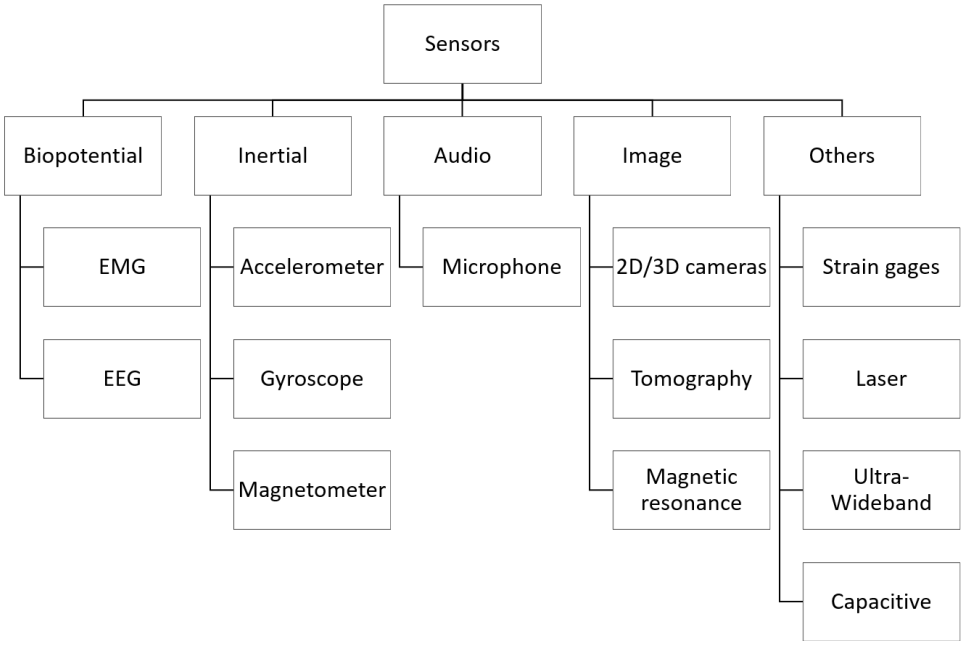

Figure 3.1: Commonly used sensors for detection and quantification of signs and symptoms of PD.

evaluation of movements and biopotentials.

In this sense, this survey aimed to answer the following question: *Is there a portable non-contact sensor capable to quantify the PD motor signs?*

3.1 Leap Motion controller

Leap Motion controller (LMC) is a controller that allows the tracking of multiple hands, fingers, and small objects in free space. The controller's capabilities in realistic environments were analyzed by Weichert [45] and Guna [46]. However, on 2014 and 2015, the studies did not evaluate the specific hand tracking behavior.

The LMC is a consumer-grade sensor developed by Leap Motion company. The sensor was primarily designed for hand gestures and finger position detection in interactive software applications. LMC uses infrared (IR) imaging to determine the position of predefined objects in a limited space in real time. Technically, very few details are known about the precise nature of the algorithms used due to patent and trade restrictions. However, from inspection of the controller, it is clear that three separate IR light-emitting diode (LED) emitters are used in conjunction with two IR cameras [45]. The controller's field of view is an inverted pyramid centered on the device. The effective range of the controller extends from approximately 25 to 600 millimeters above the device.

The cartesian coordinate system used to describe positions in the controller's sensory

Table 3.1: Information about some of the sensors commonly used to quantify motor signs of PD.

Category	**Sensor**	**Does it need contact with the limb?**	**Basic operation**	**Measurement unit**	**Example of use**
Inertial	Accelerometer	Yes	Measures accelaration based on Newton's second law.	g *(or* m/s^2*)*	[36, 37]
Inertial	Gyroscope	Yes	Measures angular velocity based on Coriolis force.	$^\circ/s$	[36, 37]
Inertial	Magnetometer	Yes	Measures the change in rotation of a body relative to the earth's magnetic field.	*Gauss*	[38]
Biopotential	Electromyographic	Yes	Measures the electrical activity of the excitable membranes of muscle cells.	mV	[39, 4]
Image	3D camera (or depth sensor)	No	Scructured light, Time of Flight and Stereo vision.	*x, y and z coordinates*	[40, 41]
Others	Laser	No	Measures the reflection of the projected laser light.	*Pixel*	[42]
Others	Ultra-Wideband	No	Measures the reflection of the projected EM pulse.	V	[43]

space is shown in Figure 3.2. It should be noted that the sampling frequency of the sensor is not stable, it can not be set, and varies significantly [46].

LMC could be an option of sensor for the assessment of PD motor signs. Hand tremor, for instance, is one of the cardinal signs of PD and its analysis has particular requirements such as high accuracy and high precision [47]. These requirements are desired due to the two common tremor parameters, amplitude that can reach small values (around millimeters) and frequency, which can reach up to around 12 Hz [47].

Weichert *et al.* (2013) [45] analyzed the accuracy and robustness of the LMC using an industrial robot equipped with a pen in a controlled environment. They found a static accuracy of 0.2 mm and a dynamic accuracy of 1.2 mm for the pointer mode. The

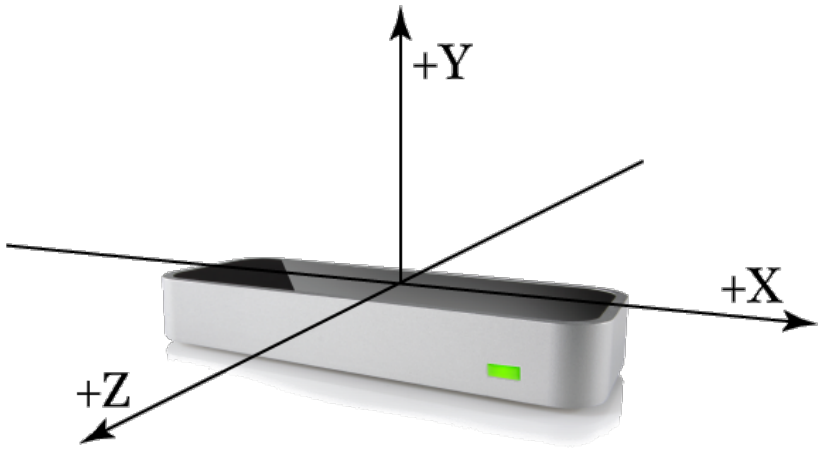

Figure 3.2: The cartesian coordinate system used describe positions in the controller's sensory space.

authors highlighted that the majority of applications for the LMC are gesture-based user interfaces. Also, the achievable accuracy of measurement of the motion of a human hand is the most relevant factor, which is essentially affected by the so-called tremor.

Guna *et al.* (2014) [46] went beyond, analyzing the precision and reliability of the LMC and its suitability for static and dynamic tracking. For static measures they equipped a prosthetic hand with a passive marker. An accuracy lower than 0.5 mm was achieved, but they warned that obtaining tracking stability was challenging. When moving away from the controller, the linear correlation revealed a significant increase in the standard deviation. For the dynamic measurements, a V-shaped tool, consisting of two tracking objects maintaining a constant distance between them, was used to simulate two human fingers. The results of the dynamic scenario revealed the inconsistent performance of the controller, with a significant drop in accuracy for samples taken more than 250 mm above the controller's surface. In spite of LMC represented a revolutionary input device for gesture-based human-computer interaction, it presents limited sensory space and inconsistent sampling frequency. Due to these limitations it cannot be used as a professional tracking system.

In order to confirm the reproducibility, Chapter 5 presents an experimental method and its results to evaluate LMC as a human tremor record device.

More recently, after the experiments presented in Chapter 5, some studies were conducted focusing in the context of clinical assessment. Coton *et al.* (2016) [48] studied the feasibility of the use of LMC for hand motion analysis. The study aimed to determine if LMC could be used to realize a finger motion analysis in the contact of physiotherapist's examination. The authors employed a standard and validated protocol (i.e., measure of motor function) whose purpose is to quantify the patient's capabilities and represent

neuromuscular disease state and advance. Regarding LMC capabilities in this application setup, (i) the authors noted that smaller hands are more difficult to track and less accurate than adults' hands; (ii) a static hand will maintain its detection only for a short moment, if the hand does not move the tracking will fail; (iii) the global accuracy of the LMC decrease with the diffraction effect of glass support used in their experiment; (iv) to ensure an initial tracking of the hand by the LMC, the fingers have to be clearly visible and spaced.

Butt *et al.* (2018) [49] used LMC for objective and automatic classification of PD. The main objective of their study was to develop and test the ability of the LMC to assess the motor dysfunction in patients with PD based on MDS-UPDRS part III exercises. The results revealed that the system did not return clinically meaningful data for measuring postural tremor in people with PD. In addition, it showed limited potential to measure the forearm pronation/supination. Also, LMC has a limited angle of view to assess the motor dysfunctions in people with PD. For this reason, certain gestures could not be recorded properly depending on the placement of the LMC. Regarding the functional limitation of LMC for postural tremor assessment in PD, one possible reason could be an inconsistent frame rate of the device with respect to time.

To summarize, LMC presents severe limitations as a candidate device for the implementation of innovative service in neurodegenerative diseases and other ageing-related disorders. Improvements in software development kit (SDK) algorithm accuracy and usability are required to allow its use in medical assessment context.

3.2 Non-contact capacitive sensor

After LMC, non-contact capacitive (NCC) sensor was identified as a portable technology with potential to be used for hand motion quantification.

In this research, the investigated NCC sensor is based on electric potential sensing (EPS) technology. Table 3.2 presents a history timeline of EPS technology development and successful applications.

NCC sensors are capable to measure perturbations in the electric field (E-field) caused by objects with dielectric properties such as the human body [55]. By using this technology, it is possible to recognize various human activities. Many studies have reported the use of this sensing technology for multiple purposes such as non-invasive breathing and heart monitoring [54], wearable devices to detect hair touch and restless leg movement [56] and passive tracking of movements [52].

Table 3.2: NCC electric potential sensing technology timeline.

Year	Authors	Study title	Achievements
1991	Clippingdale *et al.* [50]	Ultra-high impedance voltage probes and non-contact electrocardiography	EPS was first introduced
2001	Harland *et al.* [51]	Electric potential probes - new directions in the remote sensing of the human body	Data showing the application of the remote, off-body, sensing of the electrical activity of the heart at distances of up to 1 m from the body
2010	Beardsmore-Rust *et al.* [52]	Passive tracking of targets using electric field sensors	Data obtained using a sparse (4-element) array of sensors to image a volume of space for target movements
2015	Fatoorechi *et al.* [53]	A comparative study of electrical potential sensors and Ag/AgCl electrodes for characterising spontaneous and event related electroencephalagram signals	Signals recorded by the novel EPS sensor were compared to a wet-gel electrode system
2016	González-Sánchez *et al.* [54]	Capacitive Sensing for Non-Invasive Breathing and Heart Monitoring in Non-Restrained, Non-Sedated Laboratory Mice	Monitoring the heart rate and breathing rate of non-restrained, non-sedated laboratory mice

There is a version of EPS sensor designed to allow detection of field disturbance due to the movement of a nearby object. In Chapter 7, a series of experiments are conducted to evaluate the employment of this sensor for PD motor signs quantification. It is important to note that we have found no report of the use of capacitive sensors for monitoring hand movements in the context of PD.

NCC EPIC sensor behavior

Plessey Semiconductors Ltd is the company responsible for the commercialization of electric potential integrated circuit (EPIC) sensors [57]. The EPIC sensors are basically composed of a metal electrode which is coupled to circuitry with an ultra-high input impedance, so, it acts as a high sensitivity, non-contacting voltmeter. It is designed to measure very small changes in electric fields. EPIC measures changes in electric potential, that could be [58], (i) the earths natural electric field (i.e., 100 V / vertical meter); (ii) the environment electric field (i.e., 50/60 Hz mains frequency); (iii) biometric electric field (i.e., ECG / EMG / EOG / EEG); (iv) an induced electric field.

In single-ended mode the sensor can be used to read electric potential; when used in differential mode, it can measure the local electric field; or it can be deployed in arrays

to provide spatial potential mapping (locating a conducting or dielectric material placed in free space).

There are several products launched by Plessey, but in this research we are interest in PS25454 (see Figure 3.3) EPIC sensor, which was specifically designed for movement detection in an open environment.

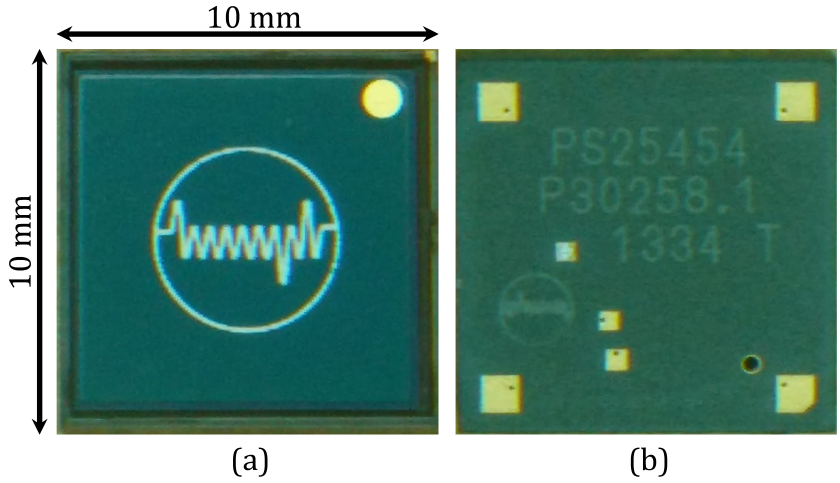

Figure 3.3: PS25454 EPIC sensor (Plessey semiconductors, UK), (a) front and (b) rear views.

PS25454 EPIC capacitive sensor (see Figure 3.3) incorporates several features to enhance the measured signals, allowing for the detection of field disturbance due to the movement of a nearby object. The main features of this sensor are ultra-high input resistance, typically 20 $G\Omega$; input capacitance as low as 15 pF; lower -3 dB point typically 0.2 Hz and upper -3 dB point typically 20 kHz. It operates with bipolar power supply from $\pm 2.4V$ to $\pm 5.5V$.

EPIC can be used in non-contact applications to sense [58], (i) field disturbance; (ii) monitoring charge; (iii) interaction with ambient field. Only interaction with ambient AC field will be detailed, because it is the operation best suitable for the objectives of this research [52].

When a person moves, the E-field is disturbed so that a proportional signal can be used to estimate various information related to position and motion. One of the main advantages of this sensor technology is its ability to operate completely passively, without the necessity to emit waves in the environment such as in the case of a radar [59]. Figure 3.4 illustrates the sensor behavior while interacting with ambient AC field plus a hand movement.

Detailing, Figure 3.4a depicts the sensor behavior while any objects are moving around. The sensor signal output is the detected ambient AC field and it oscillates

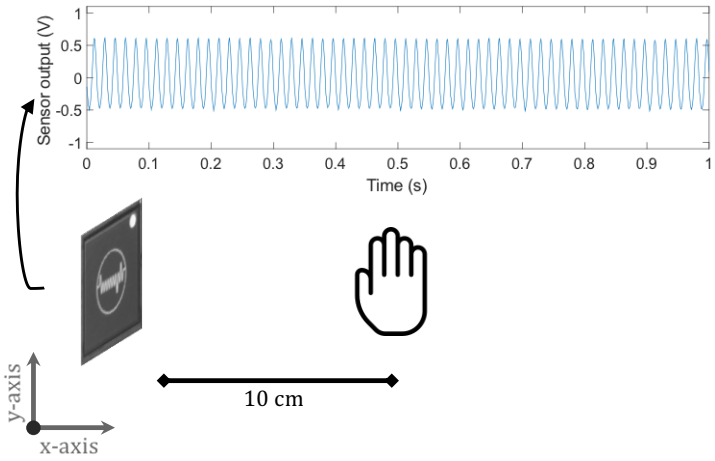

(a) Sensor behavior without nearby hand movement.

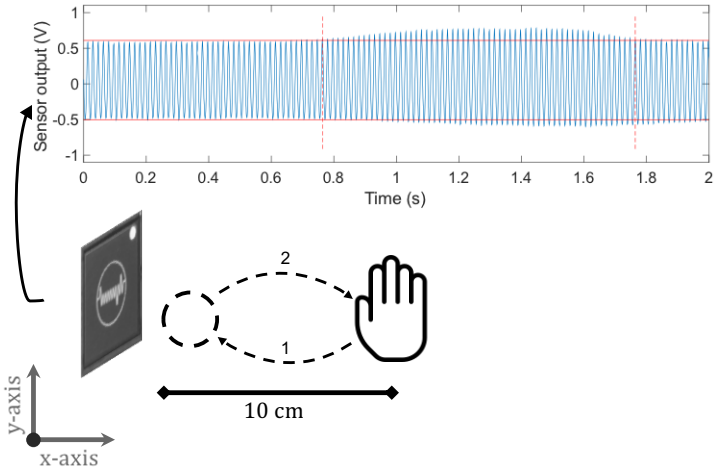

(b) Sensor behavior while the hand moves closer (i.e., back and forth movement).

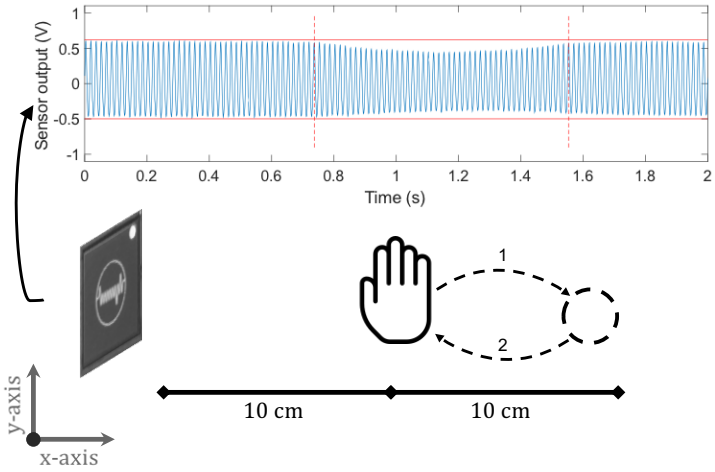

(c) Sensor behavior while the hand moves away (i.e., back and forth movement).

Figure 3.4: Interaction with ambient ac field - NCC EPIC sensor behavior.

exactly in 60 Hz. In this research, this signal component is called of *carrier* and it is related to the power line frequency. Figure 3.4b depicts what happens when the hand is moved closer to the sensor unit (i.e., back and forth movement). The upper and lower horizontal red lines denote the baseline signal amplitude and the vertical dashed lines represent a window of sensor output while a human hand was moving back and forth one time. Figure 3.4c depicts the sensor signal output while a human hand was moving away.

3.3 Conclusions and hypothesis

1. There is a massive number of studies employing contact sensors (i.e., inertial and electromyographic sensors) to measure the signs of PD and many of them show relevant outcomes and high correlation with the severity scales.

2. There are challenges intrinsic to the use of contact sensors. These sensors can cause skin irritation, require careful skin preparation and may not be indicated to be used in environments with high risk of contamination by contact.

3. Previous studies have demonstrated that LMC is a revolutionary input device for gesture-based human-computer interaction, but it presents limited sensory space and inconsistent sampling frequency. Due to these limitations it cannot be used as a professional tracking system.

4. NCC sensors based on EPS technology are capable to measure perturbations in the electric field caused by objects with dielectric properties such as the human body.

5. EPS technology has been developed and applied since 90s. The applications are mainly focused in the measurement of biopotentials. However, there is no application of this technology yet for the hand motion quantification in the context of PD.

6. There is a version of EPS sensor designed to allow detection of field disturbance due to the movement of a nearby object.

Two hypotheses were formulated as a result of the performed literature survey:

1. LMC are not suitable for the assessment of PD hand tremor or any time dependent event.

2. By means of the use of non-contact capacitive sensors, it is possible to quantify the main motor signs of PD, as well as one of the most used inertial sensor (i.e., gyroscope).

"It's not like I take two pills and then at 10am I take another two. It really depends on what chemicals are brewing in my brain that day."

- Michael J Fox

4

Visualization and classification of motor symptoms of Parkinson's disease

Currently, the ability to collect and store large datasets is tremendous. Despite that, our ability to algorithmically analyze and synthetically display clinically and disease-relevant information to physicians and patients remains limited [7]. Big data in healthcare can be useful for early detection of disease and focused treatment. Data from people with PD possess all the characteristics of big data [60, 61], which are characterized by volume, variety, velocity, veracity, value, and variability.

More and more application domains are producing progressively larger and multivariate datasets. Expressed in a space that requires many degrees of freedom, multivariate data present severe problems for data analysis and especially for visualization. Visualization is the integral part of exploratory data analysis, the first stage of data analysis where the goal is to make sense of the data before proceeding with more goal-directed modeling analyses. Since human perception (and output devices) is limited to three-dimensional space, the challenge of visualizing multivariate data is converting the data to a space of lower dimensionality that is depictable and comprehensible to the user while preserving as much information as possible. This process is called dimensionality reduction (DR) and visualization of multivariate data is one of its traditional applications.

Related to data visualization and classification, the curse of dimensionality [62] refers to various challenges that arise when analyzing data in high-dimensional spaces that do not occur in low-dimensional settings. High dimensionality coupled with large sample sizes create issues such as heavy computational cost and algorithmic instability.

4.1 Dimensionality reduction

A relevant area for data visualization is dimensionality reduction (DR). DR focuses on keeping data relationship from high-dimensional (e.g., original data) to low-dimensional (e.g., reduced data) spaces. In addition, DR methods are used to simplify data visualization, making it easier for human evaluation. Data visualization is an important application of DR. It is the study of the visual representation of data through graphical representations, and it is effective in exploratory data analysis [63, 64].

DR algorithms can be divided into different categories based on different criteria, e.g., linear and nonlinear dimensionality reduction algorithms. Classically, the problem of dimension reduction and data representation has been approached by applying linear transformations such as the well-known principal component analysis (PCA) [65, 66]. Those linear techniques focus on keeping the low-dimensional representations of dissimilar data points far apart. However, PCA is not capable of representing higher order, nonlinear, and local structure in the data. In the last decades, some nonlinear DR algorithms have been proposed to deal with complex nonlinear data.

Many nonlinear and linear DR methods are reported in the literature [67, 68]. In this research, three of these methods were employed and compared: PCA [65], Sammon's mapping [69], and t-distributed stochastic neighbor embedding (t-SNE) [70].

Sammon's mapping is one of the first nonlinear mapping algorithms for analysis of multivariate data [69]. t-SNE, on the other hand, is an improved variation of the stochastic neighbor embedding (SNE) [71].

Furthermore, there are some studies that employed PCA [61, 72], Sammon's mapping [72, 19] and t-SNE [73, 74] for visualization of PD-related data. The following subsections explain the basic principle behind Sammon's mapping and t-SNE techniques.

Sammon's mapping

Sammon's nonlinear mapping [69] is a projection method for analysing multivariate data. The method attempts to preserve the inherent structure of the data when the patterns are

projected from a higher-dimensional space to a lower-dimensional space by maintaining the distances between patterns under projection. Denote the distances between pattern X_i and pattern X_j in the input space and their projections Y_i and Y_j in the projected space as d^*_{ij} and d_{ij}, respectively. Employing Euclidean metric to measure distances, Sammon's mapping minimises the mapping error

$$E = \frac{1}{\sum_{i<j}^{n} d^*_{ij}} \sum_{i<j}^{n} \frac{[d^*_{ij} - d_{ij}]^2}{d^*_{ij}} \tag{4.1}$$

where n is the number of patterns. The mapping attempts to fit n points in the lower-space, such that their interpoint distances approximate the corresponding distances in the higher-space.

Sammon's mapping has been originaly designed and usually used to project high-dimensional data onto one to three dimensions in order to analyse the data structure, or for classification based on two projections [75, 19]. It was found that classification accuracy based on Sammon's projections is comparable with, an in some cases even superior, to that based on other feature extractors [75, 76, 77].

t-SNE

The t-SNE technique represents a recent machine learning strategy for nonlinear dimensionality reduction that is useful for embedding (e.g., scatter-plotting) of high-dimensional data into lower-dimensional (1D, 2D, 3D) spaces.

t-SNE tries to place a point from high-dimensional space in a low-dimensional one so as to preserve neighborhood identity. The SNE algorithm converts Euclidean distances between high-dimensional data points into conditional probabilities representing similarities; closer data points mean high similarity.

The similarity of data point x_j to data point x_i is represented by the conditional probability $p_{j|i}$. These similarities express the probability that x_i would select x_j as its neighbor. For the low-dimensional counterparts y_i and y_j of the high-dimensional data points x_i and x_j, it is computed a similar conditional probability denote by $q_{j|i}$.

Once conditional probability distributions are calculated for the data points in both the high- and low-dimensional representations, the goal of the algorithm is to minimize the mismatch between the two. The cost function (Equation 4.2) which should be minimized is the sum of Kullback-Leibler (KL) divergences over all points using a gradient descent

method,

$$E = \sum_i KL(P_i||Q_i) = \sum_i \sum_j p_{j|i} log \frac{p_{j|i}}{q_{j|i}} \tag{4.2}$$

in which P_i represents the conditional probability distribution over all data points given a data point x_i and Q_i represents the conditional probability distribution over all other map points given map point y_i.

t-SNE improves SNE in two points [70]: (i) by using a symmetrized version of the SNE cost function with simpler gradients and (ii) by applying Student's t-distribution rather than a Gaussian to compute the similarity between two points in the low-dimensional space.

4.2 Conclusions and hypothesis

1. Dimensionality reduction methods are frequently used as a prior step before data classification.
2. The use of DR methods prior data classification, in some cases, improve the accuracy of generated models.
3. Visualization of high-dimensional data is an important problem in many different domains, and deals with data of widely varying dimensionality.
4. The employment of t-SNE for data visualization dates from 2008, when the technique was first presented and its application in data related to PD has yet been poorly explored.
5. Until 2018, the use of t-SNE as a step prior to data classification had not yet been investigated.
6. It was not found in the literature a comparison of DR methods in the context of PD motor patterns recognition.

Two hypothesis were formulated as a result of this chapter:

1. By using t-SNE, it is possible to enhance the visualization of PD motor patterns in a 2-dimensional map.
2. By avoiding the curse of dimensionality, the use of DR methods prior PD data classification could improve the performance of machine learning models.

"I love deadlines. I love the whooshing noise they make as they go by."

- Douglas Adams

5

Experimental research using Leap Motion controller

In this chapter, the results of the experiments with the LMC are presented. The experimental research of LMC, by measuring hand displacement in a static and dynamic scenarios, are presented. This research aimed to evaluate LMC as a device to be used for quantification of hand movements before apply it in a wider study in PD motor task quantification.

In order to evaluate LMC, three experimental setups were designed: (i) measurement of induced hand tremor by means of functional electrical stimulation; (ii) measurement of wrist tremor from a subject with PD and from two subjects neurologically healthy; (iii) measurement of a static plaster hand model under two light conditions and two different distances between the controller and the hand. Additionally, a computer software (National Institute of Intellectual Property - Brazil - BR 51 2015 000133 7) was designed and implemented to control LMC and to organize the data collected for further analysis. Figure 5.1 depicts the software interface with description notes.

By using this software (see Figure 5.1) it is possible to record various data regarding the hand and its fingers, including the hand palm and fingers displacement along x-, y- and z-axes.

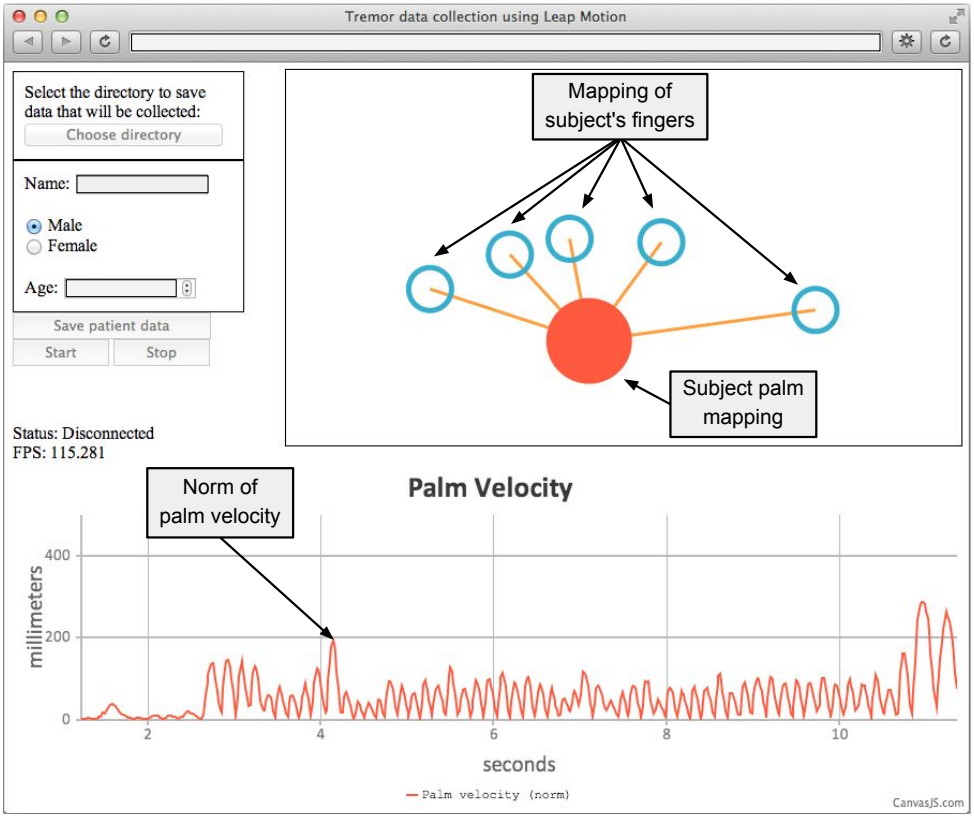

Figure 5.1: Graphical user interface of developed computer software for data collection with Leap Motion controller.

The results of the research presented in this chapter were published and presented at two national conferences: "XXIV Brazillian Congress on Biomedical Engineering" [78] and "VIII Simpósio em Engenharia Biomédica" [79].

5.1 Hand tremor quantification

In this investigation, four volunteers were invited to perform an invidual task (i.e., sustain a pose against gravity). Two distintic scenarios were evaluated: (i) induced hand tremor by means of functional electrical stimulation; (ii) wrist tremor from a subject with PD and from two subjects neurologically healthy. This study has been approved by the National Committee for Ethics in Research (CAAE: 07075413.6.0000.5152).

Signal preprocessing

In this study, only the hand palm displacement was used as information for tremor analysis. The variation of hand palm position along the time is used for estimation of velocity (v), as defined in Equation 5.1. The time-series of velocity norm ($\|\overrightarrow{v}\|$) is estimated and,

then, used to represent the voluntary and involuntary movement.

$$\overrightarrow{v} = \left[\frac{\Delta x}{\Delta t}, \frac{\Delta y}{\Delta t}, \frac{\Delta z}{\Delta t}\right] \tag{5.1}$$

Signal processing

A rectangular window of 10 seconds was considered for all collected signals in a way to make them comparable. The signals were analyzed in time and frequency domains. The instantaneous mean frequency (IMNF) was estimated by means of Hilbert Spectrum (HS) as described in [80].

Scenario: induced hand tremor by means of functional electrical stimulation

Figure 5.2 illustrates the elements employed for the experiment which involves the stimulator controller, the glove (to spread the stimulus across the hand) and the LMC (to capture the induced tremor). For tremor induction a device developed by VITAtronic®[81] company was used, with aim to emulate the human tremor commonly found in eldery people.

The electric stimulator device was powered by a 9 V battery and it is composed of two potentiometers, one for electric pulse frequency adjustment and other to control the stimulus amplitude. The electric pulse is transmitted through the cable to the conductive glove worn by volunteer.

To check and visualize the electric pulse frequency and amplitude, an oscilloscope was connected in the glove input terminals. Figure 5.3 shows a typical electric pulse generated by stimulator.

A neurologically healthy subject was the volunteer in this experiment. Table 5.1 summarizes the experiment configurations.

The data acquisition of induced hand tremor lasted at least 10 seconds for both hands considering the four frequencies, keeping pulse amplitude value, as shown in Table 5.1.

As a result, Figures 5.4 and 5.6 show the palm velocity norm ($\|\overrightarrow{v}\|$) of volunteer's left hand while stimulus frequency has been set to 2.5 Hz and 10 Hz, respectively. Figures 5.5 and 5.7 show the estimated IMNF (in green) and Figure 5.8 compare the obtained results for each case.

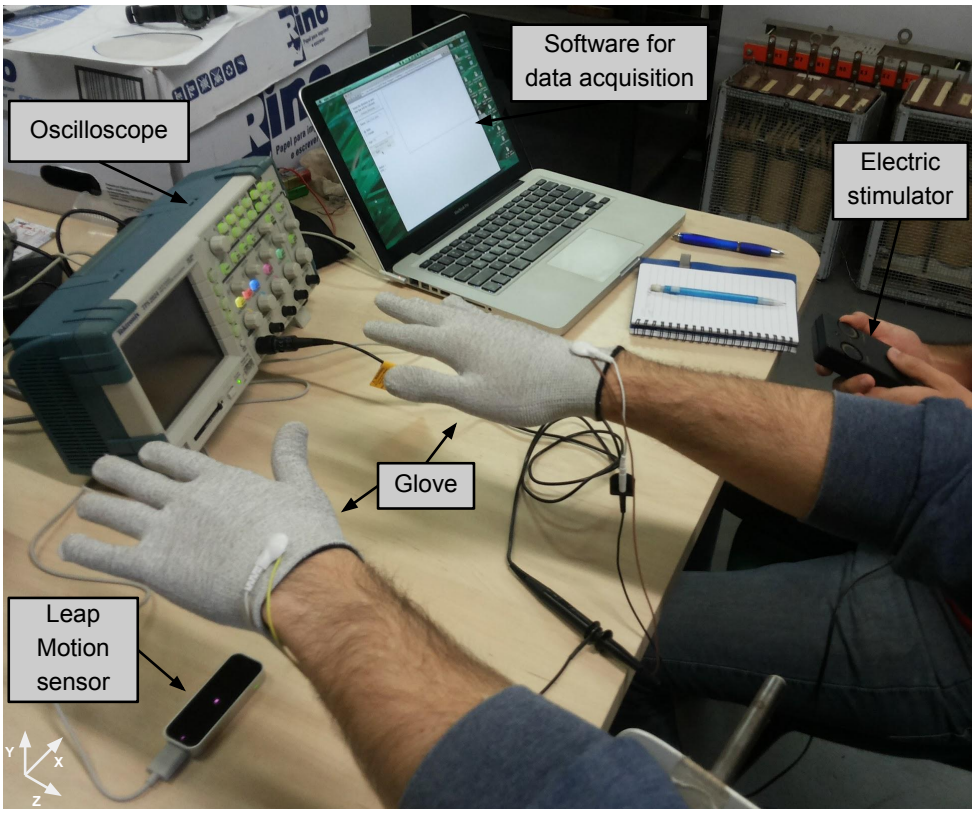

Figure 5.2: Data collection setup of induced hand tremor by means of functional electrical stimulation.

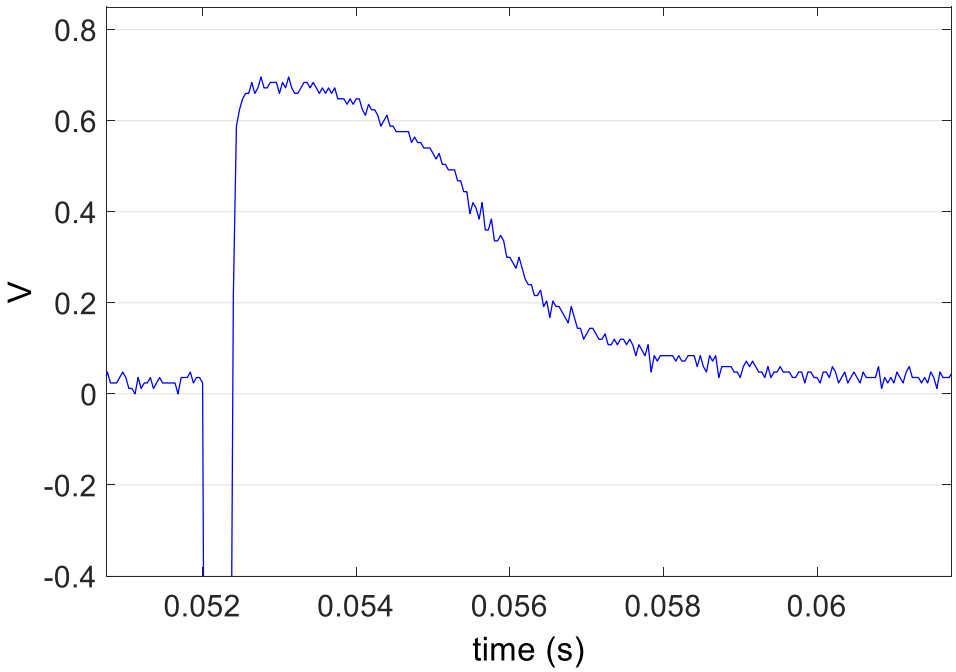

Figure 5.3: Typical electric pulse generated by hand tremor stimulator.

Figure 5.8 shows the IMNF distributions for each configuration as shown in Table 5.1. A clear visual difference between the distributions can be seen only in the case of the first

Table 5.1: Induced hand tremor experiment configuration.

Item	**Parameter**	**Configuration**
Stimulator	Amplitude	0.68 V
	Frequency	2.5 Hz / 5 Hz / 7.5 Hz / 10 Hz
Leap Motion controller	Sample frequency	60 Hz
-	Data acquisition time	>= 10 s

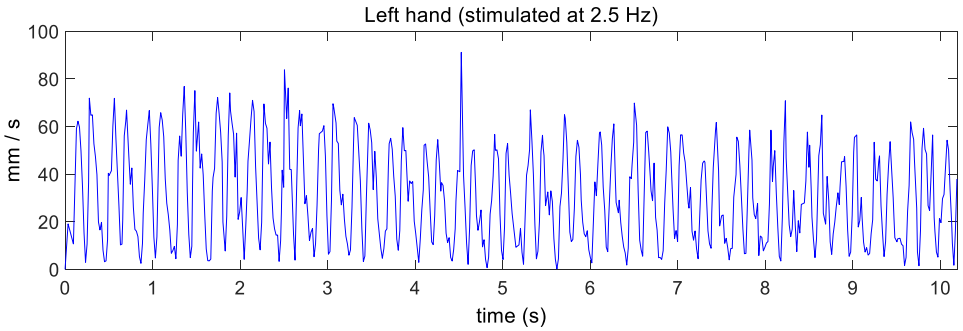

Figure 5.4: Norm of left palm velocity vector (stimulated at 2.5 Hz).

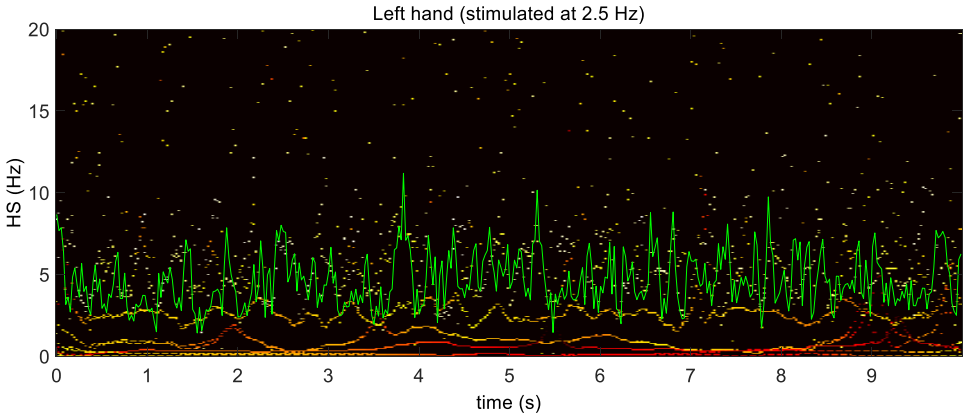

Figure 5.5: Estimated instantaneous mean frequency (in green) from the signal presented in Figure 5.4 by using Hilbert spectrum analysis.

three frequencies against the last one.

All the IMNF distributions were non-normal. The normality test was conducted by using One-sample Kolmogorov-Smirnov test. Table 5.2 presents the hypothesis test comparing each distribution in pairs by means of Mann-Whitney U-test.

In the Table 5.2, p-value equal or less than 0.05 means that compared distributions have different medians. In this sense, the distributions were statisticaly different following a pattern, e.g., taking 2.5 Hz as a reference, only 7.5 Hz and 10 Hz were different. Only the

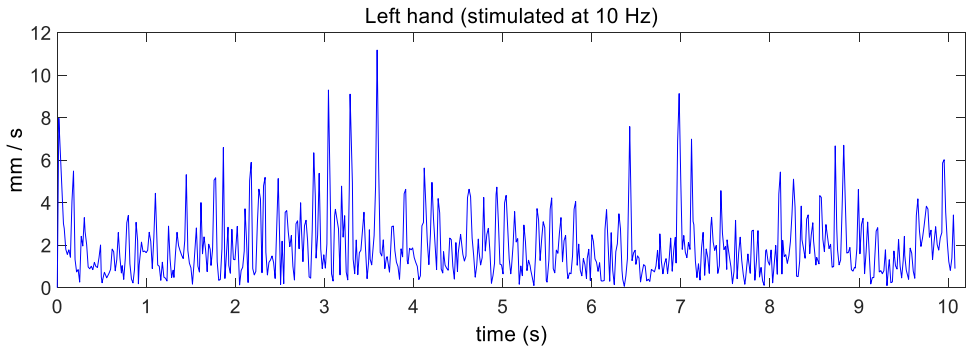

Figure 5.6: Norm of left palm velocity vector (stimulated at 10 Hz).

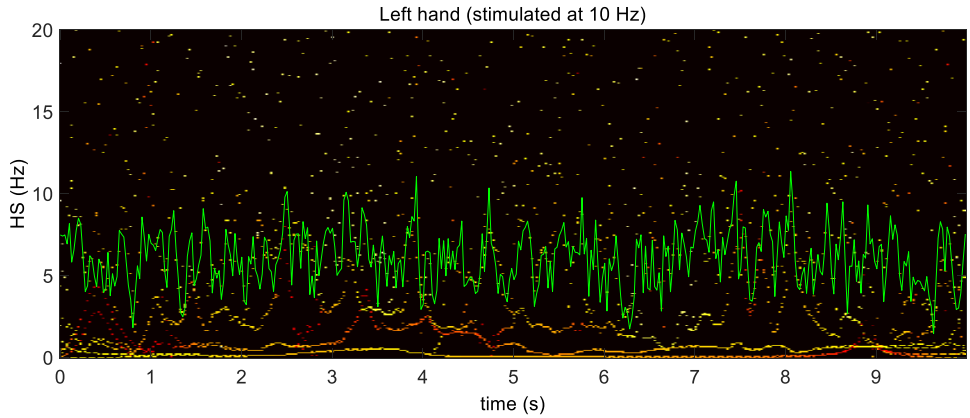

Figure 5.7: Estimated instantaneous mean frequency (in green) from the signal presented in Figure 5.6 by using Hilbert spectrum analysis.

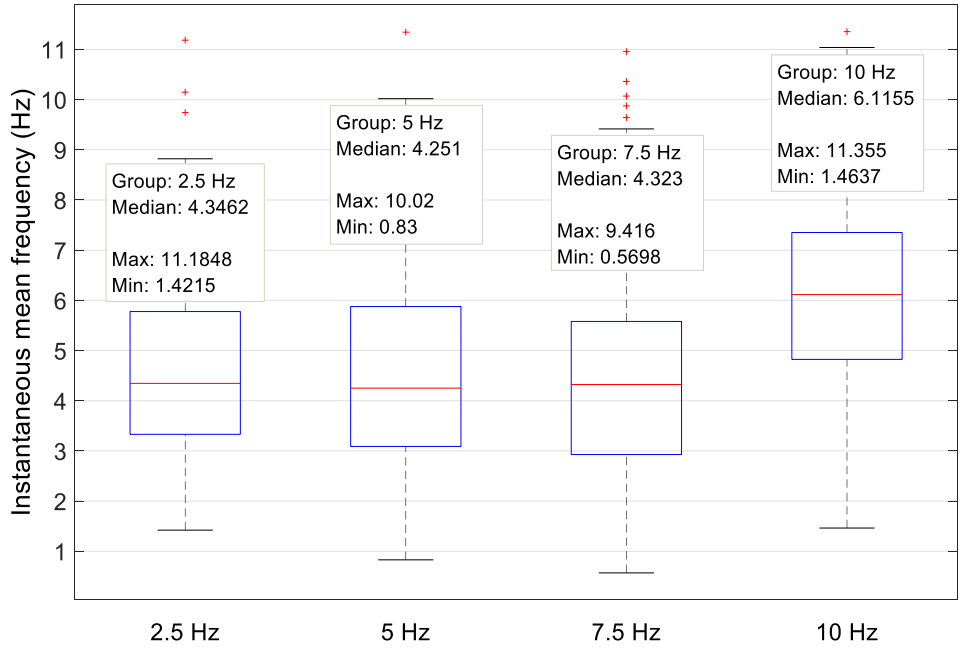

Figure 5.8: Boxplot of IMNF distributions for data acquired while electric stimulator frequency has been set at 2.5 Hz, 5 Hz, 7.5 Hz and 10 Hz.

Table 5.2: Median difference test among the four IMNF distributions by using Mann-Whitney U-test.

	P-value			
	2.5 Hz	5 Hz	7.5 Hz	10 Hz
2.5 Hz	**1.00**	0.33	0.04	0.00
5 Hz	0.33	**1.00**	0.33	0.00
7.5 Hz	0.04	0.33	**1.00**	0.00
10 Hz	0.00	0.00	0.00	**1.00**

distribution of the higher stimulus frequency the difference was confirmed while compared against the other ones.

5.2 Preliminary sensor evaluation

In this investigation, the aim was to evaluate LMC with focus on the specific hand tracking capabilities. Depending on the human age, for example, the tremor amplitude varies between 0.4 mm ± 0.2 mm for young individuals and 1.1 mm ± 0.6 mm for old individuals [82, 83]. The controller's performance was evaluated using a static hand as a reference object, this way, the hand palm position was tracked and recorded to evaluate the dispersion of the results.

The effective range of the controller extends from approximately 25 to 600 millimeters above the device. The cartesian coordinate system is used to describe positions in the controller's sensory space. It should be noted that the sampling frequency is not stable, it can not be set, and varies significantly [46].

Measurement setup

The LMC was fixed on a plane and a reference plaster hand model was fixed above it, as shown in Figure 5.9. A laptop computer, Intel Core i7-3520M CPU 2.9 GHz with 8 GB of RAM, with the developed evaluation software (Figure 5.1) were used for real-time data acquisition and logging.

During the measurements, the hand model was firmly attached using a metal structure. The static measurement was performed under four experimental conditions sets as shown in Table 5.3.

Figure 5.9: Setup of the experimental environment.

The measured positions are denoted by $p[i] = (p_x[i], p_y[i], p_z[i]) \in R^3$, where the components $p_x[i]$, $p_y[i]$ and $p_z[i]$ represent the coordinates in the LMC cartesian coordinate system of the i-th sample ($1 \leq i \leq N, i \in N$) taken at the same position, and N means the total number o samples taken.

Table 5.3: Predefined experimental conditions sets.

	Illumination intensity (lux)	**Distance from controller (cm)**
Set 1	353	27
Set 2	72	
Set 3	353	17
Set 4	72	

In the following, for each set, at least 2,500 samples were measured. In order to analyze the sensor's accuracy and precision in static scenario the deviation and standard deviation were calculated. Figure 5.10 shows deviation between each measured position and mean value for x- and y-axis from set 2.

Figure 5.10 presents one of the smallest deviations for x- and y-axis, which is less than 0.43 mm in the case of x-axis and in the y-axis case is less than 0.59 mm. The box-and-whisker plots in Figure 5.11 shows the average deviation concerning the x-, y- and z-axis at each set (see Table 5.3). The boxes are representing the interquartile range

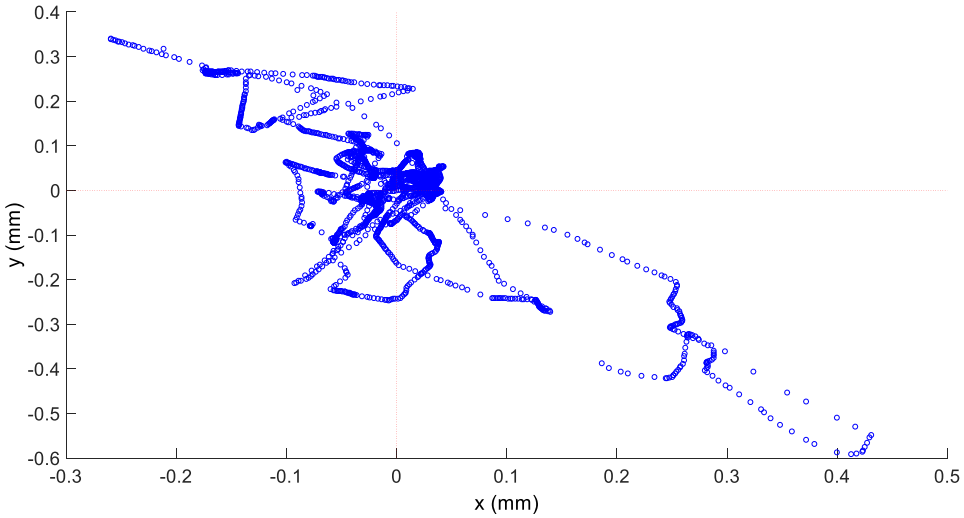

Figure 5.10: Deviation between each measured position and the mean value for x- and y-axis from set 2.

that contains 50% of the values and the whiskers are marking the minimum and maximum values, excluding outliers (marked as red points).

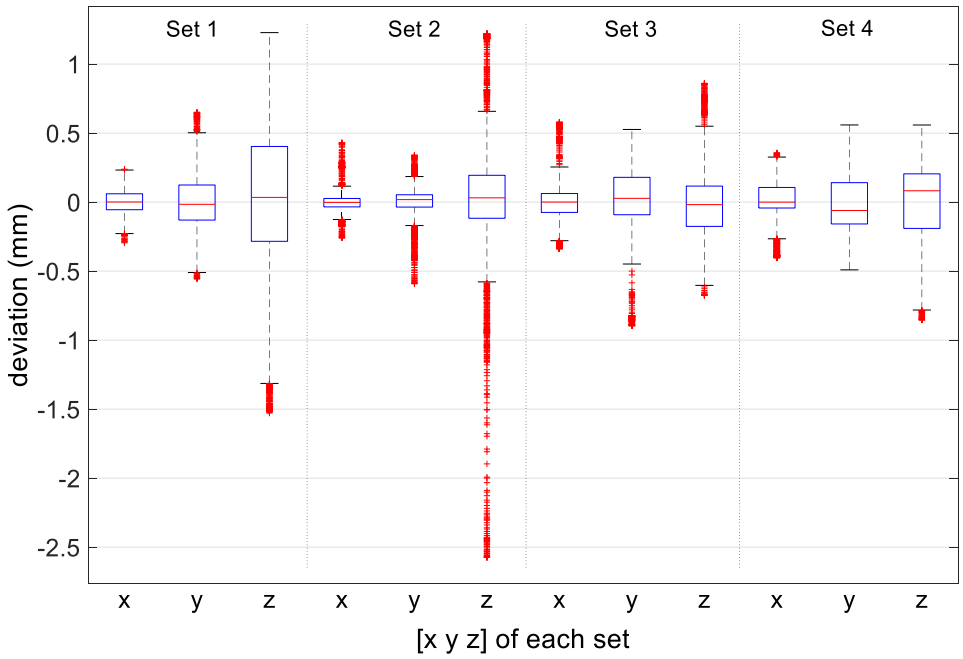

Figure 5.11: Box-and-whisker plot of x-, y- and z-axis deviations for each set.

Figure 5.12 shows a comparison of standard deviation of x-, y- and z-axis for each set. The lowest standard deviation (0.085 mm) was measured on the x-axis 27 cm above the controller with illumination intensity of 72 lux, while the highest standard deviation (0.57 mm) was measured on the z-axis at the same conditions.

This investigation described a preliminary evaluation of the hand tracking performance of the LMC in the static scenario. It should be noted that the LMC software

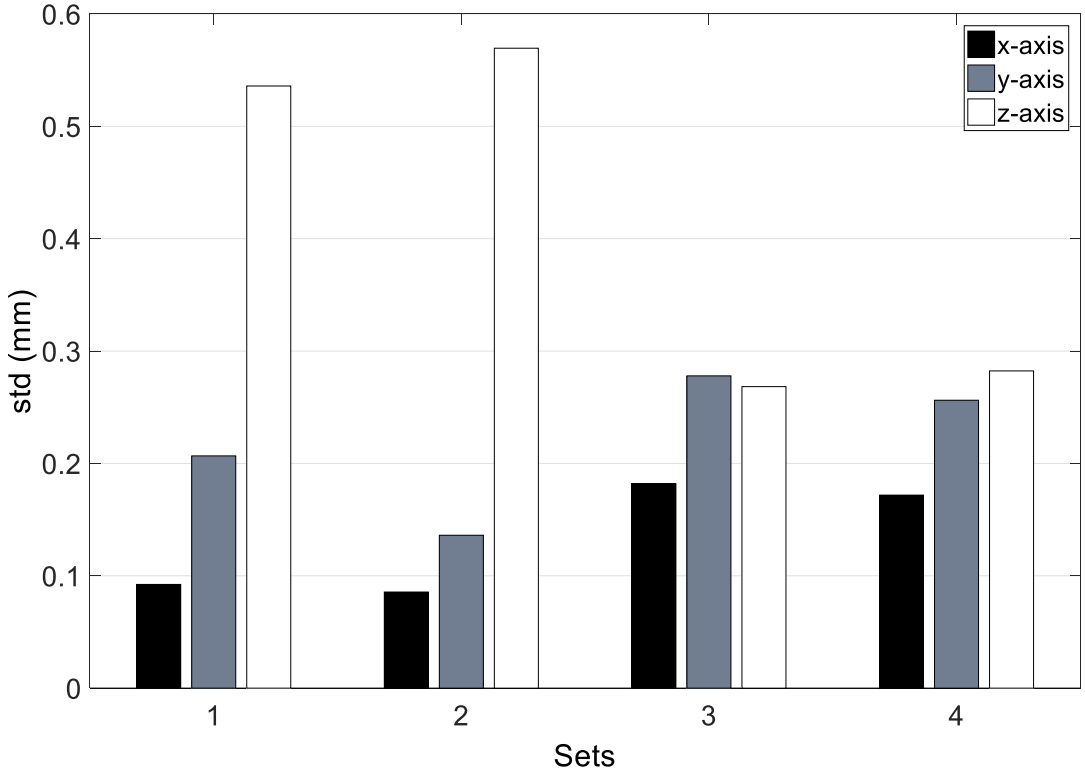

Figure 5.12: Standard deviations of x-, y- and z-axis for each set.

version used was 2.2.5 and the application programming interface (API) function used to get the hand position was Hand.palmPosition. Unlike, that information were not clear in [45] and [46] studies.

The results revealed a significant increase in the standard deviation when the hand model was moved away from the controller's surface, particularly in the z-axis, which combines with results presented by [46]. In some cases, the controller only tracked the static point for a few seconds and then stopped. The sampling frequency keeps around 58 Hz with small changes (0.5 Hz), which is below the expected value that should be 60 Hz. These two phenomena were also reported in [46].

Concerning about illumination intensity, the set of measurements revealed no significant deviation difference between the sets of 353 lux and 72 lux. Future works could focus on correlation tests to evaluate the best settings for the use of the LMC, and estimating a model of the error probability density function.

5.3 Conclusions

1. The use of LMC allied with signal preprocessing, taking into account the velocity norm and signal processing, analyzing the signal in frequency domain, allowed the

discrimination of simulated hand tremor only in some cases (see Table 5.2).

2. LMC drops considerably its accuracy while hand is moved away from the controller's surface, particularly in the z-axis.

3. Inconstant sampling frequency is a frequently issue while using the LMC.

4. Illumination intensity does not affect the LMC data acquisition.

"Without the quest, there can be no epiphany."

- Constantine Scaros

6

Experimental research for data visualization and classification

In this chapter, the results of the experiments with three DR methods are presented. PCA [65], Sammon's mapping [69] and t-SNE [70] were evaluated in terms of data visualization and classification. Features in a low-dimensional space are classified based on their ability to discriminate neurologically healthy individuals, individuals suffering from PD treated with levodopa and individuals suffering from PD treated with deep brain stimulation (DBS). The objective was to improve the PD data visualization and discrimination by using machine learning algorithms.

The research results presented in this chapter were published in a peer-reviewed scientific journal (i.e., Computational and Mathematical Methods in Medicine - [84]).

6.1 Methods

Participants and data collection

This study was conducted in the Federal University of Uberlândia (UFU), Uberlândia, Brazil, and at the University of California, Los Angeles (UCLA), USA. Both institutions

provided ethical approval for the experimental procedures (CAAE 07075413.6.0000.5152; UCLA IRB 14-001491). A complete description of the procedure employed for data collection is available in [19].

The data were collected by means of the TREMSEN (Precise Tremor Sensing Technology) system (National Institute of Intellectual Property - Brazil - BR 10 2014 023282 6) [19]. The system uses a surface EMG sensor, in a differential configuration, and triaxial inertial measurement unit (IMU) based on MEMS technology consisting of a gyroscope, an accelerometer and a magnetometer (L3G4200D, LSM303DLM).

The dataset consists of motor task measurements collected from 38 subjects. The subjects were divided into the following groups: neurologically healthy individuals ($S_H = 10$), individuals suffering from PD treated with levodopa ($S_{PD} = 16$), and individuals suffering from PD treated with DBS ($S_{DBS} = 12$). All the subjects with PD that participated in this study were rated as 2 (i.e., bilateral or midline involvement without impairment of balance) or 3 (i.e., bilateral disease: mild-tomoderate disability with impaired postural reflexes; physically independent) by using Hoehn and Yahr scale [85].

The dataset used in this study resulted from four motor tasks depicted in Figure 6.1, performed by the volunteers: finger taps (Task 1 - T1), finger to nose (Task 2 - T2), supination and pronation (Task 3 - T3) and rest (Task 4 - T4). All of these tasks are well established, described in the UPDRS [29] and used in clinical evaluation.

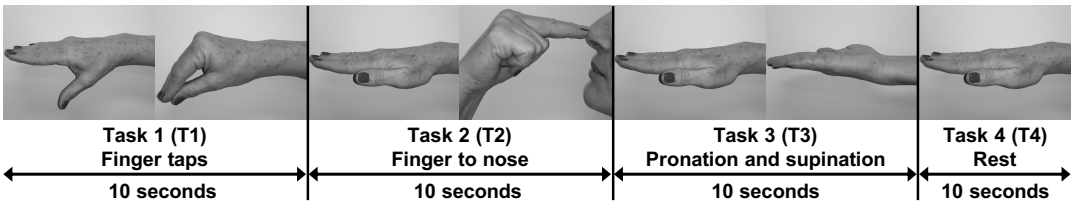

Figure 6.1: Basic sequence of executed tasks.

Each subject executed the sequence of four tasks depicted in Figure 6.1 five times. At least 30 s was allowed for rest after the end of the execution of each sequence (from tasks 1 to 4).

During the execution of the tasks, two sets of three-axial inertial sensors (i.e., accelerometer, gyroscope, and magnetometer), weighing 1 g each, were positioned on the dorsal surface of hand and forearm. Two pairs of disposable EMG sensors were placed on the muscles flexor and extensor located in the forearm. Both inertial and the envelope of EMG signals were digitized at 50 Hz.

Figure 6.2 illustrates typical waveforms of resultant components (i.e., a combination of x, y, and z coordinates) for the inertial sensors and the signal envelope for the elec-

tromyographic activity. The periods of the sequence of executed tasks (T1, T2, T3 and T4) are delimited by rectangular windows, indicating the beginning and end of each task.

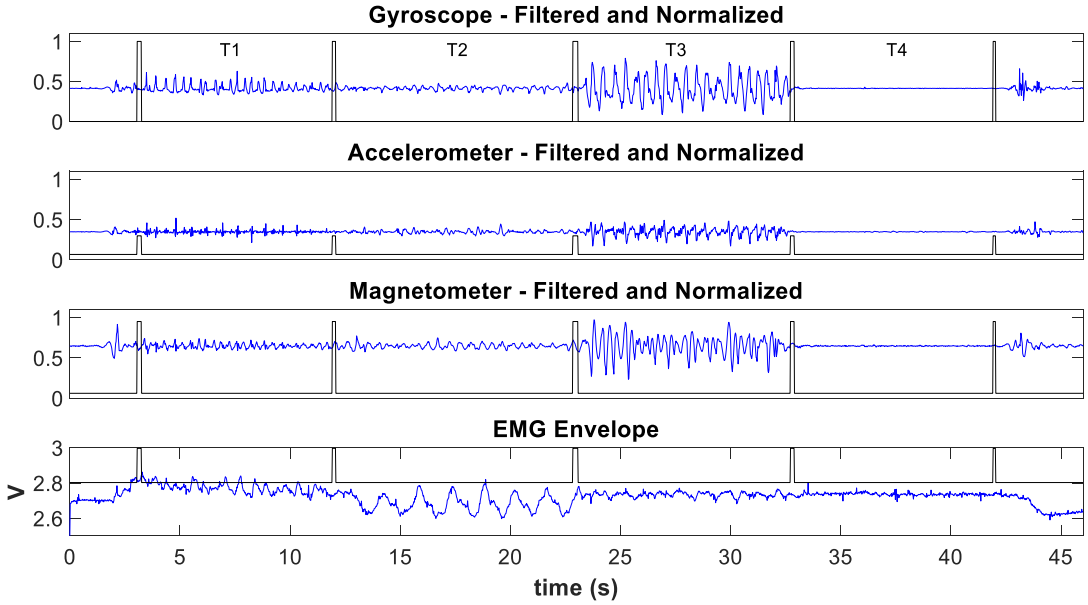

Figure 6.2: Typical example of preprocessed signals. Results of the application of the windowing and filtering steps described in [19]. The distinct tasks (T1, T2, T3, and T4) are separated by pulses.

Since each subject repeated each task five times, it was computed the coefficient of variation (CV) [86] to estimate the ratio of the standard deviation to the mean among the repetitions. For the reproducibility perspective, CV value can be used as one parameter to guide other studies in the reproduction of the experiment results.

On average, Table 6.1 shows the CV for the subjects per group. Empirically, S_H presented lower mean CV value among the three groups indicating that the subjects from this group may not vary in terms of the motor pattern as much as subjects from S_{PD} and S_{DBS} groups. On the hand, subjects from S_{PD} and S_{DBS} groups may vary more, which is expected once they suffer from PD presenting different motor patterns according to their physiological conditions (e.g., under medication and anxiety).

Table 6.1: Overall mean coefficient of variation (1 = 100%) among each repetition of the subject.

Coefficient of variation per group		
S_H	S_{PD}	S_{DBS}
0.21 ± 0.14	0.24 ± 0.15	0.30 ± 0.21

Steps for data processing

Focusing on data visualization and the discrimination between healthy subjects from those suffering from PD, the present study assesses features estimated from data projection techniques (PCA, Sammon's mapping and t-SNE) classified by a support vector machine (SVM) classifier. The main steps of this study are shown in Figure 6.3.

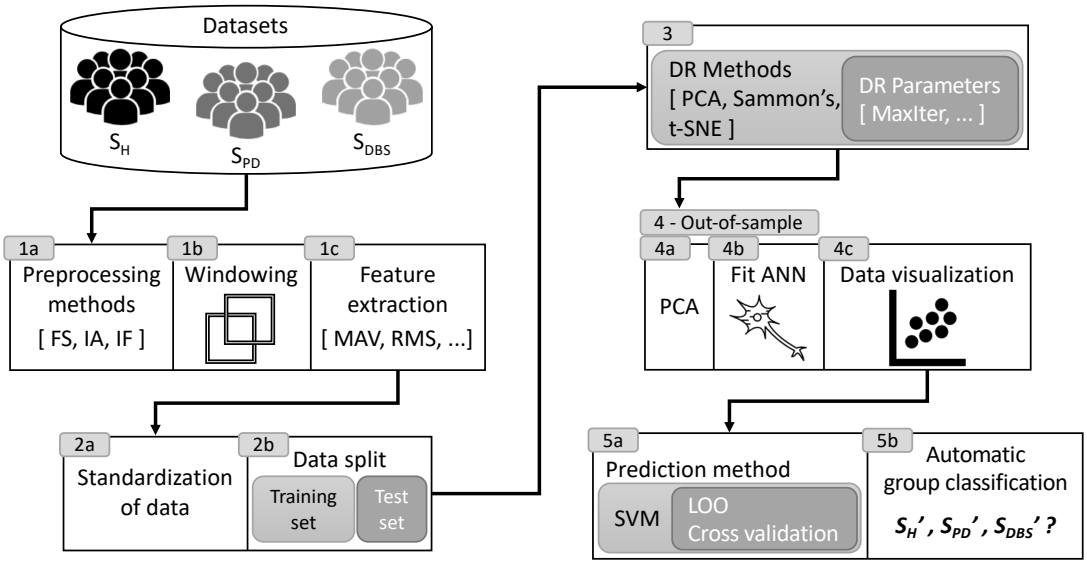

Figure 6.3: Diagram depicting the main steps.

The extracted features were standardized (step 2a in Figure 6.3) and then split into training and test sets (step 2b in Figure 6.3). The high-dimensional feature vectors of the training set were submitted to dimension reduction (step 3 in Figure 6.3). The corresponding low-dimensional map point for the test set was produced by means of an out-of-sample extension technique (step 4 in Figure 6.3). This step was accomplished by using an artificial neural network (ANN).

Feature reduction was followed by supervised learning and classification, which was achieved through SVM [87] (step 5 in Figure 6.3). These steps aim to evaluate the DR techniques in order to explore the PD motor task data. Each used method is described in detail in the following subsections.

Feature extraction

Feature extraction was performed over the filtered signals (FS), the instantaneous amplitude (IA), and the instantaneous frequency (IF), estimated from the Hilbert transform [80], as pointed out in the step 1c of Figure 6.3. The following features, which are fully described in Table 1 of [88, 89], were estimated: mean absolute value (MAV), root mean

square (RMS), global maximum (PEAK), mean of the absolute values of the second differences of the normalized signal (MAVSDN), mean of the absolute values of the second differences (MAVSD), mean of the absolute values of the first differences of the normalized signal (MAVFDN), mean of the absolute values of the first differences of the signal (MAVFD), interquartile range of the signal (INTERQ_RANGE), difference between the maximum and minimum values of a signal (RANGE), standard deviation (STD), variance (VAR), and approximate entropy.

For each method (i.e., FS, IA, and IF), a feature matrix was created containing the features extracted from all sensors. In addition, it was analyzed the combination of features estimated from each method: FS-IA, FS-IF, IA-IF, and FS-IA-IF. The aim was to identify which combination could provide the best discrimination results. The preprocessing methods (step 1a in Figure 6.3) are fully described in [19].

Data standardization and splitting

Since we have data from different sensors (i.e., accelerometer, gyroscope, magnetometer, and electromyography) which are on different scales, it is common to standardize the data. Thus, the features were standardized by using the zscore method (step 2a in Figure 6.3),

$$z = \frac{x - \mu}{\sigma}, \tag{6.1}$$

where x is the feature to be standardized, μ is the mean of the feature including all samples, and σ is the standard deviation of that feature. The standardized feature vectors were then separated randomly into training and test sets (step 2b in Figure 6.3) comprising 90% and 10%, repectively, of the data from each group of subjects (S_H, S_{PD}, and S_{DBS}) before proceeding. A strict separation between training and test sets is crucial for a more real and reliable evaluation of the automated classification task. This is an improvement while compared to the study described in [19], where the dimension reduction step was applied to the entire dataset prior to machine learning.

Unsupervised dimension reduction analysis

In this work, three unsupervised DR methods were evaluated (step 3 in Figure 6.3). The first one was the linear feature reduction PCA [65, 66]. The second was Sammon's mapping, one of the first nonlinear mapping algorithms for analysis of multivariate data [69]. The third, also a nonlinear mapping technique, was t-SNE of van der Maaten and Hinton [70]. These methods were explained in Chapter 4.

Experiment parameter setting

Sammon's mapping and *t*-SNE have several free parameters, such as the number of iterations for which the cost function optimization is processed and the learning rate used in the gradient descent method. In addition, *t*-SNE has perplexity parameter, which can be defined as a smooth measure of the effective number of neighbors.

In our experiments, we did an *exhaustive* search in order to evaluate the influence of each DR parameter in the quality of the generated maps. All the parameters settings are shown in Figure 6.4.

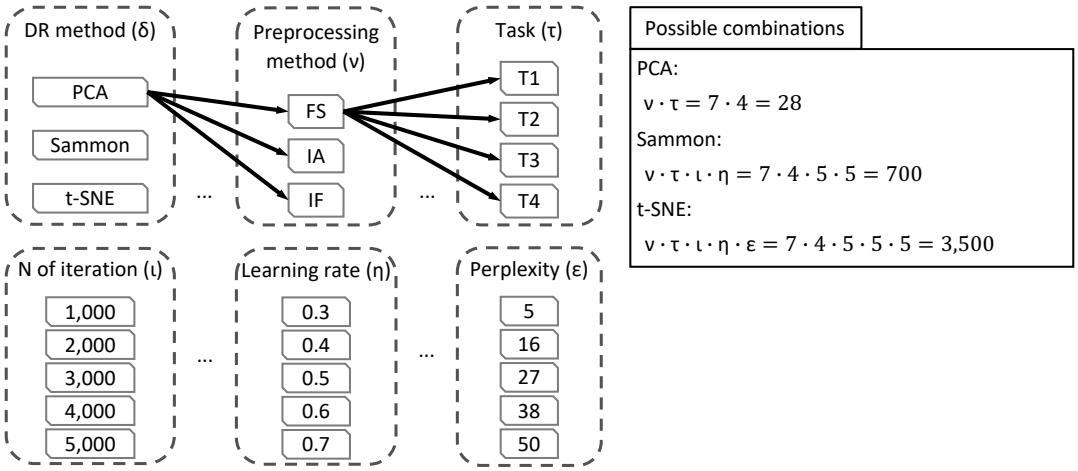

Figure 6.4: Parameter settings of the experiments. Note that for the preprocessing methods we explore all possible combinations between them (i.e., FS, IF, IA, FS-IF, FS-IA, IF-IA, and FS-IF-IA).

Each DR method was evaluated across some experiments without repetition (same combination more than once), which are composed by different parameter settings (as shown in Figure 6.4); for example, PCA experiments are arranged by the combination of preprocessing methods (ν) and tasks (τ), resulting in 28 experiments. Following, with a total of 700 experiments is Sammon's mapping by the combination of ν, τ, number of iterations (l), and learning rate (η). Lastly, *t*-SNE experiments combine all parameters depicted in Figure 6.4, which sums 3,500 experiments.

For each setup shown in Figure 6.4, the procedure was (1) execute DR method; (2) execute the out-of-sample process; (3) train and test the SVM classifier; and (4) compute performance indices in order to evaluate the parameters setup.

Out-of-sample extension

A plenty of nonlinear DR methods only map a given finite set of data points to low-dimension, not providing a built-in way to map new data points to the corresponding

low-dimensional representation. Sammon's mapping and t-SNE fall into this category of DR methods. The training set of high-dimensional data x_i and their corresponding mapped low-dimensional representation y_i was used to train a feedforward neural network with weights w, which act as a mapping function $f : x_i \longrightarrow y_i$ in which for each x_i, we have a y_i to determine the low-dimensional representation of the test set (step 4b in Figure 6.3).

Before proceeding to use an ANN, the high-dimensional training set passes through PCA by preserving 90% of the total variance of the data (step 4a in Figure 6.3). This step avoids the curse of dimensionality [90] and speeds up ANN training. Bayesian regularization backpropagation [91] was the training method used to update w and bias values.

The analysis of the lower dimensional data was performed by means of the evaluation of classification results.

Classification analysis

In order to evaluate the DR techniques, a supervised machine learning classifier, SVM, was employed for data classification (step 5 in Figure 6.3). Once trained, the model was cross-validated using a leave-one-out (LOO) method and the cross validation loss of the model was calculated. It should be noted that inside the training set, we also have the validation set used during cross-validation step. Through empirical test, the best parameters for our SVM classifier were Gaussian kernel function with 0.35 for kernel scale.

Classification accuracy was defined as

$$accuracy = \frac{TP + TN}{TP + TN + FP + FN}, \tag{6.2}$$

where TP = number of true positives, TN = number of true negatives, FP = number of false positives, and FN = number of false negatives.

Success rate was defined as

$$successrate = \frac{\Sigma R_{TP}}{\nu\tau}, \tag{6.3}$$

where R_{TP} is the true positive rate, ν indicates the number of preprocessing methods, and τ represents the number of tasks.

Cross validation is a statistical method for assessing how the result models will generalize to an unknown dataset [92]. In this research was used LOO cross validation method, where the number of folds equals the number of samples in the dataset. Thus, the SVM algorithm was applied once for each sample, using all other samples as a single-item validation set. As we have three classes (i.e., S_H, S_{PD}, and S_{DBS}), it was employed a multiclass classification [93] in a one-versus-all strategy, which employs binary classifiers to assume that one class is positive and the rest are negative.

6.2 Results

The experimental results of the assessed classification methods are shown in this section.

One hundred and seventy-one training samples were collected from 38 subjects within the training set, each composed of 408 to 1,224 dimensional features, which were reduced to two-dimensional features and evaluated with LOO CV. The rest of the samples, which is 10% as described in subsection 6.1, compose the test set. Each data from the test set was submitted to the out-of-sample extension in order to be mapped in a 2-dimensional space. In the end, these 2D points were labeled by the SVM model.

Visual representation of mappings

In Figures 6.5-6.8, we show some of the results of our experiments with PCA, Sammon's mapping, and t-SNE on the datasets built with the tasks depicted in Figure 6.1. The visualizations are scatter plots representing dimensionless scores of the projection of high-dimensional feature vectors. Additionally, it was drawn the decision boundary generated by a multilayer feedforward network in such a way to enhance the visual analysis.

Each setup, as depicted in Figure 6.4, creates one scatter plot. The scatter plots shown in Figures 6.5-6.8 were selected using a quality ratio defined as

$$QR = \frac{(OSR_{LOOCV} + OSR_{TS})}{2}, \tag{6.4}$$

where OSR is the overall sucess ratio defined by

$$OSR = \frac{\Sigma TP}{TNS}, \tag{6.5}$$

where TP is the number of true positive of all classes and TNS is the total number of

samples. Since OSR is given in percentage and could range from 0 to 100%, QR also follows this interval.

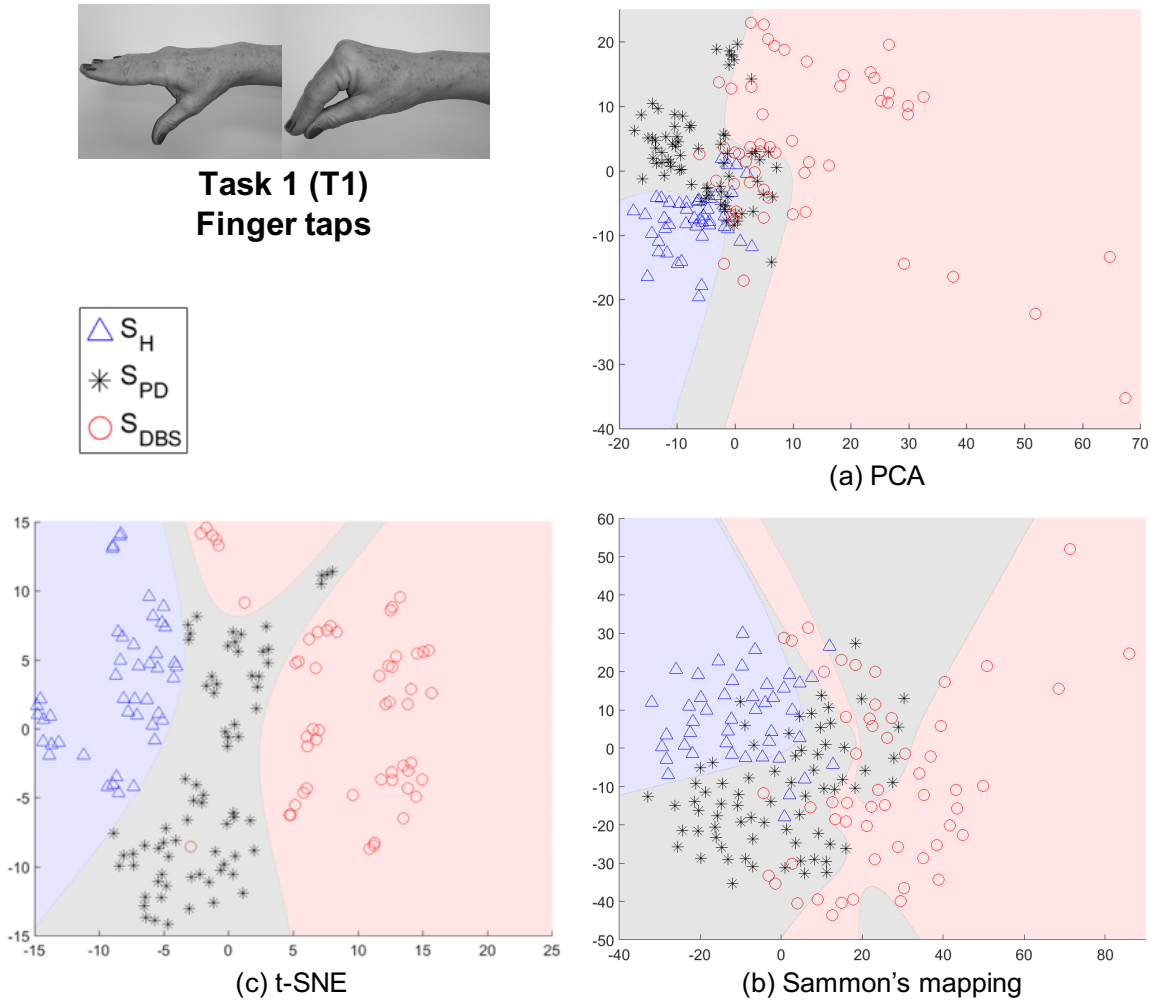

Figure 6.5: Visualization of projected data onto a lower dimensional space (step 3 in Figure 6.3). The visualizations are scatter plots representing dimensionless scores of the projection of high-dimensional feature vectors onto the first (x-axis) against the second (y-axis) estimated components. The data are from Task 1, which is the movement of finger taps. Triangles represent S_H, asterisks S_{PD}, and circles S_{DBS}. (a) The projections of PCA technique, (b) projections of Sammon's mapping, and (c) t-SNE map.

This ratio aims to guide in the selection of scatter plots which reach best results in the classification process, considering each DR method and each task. In this way, Figures 6.5-6.8 represent the scenarios which achieved higher quality ratio. Table 6.2 summarizes the parameters and performance values for each selected scenario.

Analyzing Table 6.2, t-SNE achieved better performance in all scenarios, reaching mean QR of 99.42%. Secondly it was Sammon's mapping with mean QR of 90.72% and finally PCA with mean QR of 81.36%. Finger to nose (T2) was the task with highest QR value considering all DR methods, and Rest (T4) was the task with the lowest performance.

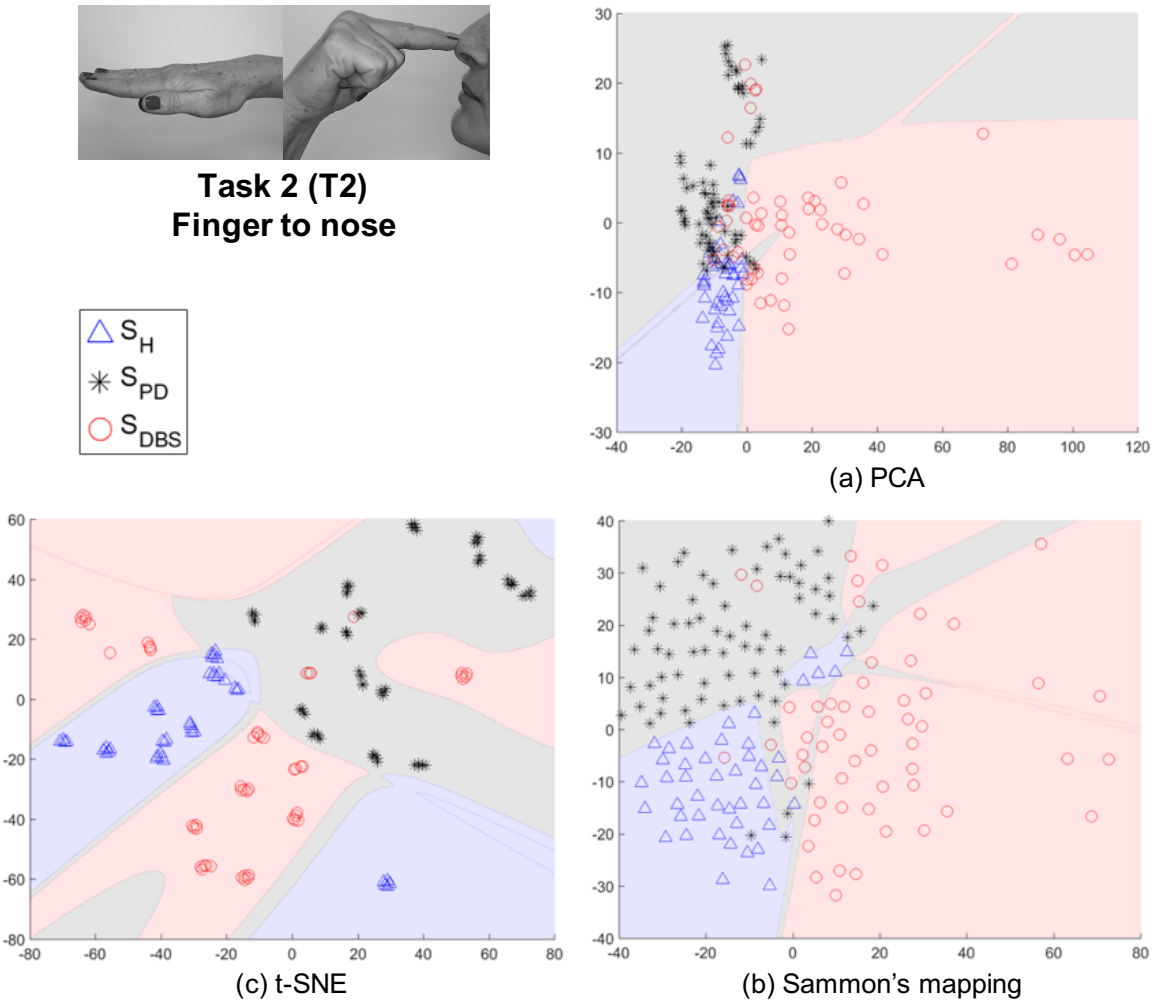

Figure 6.6: Visualization of projected data onto a lower dimensional space (step 3 in Figure 6.3). The visualizations are scatter plots representing dimensionless scores of the projection of high-dimensional feature vectors onto the first (x-axis) against the second (y-axis) estimated components. The data are from Task 2, which is the movement of finger to nose. Triangles represent S_H, asterisks S_{PD}, and circles S_{DBS}. (a) The projections of PCA technique, (b) projections of Sammon's mapping, and (c) t-SNE map.

Classification performance of projected data

Figures 6.9 and 6.10 present the boxplots of success rate (normalized between 0 and 1, in which 1 means 100%) for the data from the training set and test set, respectively. In Figure 6.9, for all three classes of data, the true positive success rate distribution remains similar, except for PCA for the S_{PD} class. In Figure 6.10, the true positive success rate of Sammon's mapping and t-SNE were similar and higher than PCA for S_H class. For S_{PD} and S_{DBS} classes, t-SNE yielded superior performance.

Analyzing the boxplots of Figure 6.9, it is observed that there is a clear difference among all DR methods, whereas in Figure 6.10 for S_{DBS} group, there also was a difference among DR methods, but for S_H and S_{PD} groups, the difference was not clear.

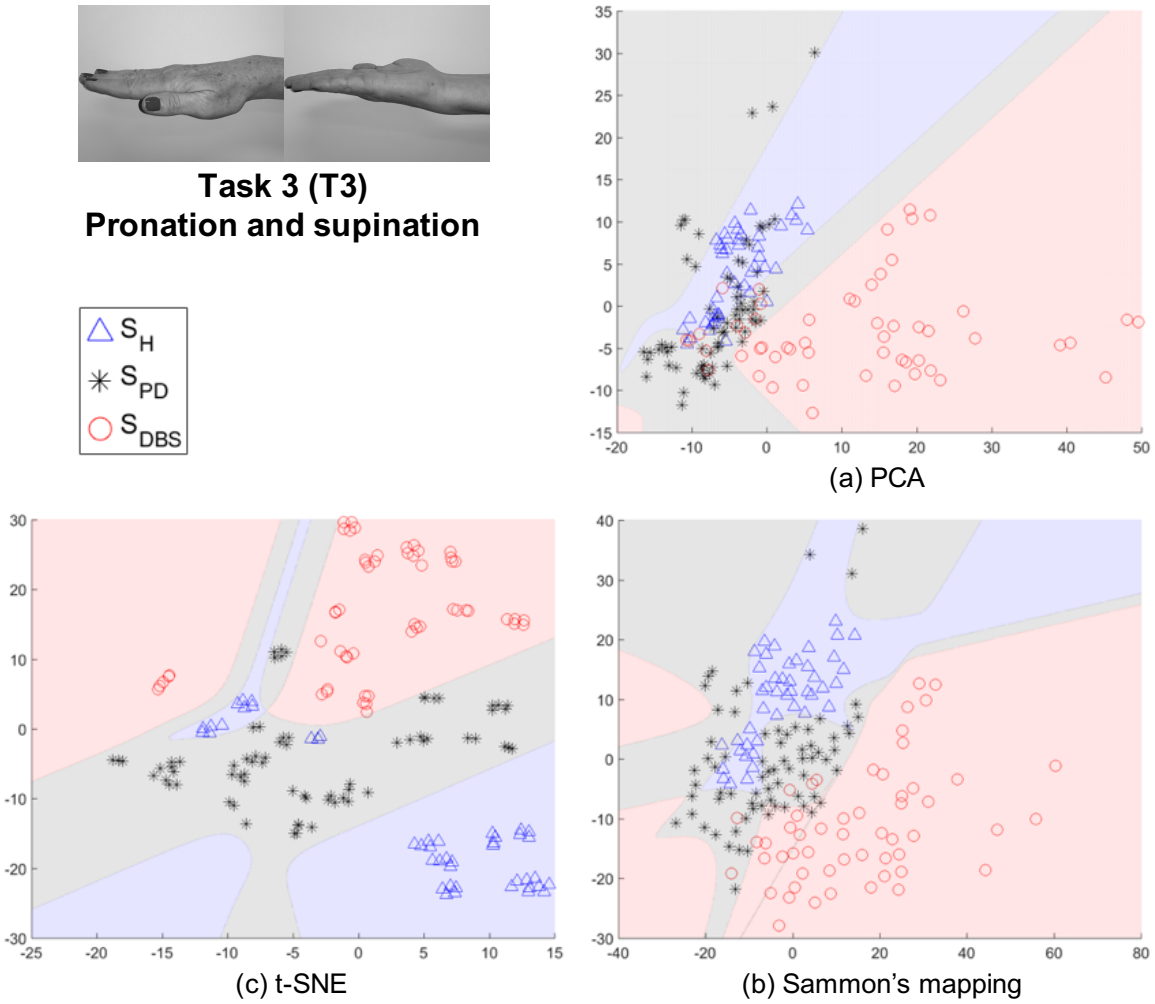

Figure 6.7: Visualization of projected data onto a lower dimensional space (step 3 in Figure 6.3). The visualizations are scatter plots representing dimensionless scores of the projection of high-dimensional feature vectors onto the first (x-axis) against the second (y-axis) estimated components. The data are from Task 3, which is the movement of pronation and supination. Triangles represent S_H, asterisks S_{PD}, and circles S_{DBS}. (a) The projections of PCA technique, (b) projections of Sammon's mapping, and (c) t-SNE map.

In order to confirm the analysis of boxplots, a statistical test was conducted. Only Sammon's mapping and t-SNE were considered for statistical analysis, since the PCA method has one value in the context of boxplots. The normality presupposition was not satisfied for any of the distributions. The normality presupposition was verified by means of the one-sample Kolmogorov-Smirnov test. Table 6.3 presents the p-values estimated by means of the two-sample Kolmogorov-Smirnov test between success ratios achieved by Sammon's and t-SNE methods. The statistical difference of 95% was confirmed for all cases, except for S_H group from the test set.

Overall, these findings show that when t-SNE is combined with either the SVM algorithm, a notable improvement is seen over other investigated DR methods. When

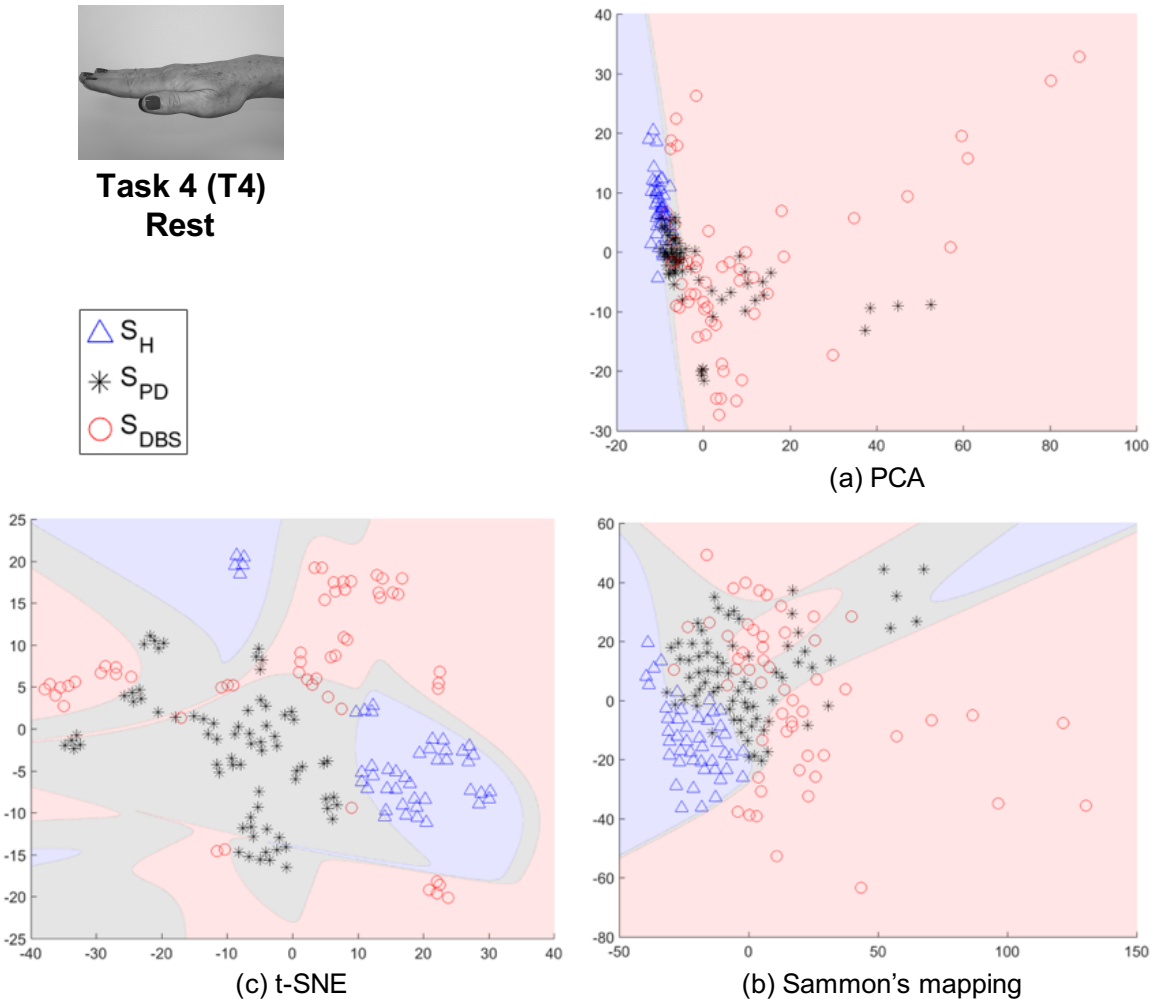

Figure 6.8: Visualization of projected data onto a lower dimensional space (step 3 in Figure 6.3). The visualizations are scatter plots representing dimensionless scores of the projection of high-dimensional feature vectors onto the first (x-axis) against the second (y-axis) estimated components. The data are from Task 4, which is the rest pose against gravity. Triangles represent S_H, asterisks S_{PD}, and circles S_{DBS}. (a) The projections of PCA technique, (b) projections of Sammon's mapping, and (c) t-SNE map.

examining the mean of each distribution shown in Figure 6.9, the improved classification was seen when compared t-SNE to Sammon's, increased 18.1%, 18.4%, and 18.8% for classes S_H, S_{PD}, and S_{DBS}, respectively. When examining the mean of each distribution shown in Figure 6.10, the improved classification was seen when compared t-SNE to Sammon's, increased 2% and 6% for classes S_{PD} and S_{DBS}, respectively, but decreased by 0.6% for class S_H.

Next, Table 6.4 shows the grand average confusion matrix of SVM classifier for all studied DR methods, including data from the training set (LOO CV) and test set. In this table, the diagonal cells in bold show the normalized percentage of correct classifications by the SVM. For example, 70 samples of S_{PD} group were correctly classified when t-SNE DR method was employed. This corresponds to 98% of all training set samples of S_{PD}

Table 6.2: Parameters and performance values of best scenarios according to its quality ratio (QR).

Task	**DR methods**	**Parameter settings**			**Performance value**
		l	η	ε	**QR (%)**
Finger taps (T1)	PCA	-	-	-	79.82 ± 6.2
	Sammon's	575	0.6	-	88.60 ± 8.6
	t-SNE	5000	0.6	27	99.42 ± 0.8
Finger to nose (T2)	PCA	-	-	-	86.26 ± 4.5
	Sammon's	423	0.4	-	94.44 ± 7.8
	t-SNE	5000	0.4	5	99.71 ± 0.4
Pronation and supination (T3)	PCA	-	-	-	83.92 ± 15.2
	Sammon's	742	0.6	-	93.57 ± 9.0
	t-SNE	1000	0.6	16	100 ± 0.0
Rest (T4)	PCA	-	-	-	75.44 ± 2.4
	Sammon's	1080	0.4	-	86.26 ± 11.9
	t-SNE	3000	0.5	16	98.54 ± 2.0

Table 6.3: P-value from two-sample Kolmogorov-Smirnov test between success ratios achieved by Sammon's and t-SNE methods.

Group	**P-value**	
	Leave-one-out cross validation	**Test set**
S_H	0.00	0.32
S_{PD}	0.00	0.02
S_{DBS}	0.00	0.00

group. Similarly, 6 samples of the same group were correctly classified when, again, t-SNE DR method was employed. This corresponds to 78% of the test set samples of S_{PD} group.

Overall, using the PCA DR method 73.5% of the training set and 67.8% of the test set was correctly classified. For Sammon's mapping, considering the training and test sets, respectively, 78.6% and 74.1% of the predictions were correct. Lastly, t-SNE yielded the highest percentage of correct predictions for both, training (96.9%) and test sets (76.6%).

Figures 6.11 - 6.13 show the receiver operating characteristic (ROC) curves of the LOO CV of the training set and test set validations for each class along with the mean area under the curve (AUC) while each DR method was employed as a step before classification

Figure 6.9: Boxplots of grand average of true positive rate achieved by SVM using LOO CV for PCA, Sammon's, and t-SNE DR techniques for participants of S_H (left), and S_{PD} (center), and S_{DBS} (right) groups. As this study PCA has no parameters to be varied (Figure 6.4), it is depicted by one value, which represents all possible combinations for the PCA DR method.

Table 6.4: Grand average confusion matrix of SVM for each DR method. The bold diagonal cells show the normalized (0-1) percentage of correct classifications by the SVM.

DR method			**Target class**					
			Leave-one-out cross validation			**Test set**		
			S_H	S_{PD}	S_{DBS}	S_H	S_{PD}	S_{DBS}
PCA	Predicted class	S_H	**0.70**	0.11	0.07	**0.60**	0.08	0.10
		S_{PD}	0.24	**0.78**	0.20	0.31	**0.79**	0.26
		S_{DBS}	0.05	0.11	**0.72**	0.09	0.13	**0.64**
Sammon's	Predicted class	S_H	**0.79**	0.08	0.05	**0.78**	0.11	0.08
		S_{PD}	0.15	**0.79**	0.18	0.17	**0.76**	0.24
		S_{DBS}	0.05	0.13	**0.77**	0.06	0.13	**0.68**
t-SNE	Predicted class	S_H	**0.98**	0.01	0.01	**0.77**	0.08	0.07
		S_{PD}	0.02	**0.98**	0.03	0.14	**0.78**	0.19
		S_{DBS}	0.01	0.01	**0.95**	0.09	0.14	**0.74**

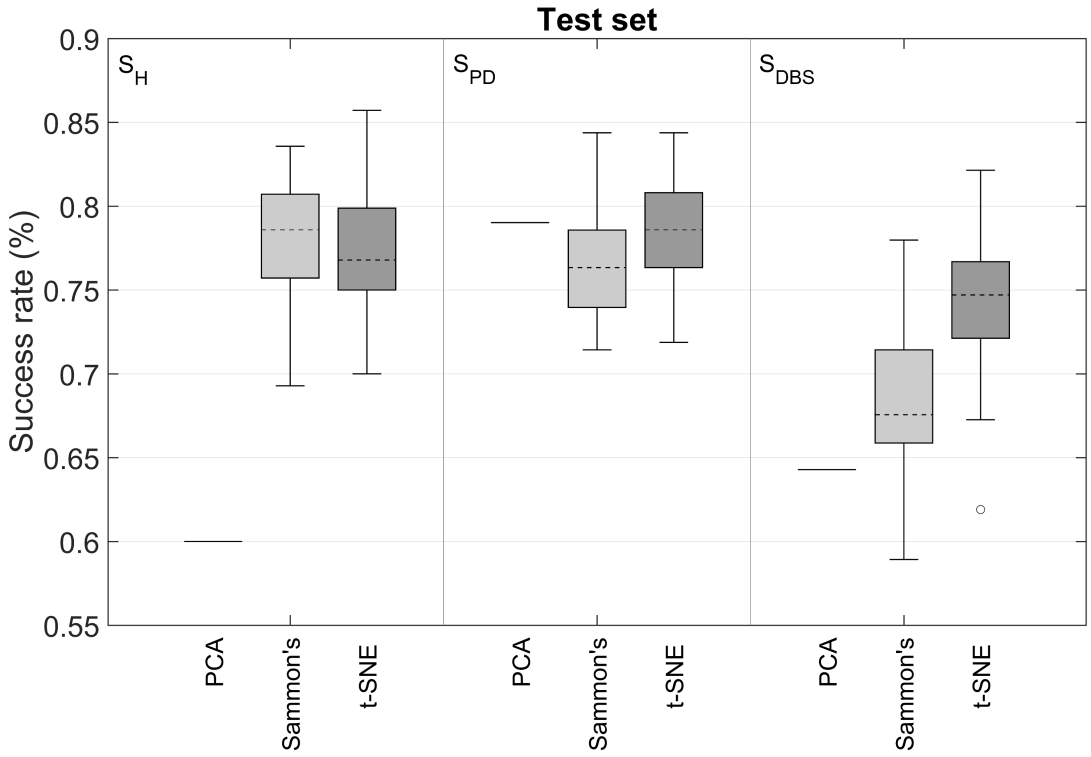

Figure 6.10: Boxplots of grand average of true positive rate achieved by SVM using the test set for PCA, Sammon's, and t-SNE DR techniques for participants of S_H (left), and S_{PD} (center), and S_{DBS} (right) groups. As this study PCA has no parameters to be varied (Figure 6.4), it is depicted by one value, which represents all possible combinations for the PCA DR method.

process. For the LOO CV, the confidence bounds of 95% were computed for ROC curves by means of Bootstrap, with 1,000 replicas.

For the S_H class, t-SNE achieved remarkable performance considering LOO CV, with the highest mean AUC (0.99) and with the lowest deviation from the mean. Sammon's mapping and PCA reached mean AUC of 0.91 and 0.85, repectively, and both showed a similar deviation from the mean. Considering the test set, t-SNE and Sammon's mapping show similar responses when observing the shape of the curve, mean AUC, and the balance point (i.e., the point where the ROC curve reaches the equality between specificity and sensitivity - diagonal dashed line in Figures 6.11 - 6.13). PCA, on the other hand, had the lowest performance.

The ROC curves of Figure 6.12 show the discrimination ability of the SVM classifier for S_{PD} class for both, training (LOO CV) and test validation sets. Examining Figure 6.12a, the results indicate that t-SNE obtained similar results when compared to the same method applied in S_H group, whereas Sammon's and PCA decreased their performance. Note that for S_{PD} class, these two methods present overlapped area in ROC curve along with confidence bounds as much as for S_H class. However, for S_{PD} class, the confidence

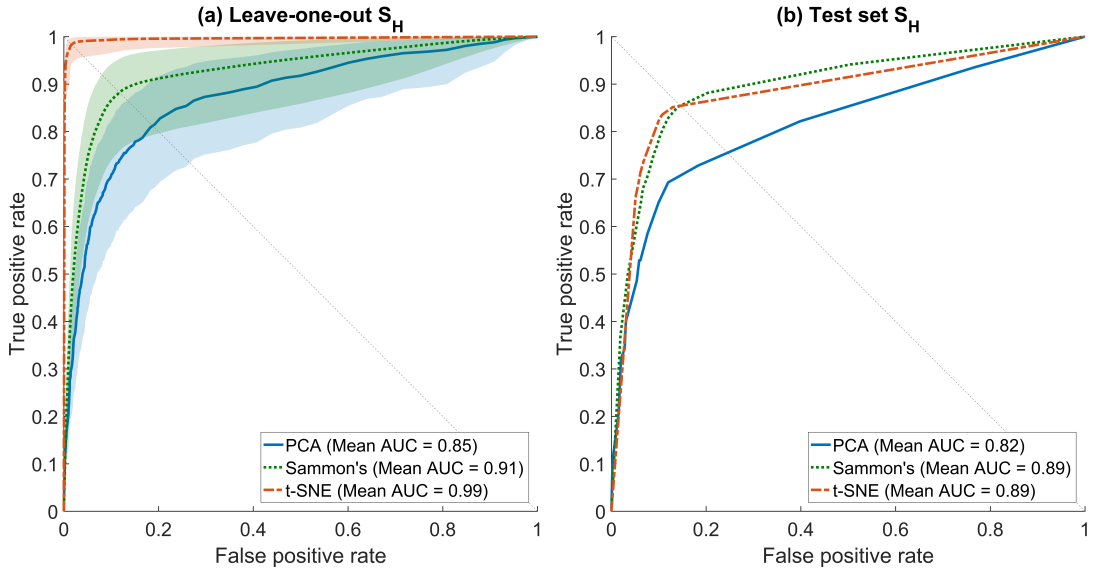

Figure 6.11: Receiver operating characteristics curves of SVM classifier for the training and test sets of S_H group. The orange, green, and blue lines show the ROC curves for t-SNE, Sammon's mapping, and PCA DR methods, respectively. AUC is the area under the curve. (a) Mean ROC curves for data from the training set and its 95% confidence bounds computed by means of Bootstrap, with 1,000 replicas. (b) Mean ROC curves for data from the test set.

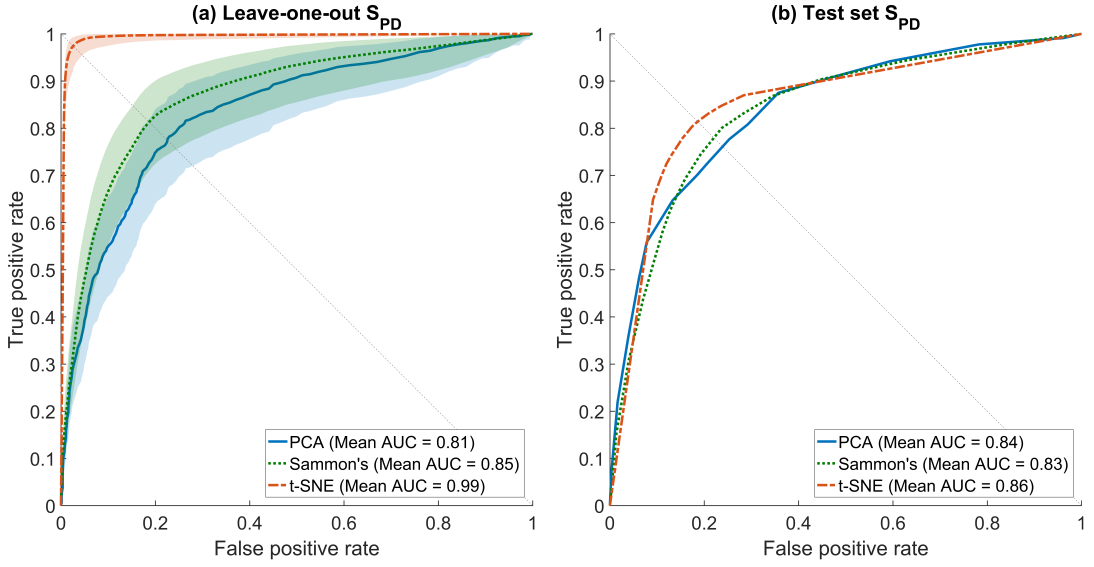

Figure 6.12: Receiver operating characteristics curves of SVM classifier for the training and test sets of S_{PD} group. The orange, green, and blue lines show the ROC curves for t-SNE, Sammon's mapping, and PCA DR methods, respectively. AUC is the area under the curve. (a) Mean ROC curves for data from the training set and its 95% confidence bounds computed by means of Bootstrap, with 1,000 replicas. (b) Mean ROC curves for data from the test set.

bounds are narrower.

Figure 6.12b shows ROC curves for the test set. The behavior of the curve for each DR

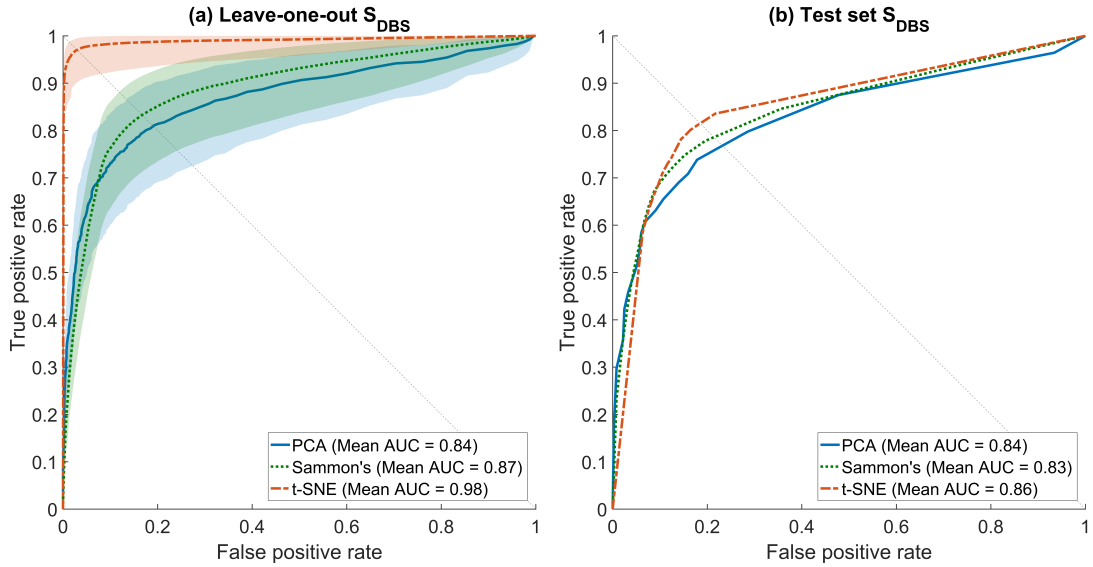

Figure 6.13: Receiver operating characteristics curves of SVM classifier for the training and test sets of S_{DBS} group. The orange, green, and blue lines show the ROC curves for t-SNE, Sammon's mapping, and PCA DR methods, respectively. AUC is the area under the curve. (a) Mean ROC curves for data from the training set and its 95% confidence bounds computed by means of Bootstrap, with 1,000 replicas. (b) Mean ROC curves for data from the test set.

method was similar, t-SNE reached the best AUC (0.86), right after are PCA (0.84) and Sammon's with AUC of 0.83. At the balance point view, t-SNE was the best method and PCA was the worst one. Considering S_H and S_{PD} classes, PCA improved for classification of S_{PD} samples from the test set. On the other hand, Sammon's and t-SNE decreased its performance for S_{PD} class.

The classification performance for S_{DBS} class is also shown in ROC curves of Figure 6.13. The results showed in Figure 6.13a present training set performance curves for S_{DBS} class, again, t-SNE achived the best performance in terms of AUC and balance point. Next, Sammon's mapping and PCA with 0.87 and 0.84 of mean AUC, respectively, showing great overlapped area between its confidence bounds. For S_{DBS} class, t-SNE showed the wider confidence bound while compared with the performance achieved for S_H and S_{PD} classes. Figure 6.13b, in turn, shows that the three DR methods yielded the same results for S_{PD} and S_{DBS} classes in terms of mean AUC.

6.3 Discussion

This kind of study is not often found in the literature. The reasons could be related to the complexity of the recruitment of volunteers since, in this study, three distinct groups (i.e., S_H, S_{PD}, and S_{DBS}) were evaluated. This type of data are expensive, and their

acquisition demands specialized professionals.

In the literature, there are a plenty of studies which propose and evaluate methods for discrimination between individuals with PD from neurologically healthy ones. However, some studies show that there are key points to be overcome for realizing the full potential of this technology in PD research and practice [7, 94], for instance (1) the machine learning methods are challenging to evaluate and apply without a basic understanding of the underlying logic on which they are based; (2) the ability to algorithmically analyze and synthetically display clinically and disease-relevant information to physicians and patients remains limited. This study brings a comparison among three DR methods with the aim to address these two points.

PD treatment is also another topic extensively discussed in the literature. The two fields inside this area related to our study are an investigation of motor behavior while using medication-based treatments and surgical ones. According to [7], it is lacking an objective way to adjust drug (e.g., levodopa) release as the patient needs. Besides that, the DBS treatment has different points for improvements, one of that concerns the implementation of closed-loop (i.e., self-adjustable parameters) DBS. The present study moves toward these directions, comparing these groups of subjects and characterizing their motor behavior.

As reported in the literature [95, 19, 96, 97, 98], our results demostrated differences between movement patterns for the three groups. On the other hand, we introduce the comparison of visualization and classification tools, which allows for an objective evaluation of subjects. Based on our review, just a few studies approached the challenge of visualizing and classifying motor activities of the three classes evaluated. Even so, the studies that explored this area did not go so far as our study.

The visual representation of mappings presented in Figures 6.5 - 6.8 show the ability of each DR technique to deal with high-dimensional data since these figures show the scenarios which achieved higher quality ratio. Considering the visual aspect (i.e., clustering and boundary of classes), *t*-SNE produces better visualizations, followed by Sammon's mapping in second place and PCA in the third one. In fact, the *t*-SNE ability to keep global and local structures implies in better visualizations as stated in [67]. Sammon's mapping, in turn, improves PCA, adding the ability to handle with nonlinear data. In every mentioned figure, the map built by Sammon's has a similar shape while compared with PCA map. This occurs due to the PCA initialization strategy for Sammon's algorithm [75].

Classification accuracy for PCA, Sammon's mapping, and *t*-SNE was, respectively, 73.5%, 78.6%, and 96.9% for the training set and 67.8%, 74.1%, and 76.6% for the test

set. According to [92], the training set is used to fit the models and the test set is used for assessment of the generalization error of the final chosen model. Furthermore, there are subtle differences between the training set and test set. The reasons of that are (1) differences in motor behavior between inter and intragroups; (2) the training and test sets are built randomly; (3) the out-of-sample step introduces error which is related to the mapping of high-dimensional information onto a 2-dimensional space; (4) the classifier generalization ability varies, and this factor impacts directly in the prediction accuracy, especially when new samples are presented.

Visual representation presented in Figures 6.5 - 6.8 could be used as a visualization tool for follow-up of treatments of PD by means of definition of the control zone, so that the closer this zone to the subject is better in terms of motor behavior. Furthermore, to achieve a smooth control of this zone, an individual analysis for each patient could help.

Our results take into account the differentiation of PD treatments and a healthy control group without considering the subtypes of the disease. The variability found in some methods may be due to this factor, since tremor, bradykinesia, and rigidity present different movement patterns. A further study with the use of our system and protocol in new group of participants, separated by PD subtypes, could address this limitation.

The tasks performed in this study are well established, described in the UPDRS [29] and used in clinical evaluation [99, 100, 101, 102, 103]. In Figure 6.5, the finger taps (Task 1) using *t*-SNE projection reached a quality ratio of 99.42% $\pm$ 0.8 as well as the clearer visual representation among all mappings shown in Figures 6.5 - 6.8. Sammon's mapping, in turn, presented a spherical projection, which is characteristic of this method and achieved 88.60% $\pm$ 8.6 of QR, around 10% less than *t-SNE*.

Finger to nose (T2) and pronation and supination (T3) were the performed tasks with highest mean QR, 93.47% and 92.50%, respectively, considering all DR methods. Both movements are more complex than the other two performed tasks, finger taps (T1), and rest (T4). The higher motor pattern complexity of T2 and T3 task reflect in a higher success rate on discrimination of the three classes (S_H, S_{PD}, and S_{DBS}). The finger to nose task shares its dominant kinematic pattern with a variety of activities of daily living (ADL) such as eating, drinking, and answering a phone. Pronation and supination task, on the other hand, is commonly used to assess bradykinesia [104].

Regarding discrimination among groups, *t*-SNE showed the highest success rate for the LOO CV followed by Sammon's mapping. Similar performance was achieved when *t*-SNE was applied as a step before proceeding with the classification using the test set. Although the success rate reached by *t*-SNE was superior, its performance was weak while compared with itself in LOO CV. This drop occurs due to the step to allow project

new data points, called out-of-sample (step 4 in Figure 6.3). The out-of-sample (OOS) process was carried out by means of a PCA along with an ANN as explained in Section 6.1. Our OOS approach reached overall mean squared error of 17.9 ± 10.5 and 3.6 ± 2.7 for Sammon's mapping and *t*-SNE, respectively, and an overall R value of 0.97 ± 0.02 and 0.95 ± 0.03 also for the same methods.

Despite our good results in OOS step, in many cases, the high variability of intragroup motor patterns, mainly in S_{PD} and S_{DBS}, turns the OOS a hard process. There are in the literature other methods to deal with OOS [105]; these methods could improve the results presented in this study.

In this study, three preprocessing methods were employed. The first (FS) was based on the filtered signal, which yields data more correlated with the original data; the second (IF) captures changes in the signal frequency over time and the third (IA) takes into account changes in the amplitude of the signal.

Concerning to the preprocessing methods, our results show that the combination of features extracted from the methods FS and IF was the one that yielded the best overall success rate (86.14% ± 4.3), in accordance with [19]. The success of this combination may be related to the cardinal symptom tremor, which induces oscillatory movements in individuals with PD. These oscillatory movements could vary around 6 Hz [103].

Proceeding to classification analysis, Table 6.4 summarizes the classification results by using the confusion matrix style. Machado et al. [19] employed a similar analysis in some points, using only Sammon's mapping. They reported an overall mean success rate as given below:

1. $S_H(S_H)$: 0.85 and 0.75 for classification and test sets, respectively;
2. $S_{PD}(S_{PD})$: 0.73 and 0.60 for classification and test sets, respectively;
3. $S_{DBS}(S_{DBS})$: 0.72 and 0.63 for classification and test sets, respectively.

In our experiments using *t*-SNE, we achieved an overall mean success rate as given below (from Table 6.4):

1. $S_H(S_H)$: 0.98 and 0.77 for classification and test sets, respectively;
2. $S_{PD}(S_{PD})$: 0.98 and 0.78 for classification and test sets, respectively;
3. $S_{DBS}(S_{DBS})$: 0.95 and 0.74 for classification and test sets, respectively.

6.4 Conclusions

This part of the study, investigated the motor behavior of three distinct groups of individuals: neurologically healthy, PD treated with levodopa, and PD treated with DBS. In order to analyze the motor behavior of each group, four motor tasks were performed by the subjects and recorded using inertial and EMG sensors. In spite of the large possibilities of sensors to be used for collecting various data that can quantify PD symptoms, the same progress cannot be seen while dealing with large and complex data such as the kind of data collected in this study.

The assessment of the classification methods showed that the visualization provided by the *t*-SNE enhanced the visual discrimination of the groups so that they could be clearly identified for all investigated tasks. For automatic discrimination among groups, SVM was used after the data reduction step. The SVM performance was higher in almost all scenarios while *t*-SNE was employed. Furthermore, the noted improvement was irrespective of the group or task or of the preprocessing method utilized, with an improvement of around 18% for the training set, considering *t*-SNE versus Sammon's mapping. For *t*-SNE versus PCA, the improvement was around 23% for the training set.

As a future studies, the following items could be highlighted: (i) analysis of redundant features to exclude features with high correlation; (ii) factorial experiment design to decrease the number of experiments and avoid the exhaustive search regarding the parameterization of DR techniques; (iii) inclusion of features related to the signal energy, e.g., Teager-Kaiser energy operator.

"If you don't have time to read, you don't have the time (or the tools) to write. Simple as that."

- Stephen King

7

Experimental research on non-contact capacitive sensor

In this chapter, the results of the experiments with PS25454 non-contact capacitive (NCC) sensor are presented. The experimental research of NCC sensor, by measuring a set of hand movements, are presented. This research aimed to evaluate NCC sensor as a component of a device to be used for quantification of hand movements. This brings innovation while applying this kind of non-contact sensor in the context of PD motor sign quantification.

In order to evaluate NCC sensor, four early experiments were conducted with different aims:

1. The first experiment [106], aimed to test and validate the developed hardware (v1), as well as the experimental protocol. In addition, a set of features were estimated from the collected signals and used to perform 2-dimensional projections, after dimension reduction. The projections aimed to show possible patterns for the different movements.

2. In the second early experiment [107], after the developement of a second version of the custom-made hardware, tests with a subject with and without PD were made. Furthermore, also in this experiment, amplitude and time-dependent features were

extracted from the collected signals and projected in 2-D to check the patterns and possible differences among the two subjects.

3. Third experiment [108] was conducted to compare the use of NCC sensor with gyroscope. Three healthy subjects performed tasks using both sensors. After that, a correlation analysis was developed.

4. Lastly, the fourth experiment [109] aimed to verify the possibility of the NCC sensor measuring postural wrist tremor and to compare data of the NCC sensor with those obtained by a gyroscope. At the end, the data was used to characterize the group of subjects, by using features related to frequency.

Besides the four early experiments, a wider one was conducted and its aim was assess hand motor tasks performed by subjects with and without PD. This last experiment [110] tackle two points: (1) the modelling of the relationship between NCC responses and displacement in a controlled scenario; (2) the experimental evaluation of the implemented system by comparison of results obtained from a gyroscope, while healthy individuals and people with PD were executing distinct hand motor tasks.

The research results presented in this chapter were published and presented at national "XXV Brazilian Congress on Biomedical Engineering" [106], "XXVI Brazilian Congress on Biomedical Engineering" [108] and international "World Congress on Medical Physics and Biomedical Engineering 2018" and "41^{st} International Engineering in Medicine and Biology Conference" scientific conferences.

Finally, this chapter focus mainly on the last and larger conducted experiment, unpublished yet.

7.1 Materials

In order to apply the NCC sensor technology in the context of PD movement analysis, a system, composed of hardware, firmware and software, was developed from scratch. Figure 7.1 shows the main window of developed software. By using this software it is possible to control the hardware device, which includes start, stop and save data collected, transmit and receive control signals to synchronize with other devices, plot and interact (e.g., pan and zoom) with recorded signals.

A crucial part of the developed system (National Institute of Intellectual Property - Brazil - BR 10 2018 069864 8) is the hardware, composed of a custom-made circuit, along with an arrangement of NCC sensors with a board with markers to assist the subjects during the execution of experimental tasks. In the actual version, four PS25454 sensors

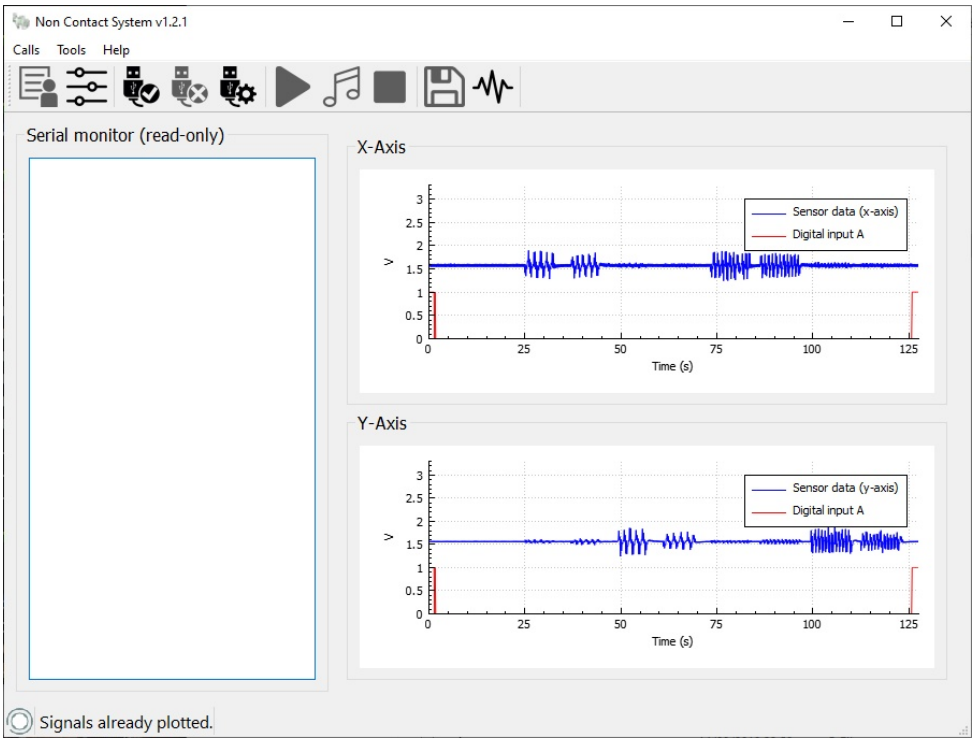

Figure 7.1: Graphical user interface of developed computer software for data collection with NCC sensors.

were used in pairs. Each pair defines a directional axis (x or y). A custom-made structure was designed using four sensors placed at the four centered edges of a squared area of size 0.21 m x 0.21 m. Figure 7.2 shows this arrangement.

The sensors were configured in differential mode to measure the local electric field. To avoid common mode noise, INA333 (Texas Instruments, Dallas, TX, USA) instrumentation amplifier was used, which has high common mode rejection, low power consumption and low price.

The sensors require a power supply voltage of $\pm 5.5V$, which is also suitable for the instrumentation amplifier. A battery was used as power supply in order to reduce the environmental electrical noise.

From both EPIC sensors, the signals were fed to the instrumentation amplifier. After that, the amplifier output is buffered by a voltage divider to adjust the signal level for analog-to-digital conversion (ADC). Figure 7.3 shows the simplified circuit diagram. The system was grounded to minimize environmental noise interference.

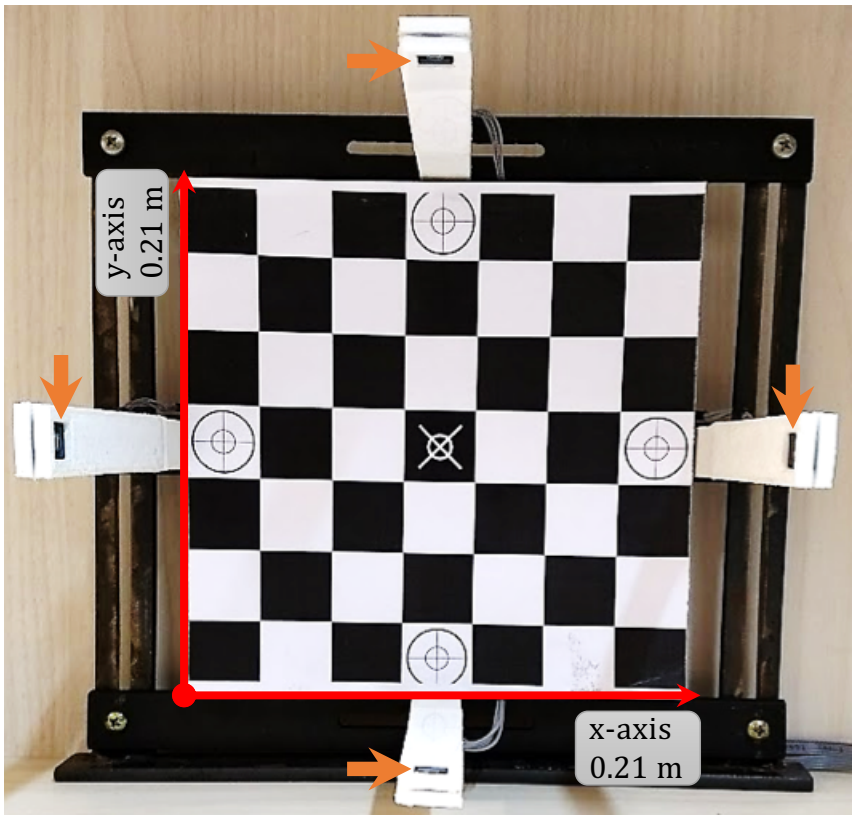

Figure 7.2: 2-D array of PS25454 sensors. Each pair of sensors provides information about movement in the x and y axes. In the background, a board with markers was specifically designed to assist the subject during the execution of experimental tasks. The orange arrows point to the four EPIC sensors.

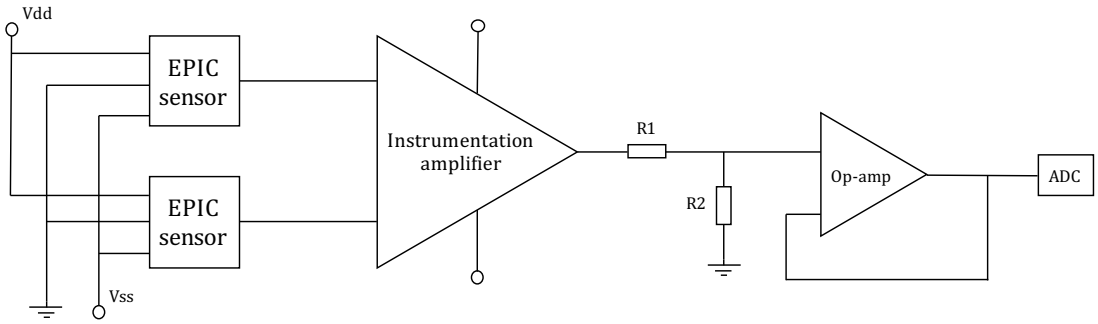

Figure 7.3: Simplified circuit diagram to use PS25454 EPIC sensors in a differential mode for movement quantification.

7.2 Methods

System validation

A micro-machine system (Minitech CNC Mini-Mill/GX, USA) with a resolution of $1\mu m$ was used as the reference for the validation of the system. Attached to the reference system, a plaster hand model was fixed in order to simulate a usage scenario. Figure 7.4

depicts the experimental setup for system calibration.

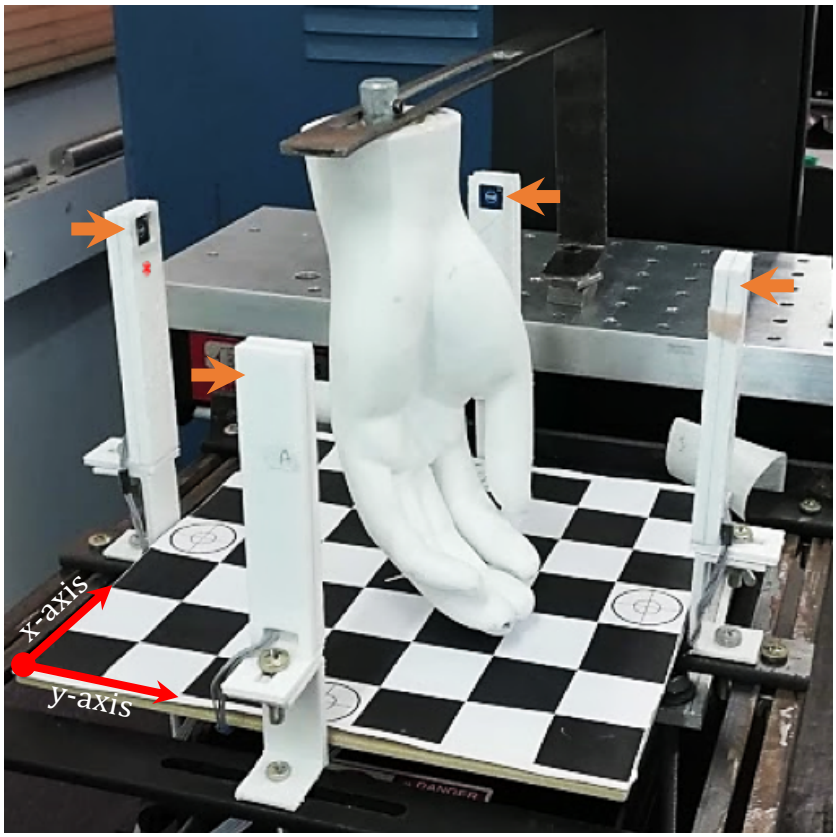

Figure 7.4: Experimental setup for NCC system calibration. The axes orientation is denoted by the red arrows and the orange arrows point to the four EPIC sensors. Each sensor is encapsulated in a custom-made structure.

With the aim of establishing the relationship between displacement and voltage amplitude range, two scenarios were considered. For the first one, the hand was fixed 8 cm apart from the sensor highlighted by a red asterisk (see Figure 7.4) and for the second one, the hand was fixed 4 cm apart from the same sensor. In both scenarios, the movements were along y-axis and they were executed 3 times each in the following sequence: (1) move 10 mm;(2) move 5 mm; (3) move 2.5 mm; (4) move 1.5 mm and (5) move 0.5 mm; always going back and forth.

The focus of this stage of the study was to determine the relationship between hand displacement and EPIC sensor response. To do this, a linear mixed model [111] was used to express the relationship between the measured variables,

$$y \sim x + (1|setup) + \varepsilon \tag{7.1}$$

where x is our fixed effect term related to the hand displacement, $1|setup$ is the random effect to model the two possible scenarios (i.e., the hand fixed at 4 cm and 8 cm apart from the reference sensor), and ε is the general error term.

Participants

A total of 57 subjects (Table 7.1) were recruited, being 30 with PD (S_{PD}) and 27 controls without PD (S_C). This research has been approved by the National Committee for Ethics in Research (CAAE: 65165416.4.0000.5152). The subjects from each group were paired in terms of age and sex. Subjects with PD were evaluated using MDS-UPDRS by three skilled raters.

Table 7.1: Participants information.

	PD (n = 30)	**Controls (n = 27)**
Age*	62.1 ± 9.7	60.7 ± 8.5
Sex	20 M, 10 F	17 M, 10 F
UPDRS Part III score**	33.4 ± 13.3	-

* Equal medians with $p = 0.56$.

** Overall mean of MDS-UPDRS Part III score.

MDS-UPDRS part III concerns to motor examination and its total score ranges from 0 to 132 [29]. The overall mean part III score presented in Table 7.1 represents the PD severity of our sample from S_{PD} group. In percentage, this value represents 25% ± 9%. In clinical terms, this score implies in a slight to mild PD motor examination severity. "Slight" refers to symptoms with sufficiently low frequency or intensity to cause no impact on function and "mild" refers to symptoms of frequency or intensity sufficient to cause a modest impact on function [29].

Experimental setup

The experiments (see experiment video available in Appendix B) were carried out in an open unshielded environment (Figure 7.5). A three-axial gyroscope (L3GD20H, STMicroelectronics, Switzerland) was positioned on the dorsal region of the hand together with a laser pointer for aiding the subject to execute a set of motor tasks (Figure 7.6). The TREMSEN (Precise Tremor Sensing Technology) system (National Institute of Intellectual Property - Brazil - BR 10 2014 023282 6) was used for data acquisition and real-time visualization of the signals [19].

Subjects were instructed to start the motor task with the visual laser point at the central region of the board (highlighted with a crossed circle). The white circles on the board were set as targets considering each type of the experimental task (Figure 7.6). For task T1, subjects were instructed to keep the hand in a pose against gravity with a visual

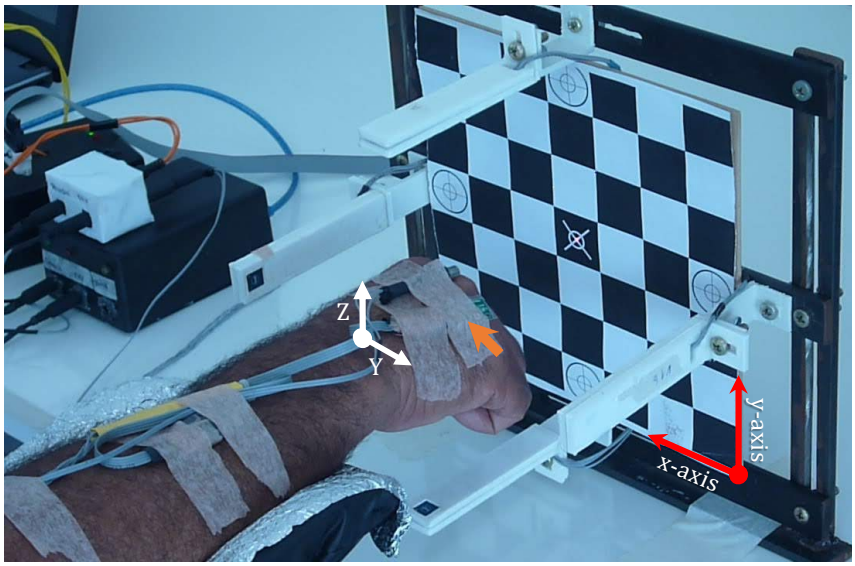

Figure 7.5: Experimental setup. The 3-axial gyroscope is positioned on the dorsal part of the hand along with the laser point. The orange arrow points to the gyroscope sensor whom the y- and z-axes are indicated. The forearm is on the support. The squared board is used for guiding the participant during the experiment.

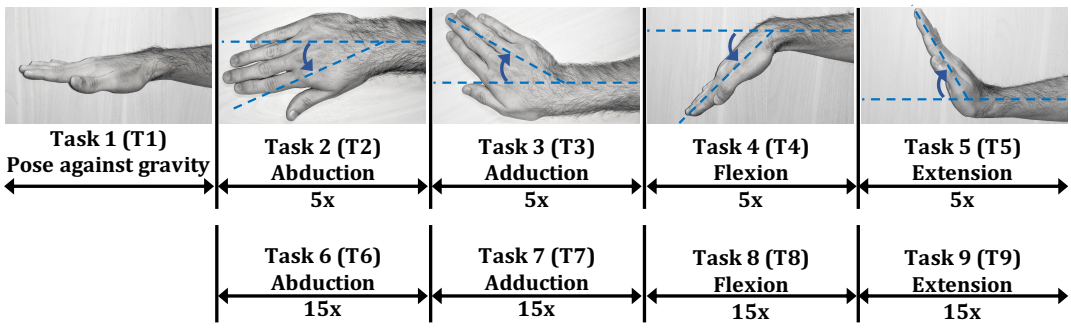

Figure 7.6: Set of tasks executed. The number of repetitions for each task is shown.

laser point at the central region of the board during 10 s. For tasks T2 to T5, subjects were asked to execute the hand movements 5 times in 10 s, whereas for tasks T6 to T9 they were asked to execute the same type of tasks 15 times in 10 s. This sequence was done three times with a rest among each execution.

Although the selected motor tasks are not in the UPDRS they are close related to the ones performed by patients during the evaluation using the UPDRS [29]. Also, gyroscopes are suitable to assess the selected movements, as they detect angular velocity, which may vary as function of the task.

Signals collected from the gyroscope were sampled at 50 Hz (with sensitivity of $\pm$ 500 $^{\circ}/s$) [112] and from the NCC system at 3 kHz. This sample rate was chosen because of the sensor behavior, in a way that, after carrier removal, 50 points are left for every second. The signals were synchronized by an external trigger. The x and y axes of the

NCC system correspond to the movements around z and y coordinates of the gyroscope, respectively.

Signal pre-processing

The NCC sensor signal comes with carrier at 60 Hz (power line frequency) with amplitude modulation, as explained in Section 3.2 of Chapter 3. So, in order to extract the relevant information from the output sensor signal, the carrier was removed by means of an envelope technique. Each sensor can measure the existing mains frequency (50 Hz / 60 Hz). When a dielectric object, such as a hand, is placed between two sensors, the level of the mains signal detected by the sensor is changed.

The signals obtained from the gyroscope were pre-processed by using a moving average filter and a nonlinear detrending technique described in [89]. For the signals detected from the NCC system, the following sequence of steps was employed, first the signal envelope of the peaks at 60 Hz component was estimated to remove the carrier signal, followed by the same sequence of steps applied to the gyroscope.

Frequency analysis

The NCC sensor detects the disturbances in the local E-field and translates this into a signal composed of the sum of all disturbances detected in the E-field. The following steps were applied for the signals from both sensors (i.e., NCC and gyroscope): (i) estimate the instantaneous mean frequency (IMNF) based on Hilbert spectrum (HS) [80]; (ii) calculate some of the key values of the descriptive statistics (i.e., min - minimum value excluding outliers, q1 - first quartile, median, q3 - third quartile and max - maximum value excluding outliers). Points are treated as outliers if they are greater than $q3 + w.(q3 - q1)$ or less than $q1 - w.(q3 - q1)$, where w is the maximum whisker length, and q1 and q3 are the 25th and 75th percentiles of the sample data, respectively; (iii) apply one-sample Kolmogorov-Smirnov test to check the normality of the distribution; (iv) apply a statistical test to check the significance of the differences between the S_{PD} and S_C groups, considering the estimated descriptive statistical features for each axis.

7.3 Results

System validation

As a result of the experiment described in Section 7.2, Figure 7.7 shows the model response of NCC EPIC sensor.

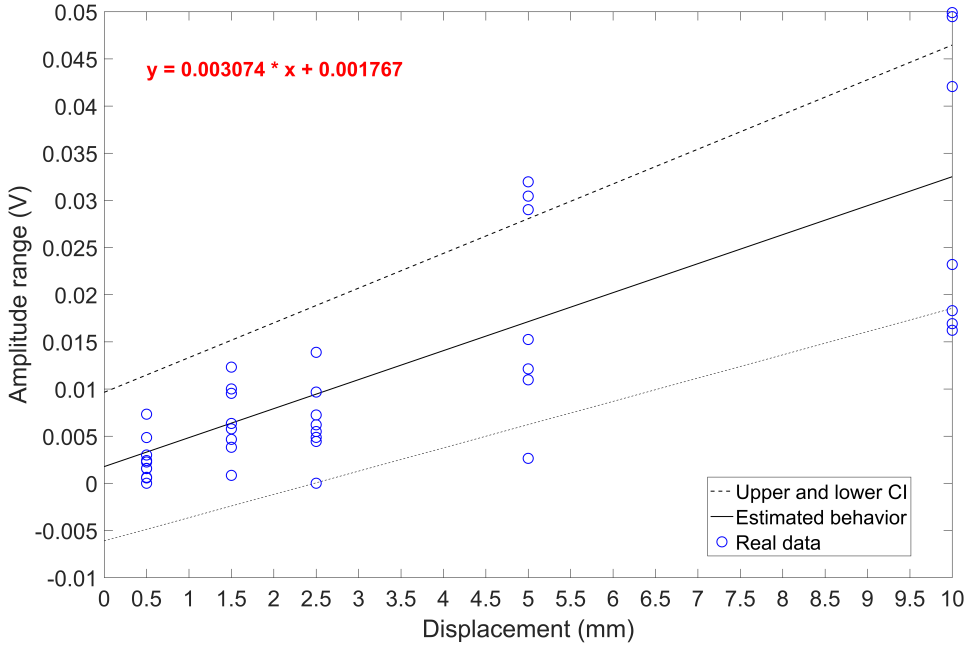

Figure 7.7: Relationship between displacement and amplitude range of NCC EPIC sensor. The dashed lines represent upper and lower 95% confidence intervals. In red on the upper left corner is the line equation of the linear mixed model.

As shown in Figure 7.7, the model presented strong linearity. R-squared and adjusted R-squared were nearly the same ($R^2 = 0.7692$ and $R^2_{adj} = 0.7631$). The following linear equation

$$y = 0.003074x + 0.001767 \tag{7.2}$$

was estimated by means of the fitted model, where x is the displacement in millimeters and y the sensor output value in volts. From Equation 7.2 it is possible to estimate the sensor behavior.

Typical waveforms

Figure 7.8 depicts typical waveforms obtained for a subject from S_C and S_{PD} groups while executing the tasks shown in Figure 7.6.

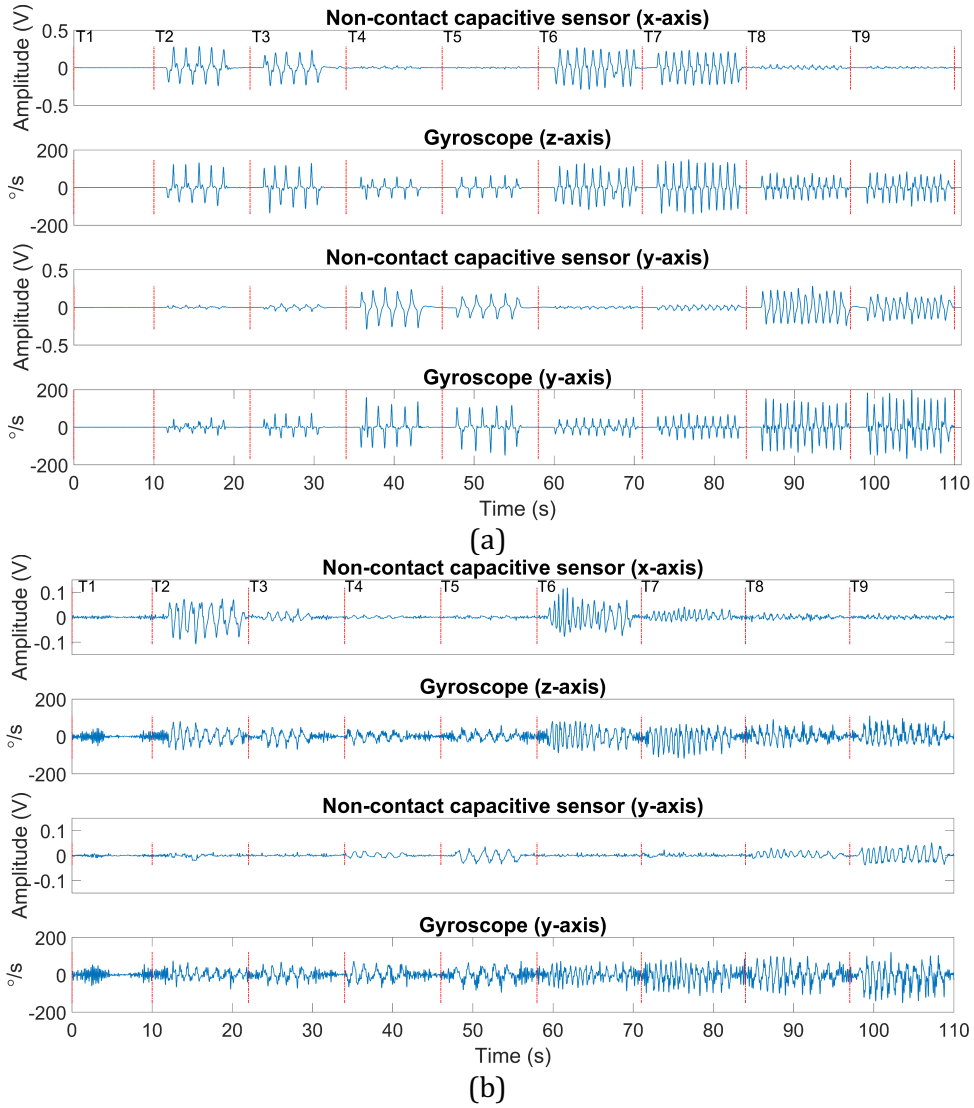

Figure 7.8: Typical signals collected. (a) subject without PD; (b) subject with PD. Each rectangular window highlighted in red represents the signal from a task.

In Figure 7.8, the signals from both sensors can be visually compared and a high similarity between their waveform can be seen. Each type of movement occurs most intensely on a specific axis. For instance, T4 and T5, i.e., flexion and extension, respectively, occur mostly on the y-axis. Nevertheless, it is also possible to observe smaller scale contribution on the z-axis to the gyroscope sensor, and on the x-axis to the NCC sensor, latter if the signal is zoomed in.

Frequency analysis

The estimation of IMNF for frequency analysis was made by means of the HS, for all subjects considering three trials and the nine tasks. Figure 7.9 shows an example of the estimation of IMNF, for signals collected from the task 2 - abduction.

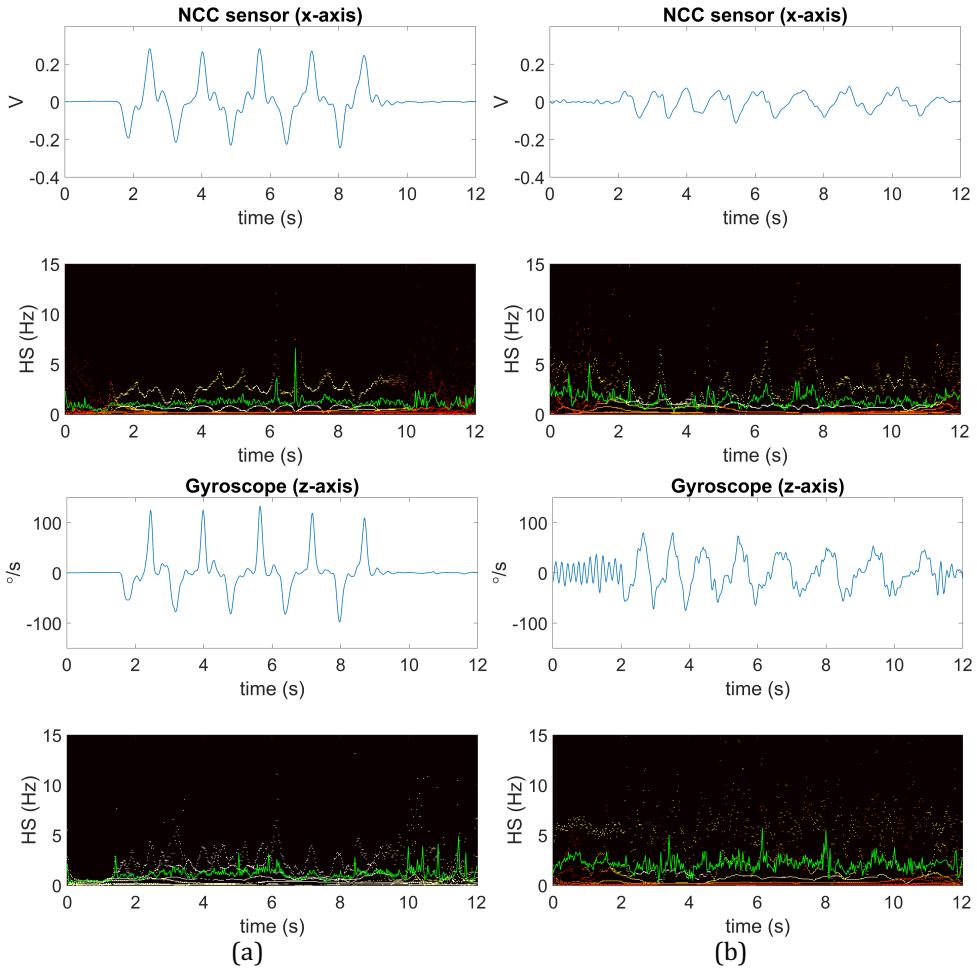

Figure 7.9: Typical IMNFs (in green), estimated through the HS, for task 2. (a) Signals and IMNFs for a subject without PD, for the x-axis of both sensors. (b) Signals and IMNFs for a subject with PD, for the x-axis of both sensors. Selected subjects are matched in age and sex.

The differences between signal waveforms for S_C and S_{PD} subjects can be seen in Figure 7.9. In the first two seconds of Figure 7.9b, it is possible to see oscillations in the signals of gyroscope and NCC sensor, latter to a lesser extent. These oscillations come from hand shaking, and they are also presented throughout the signal, similar to transients.

Table 7.2 presents a comparison between S_C and S_{PD} groups considering the estimated IMNF values for both sensors (i.e., NCC and gyroscope) and for each task. The logical values "1", also highlighted in green, help in visualization of which sensor axes and features reached a significance level of 95% ($p < 0.05$).

In most cases, both sensors were able to discriminate features from signals of each group (S_C and S_{PD}). For NCC sensor, tasks 1 and 3 were not discriminated completely by considering both axes. The gyroscope sensor, in turn, did not show statistical significance, for all features and axes, for tasks 1, 4, 5, 6, 8 and 9.

Table 7.2: Comparison of descriptive statistics based on IMNF values between S_C and S_{PD} groups by Mann-Whitney U-test.

		NCC sensor				Gyro sensor			
		p-value		logical value		p-value		logical value	
		x-axis	y-axis	x-axis	y-axis	x-axis	y-axis	x-axis	y-axis
Task 1	min	0.00	0.06	1	0	0.02	0.00	1	1
	q1	0.00	0.54	1	0	0.28	0.08	0	0
	median	0.00	0.87	1	0	0.01	0.00	1	1
	q3	0.00	0.92	1	0	0.00	0.00	1	1
	max	0.02	0.82	1	0	0.00	0.00	1	1
Task 2	min	0.00	0.00	1	1	0.00	0.00	1	1
	q1	0.00	0.00	1	1	0.00	0.00	1	1
	median	0.00	0.00	1	1	0.00	0.00	1	1
	q3	0.00	0.00	1	1	0.00	0.00	1	1
	max	0.00	0.00	1	1	0.00	0.01	1	1
Task 3	min	0.00	0.00	1	1	0.03	0.05	1	1
	q1	0.00	0.01	1	1	0.00	0.00	1	1
	median	0.00	0.01	1	1	0.00	0.00	1	1
	q3	0.00	0.03	1	1	0.00	0.00	1	1
	max	0.00	0.06	1	0	0.00	0.00	1	1
Task 4	min	0.00	0.00	1	1	0.01	0.00	1	1
	q1	0.00	0.00	1	1	0.00	0.00	1	1
	median	0.00	0.00	1	1	0.00	0.00	1	1
	q3	0.00	0.00	1	1	0.01	0.00	1	1
	max	0.00	0.00	1	1	0.05	0.00	0	1
Task 5	min	0.00	0.00	1	1	0.02	0.00	1	1
	q1	0.00	0.00	1	1	0.00	0.00	1	1
	median	0.00	0.00	1	1	0.00	0.00	1	1
	q3	0.00	0.00	1	1	0.02	0.00	1	1
	max	0.00	0.00	1	1	0.11	0.00	0	1
Task 6	min	0.00	0.00	1	1	0.00	0.00	1	1
	q1	0.00	0.00	1	1	0.00	0.02	1	1
	median	0.00	0.00	1	1	0.00	0.03	1	1
	q3	0.00	0.00	1	1	0.00	0.10	1	0
	max	0.00	0.00	1	1	0.00	0.36	1	0
Task 7	min	0.00	0.00	1	1	0.00	0.01	1	1
	q1	0.00	0.00	1	1	0.00	0.00	1	1
	median	0.00	0.00	1	1	0.00	0.00	1	1
	q3	0.00	0.00	1	1	0.00	0.00	1	1
	max	0.00	0.00	1	1	0.00	0.00	1	1
Task 8	min	0.00	0.00	1	1	0.13	0.02	0	1
	q1	0.00	0.00	1	1	0.05	0.00	1	1
	median	0.00	0.00	1	1	0.03	0.00	1	1
	q3	0.00	0.00	1	1	0.02	0.00	1	1
	max	0.00	0.00	1	1	0.02	0.00	1	1
Task 9	min	0.00	0.00	1	1	0.08	0.04	0	1
	q1	0.00	0.00	1	1	0.04	0.05	1	0
	median	0.00	0.00	1	1	0.01	0.03	1	1
	q3	0.00	0.00	1	1	0.00	0.01	1	1
	max	0.00	0.00	1	1	0.00	0.00	1	1

7.4 Discussion

This investigation proposed the employment of non-contact capacitive sensors for the assessment of people with Parkinson's disease. The results showed that NCC sensor performs as well as a gyroscope sensor for discrimination of movements executed by people with and without PD.

Many sensors and techniques are employed to quantify the cardinal signs of PD. Most studies [2, 3, 4] address this challenge by using contact sensors (e.g., inertial sensors), and this approach has limitations. So, the alternative of use NCC sensors bring new possibilities, besides overcoming some drawbacks related to the contact approach.

The analysis of the tasks depicted in Figure 7.6 can support the development of a score to quantify the severity of some of cardinal signs. Rabelo et al. [112], for example, analyzed the bradykinesia by means of quantification of flexion and extension movement of the wrist. Pose against gravity was evaluated in [42] in order to estimate hand tremor parameters.

Furthermore, NCC system can be beneficial in many ways: (i) for people who have sensitive skin such as the elderly, being this most people suffering from PD [5]; (ii) for invisible application, once they work without contact and even through the wall [113]; (iii) as a tool to allow exam in environments with high risk of contamination by contact [6]; (iv) less interference due to cable movements; (v) no privacy concerns and (vi) less amount of data and processing time while compared with image-based systems.

NCC system

So far, there has been just a few studies using EPIC sensors, especially the non-contact versions. The datasheet of these sensors does not present enough information, and lack of application notes turn its use challenging.

González-Sánchez et al. [54] employed EPIC sensors to develop an electrocardiography (ECG) monitoring system that does not require the preparation of the skin or direct contact. From a sensor instrumentation circuit point of view, their study presented very well the circuit design and some faced issues. PS25251 EPIC sensor was used in their study and according to its datasheet, this version of the sensor was designed to be used as a dry contact ECG sensor. However, their first tested setup two sensors in a differential mode were used in a contactless approach. In this setup a laboratory mouse was placed between the sensors. Finally, the plastic tube was surrounded with grounded aluminum foil to reduce electrical noise picked up by the sensors.

In our study, two approaches were tested. In the fist one, NCC system was designed to operate in a single-ended mode. So, each sensor individually captured the E-field disturbance in a way that the amplitude of a signal correspondent to a sensor unit increase when the subject's hand approaches it. After that, in order to establish each axis, the signals of each sensor unit, after digitization, were subtracted by each other in pairs. This approach presented to be not stable and the signals were frequently swamped by environmental noise.

In the second approach, the one considered for the results presented in this chapter, it was adopted a differential mode between a pair of sensors. Using this approach, the signal of interest, most of times, was not swamped by environmental noise. After digitization, 60 Hz signal appeared as a carrier and the signal of interest varied the amplitude of the carrier, in the same way it happens in amplitude modulation (AM). However, even employing differential mode design, sometimes the signal of interest (i.e., voluntary and involuntary movements of the hand) appeared weak and it was considerable swamped by environmental noise. To overcome this limitation, a grounding technique also mentioned in [54] was employed, i.e., the arm support was covered with aluminum foil connected to a ground (GND). By using this grounding technique, signals were stable during all data collections.

Regarding system validation, the estimated model depicted in Figure 7.7 presented agreement with the measurements made by Aydin et al. [114]. The differences in amplitude range among our results and the one presented in [114] are due to measured phenomena. In our experiment, the electric field disturbance due to hand displacement was measured, and in their experiment the aim was to calibrate the EPIC sensor as a field meter, so, a known electric field was created in laboratory.

Although the differences between the movements performed in system validation (i.e., hand translation) and experimental method (i.e., hand rotation), the basic principle of NCC EPIC sensor was modelled and presented in Figure 7.7. This step was relevant to confirm the previous results [114] and move forward. This kind of system validation could be extended, considering, for instance, a variety of hand movements.

Waveforms

The obtained results indicate that both sensors, the NCC and gyroscope, can measure all evaluated movements (i.e., T1 to T9). The signals shapes from NCC and gyroscope sensor are very similar as shown in Figure 7.8. In [108], for instance, a correlation analysis was made and the results showed high agreement between both sensors. This similar behavior between them are relevant once gyroscope sensor is largely used and well established in

the field of movement analysis, including PD motor symptom evaluation [2].

On the other hand, NCC system is highly dependent of sensors arrangement and setup. This concern may be seen in Figure 7.8b, in which the signal amplitude of NCC sensor for x-axis is higher than for y-axis. There are at least two possible reasons for this phenomena: (i) the subject's hand is closer to the sensors of x-axis, once the human hand is wider in frontal plane than in sagital plane; (ii) in the case of Figure 7.8b, the subject has PD and he suffers from bradykinesia (score 3 for item 3.4 of MDS-UPDRS) and rigidity (score 2 for item 3.3 of MDS-UPDRS), which normally contribute to the slowness of the movement and a reduced range of motion. These two symptoms affect directly subject hand's movements which reflects in the captured NCC sensor signal. The latter reason can also be noted in gyroscope sensor signal, but to a lesser extent.

Frequency analysis

Information related to frequency domain is relevant and widely used to analyze PD motor symptoms [3, 4, 115].

In Figure 7.9, for example, the IMNFs were estimated over time. Figure 7.9b illustrates a task signal and its IMNF for a subject with PD. Tremor symptom appears while analyzing the signal from both sensors and the employed method for frequency estimation was able to track the signal frequency oscillation. This phenomenon can be visually noted in the first two seconds in Figure 7.9b for both sensors where the subject presented severe hand tremor.

A comparison of descriptive statistics based on IMNF values among S_C and S_{PD} groups is shown in Table 7.2. Both sensors discriminate the motor patterns of both groups very well. Overall, NCC sensor performed better. In many cases where NCC or gyroscope did not present statistical significance for a particular axis, the possible reason is that the analyzed movement occurred mainly on the other axis. For instance, task 3 occurs mainly on the x-axis. The results for NCC sensor in task 1 on the y-axis should be highlighted. In task 1, the subject was asked to keep a pose against gravity, and in this pose, even if the subject's hand shakes, it will be closer to the x-axis sensors and proportionally far from y-axis sensors, given the anatomical dimensions of the hand.

7.5 Conclusions

This experimental investigation described a new application of a non-contact sensing technology which is entirely passive and works detecting changes in the ambient electric

field. We showed that, with a custom-made arrangement of Electric Potential Sensors, it is possible to quantify hand movements. The created system was calibrated and applied for the assessment of wrist motor tasks performed by subjects with and without Parkinson's disease. This technology and the application presented in this dissertation open new possibilities to the movement analysis field.

A comparison by using frequency features estimated from NCC and gyroscope signals was conducted along with a statistical significance test. Considering this scenario, NCC system showed to be as effective as the system based on gyroscope sensor.

In addition to the practicality of using the proposed system on a daily basis, it is also suitable to be used for people with skin problems, like sensitive skin in the case of elderly. It could be used in environments with high risk of contamination by contact. While compared with image-based systems, there is no privacy concerns once in the proposed system there is no need to capture and nor store real world images and less amount of data to be processed.

Furthermore, other experimental setups could be evaluated in future studies, as the literature shows that distance and number of sensors impact directly in the acquired signal [54, 114]. Also, studies to turn this system into wearable could be relevant to the field.

"Stay hungry. Stay foolish."

- Steve Jobs

8

General conclusions

Our ability to move around is vital in our daily life. However, there are many diseases that limit the human capacity of movement. Parkinson's disease is one of these, that goes beyond and also affects the non-motor abilities of the subject. As PD is a neurodegenerative disease, the diagnosis and follow-up of it are crucial to help the ill person and minimize the impairments that will appear over time.

Nowadays, the diagnostic process of PD is painful and often take more than a year to get the initial diagnosis [116]. Since there is no test available to make a definitive diagnosis, the diagnosis is based on the results of the clinical assessment. Therefore, the experience and expertise of the clinician are critical, as the diagnosis is primarily based on patient history, clinical signs and symptoms, and response to medications [33]. The accuracy of diagnosis improves with time and repeated assessments. Previous studies concluded that initial diagnosis of PD made by general neurologists were incorrect in 24% to 35% of the cases when patients were examined at autopsy. In comparison, when clinical diagnosis is performed by a movement disorders expert, the incorrectness rate drops to 7% to 30% [117, 118, 119].

To minimize this problem and help during PD diagnosis, one of the promising trends involve sensor devices, which are low cost, low power, unobtrusive, and accurate in the measurements, for monitoring and managing the pathology. The miniaturization, sophistication, proliferation, and accessibility of technologies are enabling the capture of

more and previously inaccessible phenomena in PD. However, more information has not translated into a greater understanding of disease complexity to satisfy diagnostic and therapeutic needs [7, 94].

The experiments presented in this dissertation brought the following contributions to the field:

1. Leap Motion sensor is not yet suitable to record the commonly used movements for PD diagnosis, mainly due to three aspects: (i) inconstant sample rate; (ii) tracking issues; (iii) small (i.e., around 17 cm^3) field of view to increase sensor accuracy.

2. Evaluation of non-contact capacitive sensor (e.g., comparison with gyroscope and sensor response modeling) as a novelty sensor technology for PD motor signs quantification by means of experiments with subjects with and without PD.

3. Assessment of the classification methods showed that the visualization provided by the *t*-distributed stochastic neighbor embedding (*t*-SNE) enhanced the visual discrimination of samples of movements executed by the following individuals: neurologically healthy, PD treated with levodopa, and PD treated with deep brain stimulation (DBS). For automatic discrimination among groups, support vector machine (SVM) was used after the data reduction step. The SVM performance was higher in almost all scenarios while *t*-SNE was employed.

The results of this dissertation provide a new way to quantify movement disorders and suggest a pipeline to improve data classification and visualization. The visual representation presented in our research could be used as a visualization tool for follow-up of treatments of PD.

By the end, future studies can focus on the improvement of hardware stability to avoid interferences from the environment (e.g., dielectric objects moving around the sensor in the same room). It is also suggested to increase the number of sensors, in order to acquire more components related to hand movement and allow the analysis of more complex movements.

"So many books, so little time."

- Frank Zappa

References

[1] A. Elbaz, L. Carcaillon *et al.*, "Epidemiology of Parkinson's disease," *Revue Neurologique*, vol. 172, no. 1, pp. 14–26, jan 2016. [Online]. Available: http://dx.doi.org/10.1016/j.neurol.2015.09.012

[2] Á. Sánchez-Ferro, M. Elshehabi *et al.*, "New methods for the assessment of Parkinson's disease (2005 to 2015): A systematic review," *Movement Disorders*, vol. 31, no. 9, pp. 1283–1292, sep 2016. [Online]. Available: https://doi.org/10.1002/mds.26723

[3] S. Patel, K. Lorincz *et al.*, "Monitoring motor fluctuations in patients with Parkinson's disease using wearable sensors," *IEEE transactions on information technology in biomedicine : a publication of the IEEE Engineering in Medicine and Biology Society*, vol. 13, no. 6, pp. 864–73, nov 2009. [Online]. Available: https://doi.org/10.1109/TITB.2009.2033471

[4] S. H. Roy, B. T. Cole *et al.*, "High-resolution tracking of motor disorders in Parkinson's disease during unconstrained activity," *Movement Disorders*, vol. 28, no. 8, pp. 1080–1087, 2013. [Online]. Available: https://doi.org/10.1002/mds.25391

[5] Y. Sun and X. B. Yu, "Capacitive Biopotential Measurement for Electrophysiological Signal Acquisition: A Review," *IEEE Sensors Journal*, vol. 16, no. 9, pp. 2832–2853, may 2016. [Online]. Available: https://doi.org/10.1109/JSEN.2016.2519392

[6] J. D. Siegel, E. Rhinehart *et al.*, "2007 Guideline for Isolation Precautions: Preventing Transmission of Infectious Agents in Health Care Settings," *American Journal of Infection Control*, vol. 35, no. 10, pp. S65–S164, dec 2007. [Online]. Available: https://doi.org/10.1016/j.ajic.2007.10.007

[7] A. J. Espay, P. Bonato *et al.*, "Technology in Parkinson's disease: Challenges and opportunities," *Movement Disorders*, no. April, apr 2016. [Online]. Available: https://doi.org/10.1002/mds.26642

[8] T. e. I. E. Secretaria de Ciência and D. de Ciência e Tecnologia, "Agenda de prioridades de pesquisa do Ministério da Saúde," Brasília, p. 26, 2018. [Online]. Available: http://bvsms.saude.gov.br/bvs/publicacoes/agenda_prioridades_pesquisa_ms.pdf

[9] E. R. Dorsey, A. Elbaz *et al.*, "Global, regional, and national burden of Parkinson's disease, 1990–2016: a systematic analysis for the Global Burden of Disease Study 2016," *The Lancet Neurology*, vol. 17, no. 11, pp. 939–953, nov 2018. [Online]. Available: https://doi.org/10.1016/S1474-4422(18)30295-3

[10] A. Lee and R. M. Gilbert, "Epidemiology of Parkinson Disease," *Neurologic Clinics of NA*, vol. 34, no. 4, pp. 955–965, 2016. [Online]. Available: http://dx.doi.org/10.1016/j.ncl.2016.06.012

[11] E. R. Dorsey, R. Constantinescu *et al.*, "Projected number of people with Parkinson disease in the most populous nations, 2005 through 2030," *Neurology*, vol. 68, no. 5, pp. 384–386, 2007. [Online]. Available: https://doi.org/10.1212/01.wnl.0000271777.50910.73

[12] S. L. Kowal, T. M. Dall *et al.*, "The current and projected economic burden of Parkinson's disease in the United States," *Movement Disorders*, vol. 28, no. 3, pp. 311–318, mar 2013. [Online]. Available: https://doi.org/10.1002/mds.25292

[13] A. Gustavsson, M. Svensson *et al.*, "Cost of disorders of the brain in Europe 2010," *European Neuropsychopharmacology*, vol. 21, no. 10, pp. 718–779, oct 2011. [Online]. Available: https://doi.org/10.1016/j.euroneuro.2011.08.008

[14] S. Bohingamu Mudiyanselage, J. J. Watts *et al.*, "Cost of Living with Parkinson's Disease over 12 Months in Australia: A Prospective Cohort Study," *Parkinson's Disease*, vol. 2017, pp. 1–13, 2017. [Online]. Available: https://doi.org/10.1155/2017/5932675

[15] T. Bovolenta, S. Azevedo Silva *et al.*, "Average annual cost of Parkinson's disease in São Paulo, Brazil, with a focus on disease-related motor symptoms," *Clinical Interventions in Aging*, vol. Volume 12, pp. 2095–2108, dec 2017. [Online]. Available: https://doi.org/10.2147/CIA.S151919

[16] S. S. Rao, L. a. Hofmann, and A. Shakil, "Parkinson's disease: diagnosis and treatment," *American family physician*, vol. 74, no. 12, pp. 2046–54, dec 2006. [Online]. Available: http://www.ncbi.nlm.nih.gov/pubmed/17186710

[17] R. B. Postuma, D. Berg *et al.*, "MDS clinical diagnostic criteria for Parkinson's disease," *Movement Disorders*, vol. 30, no. 12, pp. 1591–1601, oct 2015. [Online]. Available: https://doi.org/10.1002/mds.26424

[18] O.-B. Tysnes and A. Storstein, "Epidemiology of Parkinson's disease," *Journal of Neural Transmission*, vol. 124, no. 8, pp. 901–905, aug 2017. [Online]. Available: https://doi.org/10.1007/s00702-017-1686-y

[19] A. R. P. Machado, H. C. Zaidan *et al.*, "Feature visualization and classification for the discrimination between individuals with Parkinson's disease under levodopa and DBS treatments," *BioMedical Engineering OnLine*, vol. 15, no. 1, p. 169, dec 2016. [Online]. Available: https://doi.org/10.1186/s12938-016-0290-y

[20] H. Braak, E. Ghebremedhin *et al.*, "Stages in the development of Parkinson's disease-related pathology," *Cell and Tissue Research*, vol. 318, no. 1, pp. 121–134, 2004. [Online]. Available: https://doi.org/10.1007/s00441-004-0956-9

[21] J. Jankovic, "Parkinson's disease: clinical features and diagnosis," *Journal of Neurology, Neurosurgery & Psychiatry*, vol. 79, no. 4, pp. 368–376, apr 2008. [Online]. Available: https://doi.org/10.1136/jnnp.2007.131045

[22] E. Lukhanina, I. Karaban, and N. Berezetskay, "Diagnosis of Parkinson's Disease by Electrophysiological Methods," in *Diagnostics and Rehabilitation of Parkinson's Disease*. InTech, dec 2011, pp. 27–58. [Online]. Available: https://doi.org/10.5772/17761

[23] J. M. Dickson and R. A. Grünewald, "Somatic symptom progression in idiopathic Parkinson's disease," *Parkinsonism & Related Disorders*, vol. 10, no. 8, pp. 487–492, dec 2004. [Online]. Available: https://doi.org/10.1016/j.parkreldis.2004.05.005

[24] M. E. Morris and R. Iansek, "Characteristics of motor disturbance in Parkinson's disease and strategies for movement rehabilitation," *Human Movement Science*, vol. 15, no. 5, pp. 649–669, oct 1996. [Online]. Available: https://doi.org/10.1016/0167-9457(96)00020-6

[25] B. Rossi, G. Siciliano *et al.*, "Muscle modifications in Parkinson's disease: myoelectric manifestations," *Electroencephalography and Clinical Neurophysiology/Electromyography and Motor Control*, vol. 101, no. 3, pp. 211–218, jun 1996. [Online]. Available: https://doi.org/10.1016/0924-980x(96)94672-x

[26] D. J. Gelb, E. Oliver, and S. Gilman, "Diagnostic Criteria for Parkinson Disease," *Archives of Neurology*, vol. 56, no. 1, p. 33, jan 1999. [Online]. Available: https://doi.org/10.1001/archneur.56.1.33

[27] P. H. G. Mansur, L. K. P. Cury *et al.*, "A Review on Techniques for Tremor Recording and Quantification," *Critical Reviews™ in Biomedical Engineering*, vol. 35, no. 5, pp. 343–362, 2007. [Online]. Available: https://doi.org/10.1615/critrevbiomedeng.v35.i5.10

[28] N. Quinn, P. Critchley, and C. D. Marsden, "Young onset Parkinson's disease," *Movement Disorders*, vol. 2, no. 2, pp. 73–91, 1987. [Online]. Available: https://doi.org/10.1002/mds.870020201

[29] C. G. Goetz, B. C. Tilley *et al.*, "Movement Disorder Society-Sponsored Revision of the Unified Parkinson's Disease Rating Scale (MDS-UPDRS): Scale presentation and clinimetric testing results," *Movement Disorders*, vol. 23, no. 15, pp. 2129–2170, 2008. [Online]. Available: https://doi.org/10.1002/mds.22340

[30] J. Massano, "[Parkinson's disease: a clinical update]." *Acta medica portuguesa*, vol. 24 Suppl 4, pp. 827–34, dec 2011. [Online]. Available: http://www.ncbi.nlm.nih.gov/pubmed/22863490

[31] T. Mds, C. G. Goetz *et al.*, "The Unified Parkinson's Disease Rating Scale (UPDRS): Status and recommendations," *Movement Disorders*, vol. 18, no. 7, pp. 738–750, jul 2003. [Online]. Available: https://doi.org/10.1002/mds.10473

[32] L. W. Ferguson, A. H. Rajput, and A. Rajput, "Early-onset vs. Late-onset Parkinson's disease: A Clinical-pathological Study," *Canadian Journal of Neurological Sciences / Journal Canadien des Sciences Neurologiques*, vol. 43, no. 01, pp. 113–119, jan 2016. [Online]. Available: https://doi.org/10.1017/cjn.2015.244

[33] K. E. Lyons and R. Pahwa, "Diagnosis and Initiation of Treatment in Parkinson's Disease," *International Journal of Neuroscience*, vol. 121, no. sup2, pp. 27–36, sep 2011. [Online]. Available: https://doi.org/10.3109/00207454.2011.620197

[34] K. Yang, W.-X. Xiong *et al.*, "Objective and quantitative assessment of motor function in Parkinson's disease—from the perspective of practical applications," *Annals of Translational Medicine*, vol. 4, no. 5, pp. 90–90, mar 2016. [Online]. Available: https://doi.org/10.21037/atm.2016.03.09

[35] Q. Oung, H. Muthusamy *et al.*, "Technologies for Assessment of Motor Disorders in Parkinson's Disease: A Review," *Sensors*, vol. 15, no. 9, pp. 21 710–21 745, aug 2015. [Online]. Available: https://doi.org/10.3390/s150921710

[36] A. Tzallas, M. Tsipouras *et al.*, "PERFORM: A System for Monitoring, Assessment and Management of Patients with Parkinson's Disease," *Sensors*, vol. 14, no. 11, pp. 21 329–21 357, nov 2014. [Online]. Available: https://doi.org/10.3390/s141121329

[37] H. Dai, P. Zhang, and T. Lueth, "Quantitative Assessment of Parkinsonian Tremor Based on an Inertial Measurement Unit," *Sensors*, vol. 15, no. 10, pp. 25 055–25 071, sep 2015. [Online]. Available: https://doi.org/10.3390/s151025055

[38] P. Y. Chan and Z. M. Ripin, "Development of wearable inertial sensors for measurement of hand arm tremors," in *2013 IEEE International Conference on Smart Instrumentation, Measurement and Applications (ICSIMA)*, no. November. IEEE, nov 2013, pp. 1–6. [Online]. Available: https://doi.org/10.1109/ICSIMA.2013.6717926

[39] S. M. Rissanen, M. Kankaanpaä *et al.*, "Analysis of EMG and Acceleration Signals for Quantifying the Effects of Deep Brain Stimulation in Parkinson's Disease," *IEEE Transactions on Biomedical Engineering*, vol. 58, no. 9, pp. 2545–2553, sep 2011. [Online]. Available: https://doi.org/10.1109/TBME.2011.2159380

[40] M. J. Johnson, "Detection of Parkinson Disease Rest Tremor," Ph.D. dissertation, Washington University, 2014. [Online]. Available: https://doi.org/10.7936/K7W66HQ8

[41] B. Dror, E. Yanai *et al.*, "Automatic assessment of Parkinson's Disease from natural hands movements using 3D depth sensor," in *2014 IEEE 28th Convention of Electrical & Electronics Engineers in Israel (IEEEI)*. IEEE, dec 2014, pp. 1–5. [Online]. Available: https://doi.org/10.1109/EEEI.2014.7005763

[42] R.-S. Chang, J.-H. Chiu *et al.*, "A Parkinson's disease measurement system using laser lines and a CMOS image sensor," *Sensors (Basel, Switzerland)*, vol. 11, no. 2, pp. 1461–75, jan 2011. [Online]. Available: https://doi.org/10.3390/s110201461

[43] G. Blumrosen, M. Uziel *et al.*, "Noncontact Tremor Characterization Using Low-Power Wideband Radar Technology," *IEEE Transactions on Biomedical Engineering*, vol. 59, no. 3, pp. 674–686, mar 2012. [Online]. Available: https://doi.org/10.1109/TBME.2011.2177977

[44] T. Ilias, B. Filip *et al.*, "Using measurements from wearable sensors for automatic scoring of Parkinson's disease motor states: Results from 7 patients," in *2017 39th Annual International Conference of the IEEE Engineering in Medicine and Biology Society (EMBC)*, 2017, pp. 131–134. [Online]. Available: https://doi.org/10.1109/embc.2017.8036779

[45] F. Weichert, D. Bachmann *et al.*, "Analysis of the Accuracy and Robustness of the Leap Motion Controller," *Sensors*, vol. 13, no. 5, pp. 6380–6393, may 2013. [Online]. Available: https://doi.org/10.3390/s130506380

[46] J. Guna, G. Jakus *et al.*, "An Analysis of the Precision and Reliability of the Leap Motion Sensor and Its Suitability for Static and Dynamic Tracking," *Sensors*, vol. 14, no. 2, pp. 3702–3720, feb 2014. [Online]. Available: https://doi.org/10.3390/s140203702

[47] A. Andrade, A. Alves *et al.*, "Human Tremor: Origins, Detection and Quantification," in *Practical Applications in Biomedical Engineering*. InTech, jan 2013, pp. 3–24. [Online]. Available: http://dx.doi.org/10.5772/54524

[48] J. Coton, J. Veytizou *et al.*, "Feasibility Study of Hand Motion Analysis by the Leap Motion Sensor," *AMSE IFRATH*, vol. 77, pp. 73–83, 2016.

[49] A. H. Butt, E. Rovini *et al.*, "Objective and automatic classification of Parkinson disease with Leap Motion controller," *BioMedical Engineering OnLine*, vol. 17, no. 1, p. 168, 2018. [Online]. Available: https://doi.org/10.1186/s12938-018-0600-7

[50] A. J. Clippingdale, R. J. Prance *et al.*, "Ultra-high impedance voltage probes and non-contact electrocardiography," in *Sensors: Technology, systems and applications*, K. Grattan, Ed. Institute Of Physics Publishing, 1991, pp. 469–472.

[51] C. J. Harland, T. D. Clark, and R. J. Prance, "Electric potential probes - new directions in the remote sensing of the human body," *Measurement Science and Technology*, vol. 13, no. 2, pp. 163–169, feb 2002. [Online]. Available: https://doi.org/10.1088/0957-0233/13/2/304

[52] S. Beardsmore-Rust, P. B. Stiffell *et al.*, "Passive tracking of targets using electric field sensors," in *Sensors, and Command, Control, Communications, and Intelligence (C3I) Technologies for Homeland Security and Homeland Defense Ix*, E. M. Carapezza, Ed., vol. 7666, apr 2010, p. 766622. [Online]. Available: https://doi.org/10.1117/12.849642

[53] M. Fatoorechi, J. Parkinson *et al.*, "A comparative study of electrical potential sensors and Ag/AgCl electrodes for characterising spontaneous and event related electroencephalagram signals," *Journal of Neuroscience Methods*, vol. 251, pp. 7–16, aug 2015. [Online]. Available: http://dx.doi.org/10.1016/j.jneumeth.2015.04.013

[54] C. González-Sánchez, J.-C. Fraile *et al.*, "Capacitive Sensing for Non-Invasive Breathing and Heart Monitoring in Non-Restrained, Non-Sedated Laboratory Mice," *Sensors*, vol. 16, no. 7, p. 1052, jul 2016. [Online]. Available: https://doi.org/10.3390/s16071052

[55] A. Braun, R. Wichert *et al.*, "Capacitive proximity sensing in smart environments," *Journal of Ambient Intelligence and Smart Environments*, vol. 7, no. 4, pp. 483–510, jul 2015. [Online]. Available: https://doi.org/10.3233/AIS-150324

[56] A. Pouryazdan, R. J. Prance *et al.*, "Wearable electric potential sensing," in *Proceedings of the 2016 ACM International Joint Conference on Pervasive and Ubiquitous Computing Adjunct - UbiComp '16*. New York, New York, USA: ACM Press, 2016, pp. 846–850. [Online]. Available: https://doi.org/10.1145/2968219.2968286

[57] R. Bogue, "Plessey launches range of unique electric field sensors," *Sensor Review*, vol. 32, no. 3, pp. 194–198, jun 2012. [Online]. Available: https://doi.org/10.1108/02602281211233160

[58] Plessey Semiconductors Ltd., "EPIC SENSOR APPLICATIONS GUIDEBOOK," p. 118.

[59] ——, "Application Note # 291554 Movement and gesture applications of EPIC sensors," Swindon, pp. 1–3.

[60] A. Gani, A. Siddiqa *et al.*, "A survey on indexing techniques for big data: taxonomy and performance evaluation," *Knowledge and Information Systems*, 2016. [Online]. Available: https://doi.org/10.1007/s10115-015-0830-y

[61] M. Senthilarumugam Veilukandammal, "Big data and Parkinson's: Exploration, analyses, data challenges and visualization," Ph.D. dissertation, Iowa State University, Digital Repository, Ames, 2017. [Online]. Available: https://doi.org/10.31274/etd-180810-5841

[62] I. D. Dinov, B. Heavner *et al.*, "Predictive big data analytics: A study of Parkinson's disease using large, complex, heterogeneous, incongruent, multi-source and incomplete observations," *PLoS ONE*, vol. 11, no. 8, pp. 1–28, 2016. [Online]. Available: https://doi.org/10.1371/journal.pone.0157077

[63] J. Venna, S. Kaski *et al.*, "Information retrieval perspective to nonlinear dimensionality reduction for data visualization," *Journal of Machine Learning Research*, vol. 11, pp. 451–490, 2010. [Online]. Available: http://www.jmlr.org/papers/v11/venna10a.html

[64] C. Bartenhagen, H. Klein, and C. Ruckert, "Comparative study of unsupervised dimension reduction techniques for the visualization of microarray gene expression data," *BMC Bioinformatics*, vol. 11, no. 1, pp. 567–578, 2010. [Online]. Available: https://doi.org/10.1186/1471-2105-11-567

[65] H. Hotelling, "Analysis of a complex of statistical variables into principal components," *Journal of Educational Psychology*, vol. 24, no. 6, pp. 417–441, 1933. [Online]. Available: https://doi.org/10.1037/h0071325

[66] C. Bouveyron and C. Brunet-Saumard, "Model-based clustering of high-dimensional data: A review," *Computational Statistics and Data Analysis*, vol. 71, pp. 52–78, 2014. [Online]. Available: http://dx.doi.org/10.1016/j.csda.2012.12.008

[67] L. Van Der Maaten, E. O. Postma *et al.*, "Dimensionality Reduction: A Comparative Review," *Journal of Machine Learning Research*, vol. 10, no. February, pp. 1–41, 2009.

[68] J. Venna, "Dimensionality reduction for visual exploration of similarity structures," Ph.D. dissertation, Helsinki University of Technology, 2007.

[69] J. Sammon, "A Nonlinear Mapping for Data Structure Analysis," *IEEE Transactions on Computers*, vol. C-18, no. 5, pp. 401–409, may 1969. [Online]. Available: https://doi.org/10.1109/T-C.1969.222678

[70] L. Van Der Maaten and G. Hinton, "Visualizing Data using t-SNE," *Journal of Machine Learning Research*, vol. 9, no. 1, pp. 2579–2605, nov 2008.

[71] G. E. Hinton and S. T. Roweis, "Stochastic neighbor embedding," in *Advances in Neural Information Processing Systems*, 2002, pp. 833–840. [Online]. Available: http://papers.nips.cc/paper/2276-stochastic-neighbor-embedding

[72] S. Patel, D. Sherrill *et al.*, "Analysis of the Severity of Dyskinesia in Patients with Parkinson's Disease via Wearable Sensors," in *International Workshop on Wearable and Implantable Body Sensor Networks (BSN'06)*, vol. 2006. IEEE, 2006, pp. 123–126. [Online]. Available: https://doi.org/10.1109/BSN.2006.10

[73] E. Vaiciukynas, A. Verikas *et al.*, "Detecting Parkinson's disease from sustained phonation and speech signals," *PLOS ONE*, vol. 12, no. 10, p. e0185613, oct 2017. [Online]. Available: https://doi.org/10.1371/journal.pone.0185613

[74] X. Zhang, J. Chou *et al.*, "Data-Driven Subtyping of Parkinson's Disease Using Longitudinal Clinical Records: A Cohort Study," *Scientific Reports*, vol. 9, no. 1, p. 797, dec 2019. [Online]. Available: http://dx.doi.org/10.1038/s41598-018-37545-z

[75] B. Lerner, H. Guterman *et al.*, "On pattern classification with Sammon's nonlinear mapping an experimental study," *Pattern Recognition*, vol. 31, no. 4, pp. 371–381, apr 1998. [Online]. Available: https://doi.org/10.1016/S0031-3203(97)00064-2

[76] S. De Backer, A. Naud, and P. Scheunders, "Non-linear dimensionality reduction techniques for unsupervised feature extraction," *Pattern Recognition Letters*, 1998. [Online]. Available: https://doi.org/10.1016/s0167-8655(98)00049-x

[77] B. Lerner, H. Guterman *et al.*, "A comparative study of neural network based feature extraction paradigms," *Pattern Recognition Letters*, 1999. [Online]. Available: https://doi.org/10.1016/s0167-8655(98)00120-2

[78] F. H. M. Oliveira, J. A. F. B. Júnior *et al.*, "Quantificação de tremor de punho utilizando o sensor Leap Motion," in *Anais do XXIV Congresso Brasileiro de Engenharia Biomédica*. Uberlândia: XXIV Congresso Brasileiro de Engenharia Biomédica, 2014, pp. 2762–2765.

[79] F. H. M. Oliveira and A. O. Andrade, "Preliminary evaluation of Leap Motion Controller as a human tremor record device," in *Anais do VII Simpósio em Engenharia Biomédica*, Uberlândia, 2015, pp. 241–245.

[80] A. O. Andrade, P. Kyberd, and S. J. Nasuto, "The application of the Hilbert spectrum to the analysis of electromyographic signals," *Information Sciences*, vol. 178, no. 9, pp. 2176–2193, may 2008. [Online]. Available: https://doi.org/10.1016/j.ins.2007.12.013

[81] "TENS Gerät 410 / S." [Online]. Available: http://www.tens.de/TENS410.htm

[82] P. R. Burkhard, J. W. Langston, and J. W. Tetrud, "Voluntarily simulated tremor in normal subjects," *Neurophysiologie Clinique*, vol. 32, no. 2, pp. 119–126, 2002. [Online]. Available: https://doi.org/10.1016/S0987-7053(02)00296-4

[83] M. M. Sturman, "Effects of Aging on the Regularity of Physiological Tremor," *Journal of Neurophysiology*, vol. 93, no. 6, pp. 3064–3074, jun 2005. [Online]. Available: https://doi.org/10.1152/jn.01218.2004

[84] F. H. M. Oliveira, A. R. P. Machado, and A. O. Andrade, "On the Use of t -Distributed Stochastic Neighbor Embedding for Data Visualization and Classification of Individuals with Parkinson's Disease," *Computational and Mathematical Methods in Medicine*, vol. 2018, pp. 1–17, nov 2018. [Online]. Available: https://doi.org/10.1155/2018/8019232

[85] C. G. Goetz, W. Poewe *et al.*, "Movement Disorder Society Task Force report on the Hoehn and Yahr staging scale: Status and recommendations," *Movement Disorders*, vol. 19, no. 9, pp. 1020–1028, 2004. [Online]. Available: https://doi.org/10.1002/mds.20213

[86] B. Carstensen, "Repeatability, Reproducibility and Coefficient of Variation," in *Comparing Clinical Measurement Methods*. Chichester, UK: John Wiley & Sons, Ltd, jun 2010, pp. 107–114. [Online]. Available: https://doi.org/10.1002/9780470683019.ch9

[87] C. Cortes and V. Vapnik, "Support-vector networks," *Machine Learning*, vol. 20, no. 3, pp. 273–297, sep 1995. [Online]. Available: https://doi.org/10.1007/BF00994018

[88] S. Gruss, R. Treister *et al.*, "Pain Intensity Recognition Rates via Biopotential Feature Patterns with Support Vector Machines," *PLOS ONE*, vol. 10, no. 10, p. e0140330, oct 2015. [Online]. Available: https://doi.org/10.1371/journal.pone.0140330

[89] A. O. Andrade, L. C. V. Ferreira *et al.*, "Pelvic movement variability of healthy and unilateral hip joint involvement individuals," *Biomedical Signal Processing and Control*, vol. 32, pp. 10–19, feb 2017. [Online]. Available: https://doi.org/10.1016/j.bspc.2016.10.008

[90] M. Verleysen, D. Francois *et al.*, "On the effects of dimensionality on data analysis with neural networks," *Artificial Neural Nets Problem Solving Methods*, vol. 2687, pp. 105–112, 2003. [Online]. Available: http://dx.doi.org/10.1007/3-540-44869-1_14

[91] D. J. C. MacKay, "Bayesian Interpolation," *Neural Computation*, vol. 4, no. 3, pp. 415–447, may 1992. [Online]. Available: https://doi.org/10.1162/neco.1992.4.3.415

[92] T. Hastie, R. Tibshirani, and J. Friedman, *The Elements of Statistical Learning*, ser. Springer Series in Statistics. New York, NY: Springer New York, 2009, vol. 18. [Online]. Available: https://doi.org/10.1007/978-0-387-84858-7

[93] C. Hsu and C. Lin, "A comparison of methods for multiclass support vector machines," *Neural Networks, IEEE Transactions on*, vol. 13, no. 2, pp. 415–425, 2002. [Online]. Available: https://doi.org/10.1109/72.991427

[94] K. J. Kubota, J. A. Chen, and M. A. Little, "Machine learning for large-scale wearable sensor data in Parkinson's disease: Concepts, promises, pitfalls, and futures," *Movement Disorders*, vol. 00, no. 00, pp. 1–13, 2016. [Online]. Available: https://doi.org/10.1002/mds.26693

[95] C.-L. Xie, B. Shao *et al.*, "Effects of neurostimulation for advanced Parkinson's disease patients on motor symptoms: A multiple-treatments meta-analysas of randomized controlled trials." *Scientific reports*, vol. 6, no. April, p. 25285, 2016. [Online]. Available: https://doi.org/10.1038/srep25285

[96] A. Antonini, I. U. Isaias *et al.*, "A 5-year prospective assessment of advanced Parkinson disease patients treated with subcutaneous apomorphine infusion or deep brain stimulation," *Journal of Neurology*, vol. 258, no. 4, pp. 579–585, 2011. [Online]. Available: https://doi.org/10.1007/s00415-010-5793-z

[97] P. Martinez-Martin and G. Deuschl, "Effect of medical and surgical interventions on health-related quality of life in Parkinson's disease." *Movement disorders : official journal of the Movement Disorder Society*, vol. 22, no. 6, pp. 757–65, 2007. [Online]. Available: https://doi.org/10.1002/mds.21407

[98] A. Williams, S. Gill *et al.*, "Deep brain stimulation plus best medical therapy versus best medical therapy alone for advanced Parkinson's disease (PD SURG trial): a randomised, open-label trial," *The Lancet Neurology*, vol. 9, no. 6, pp. 581–591, 2010. [Online]. Available: http://dx.doi.org/10.1016/S1474-4422(10)70093-4

[99] H. Nagasaki, H. Itoh *et al.*, "Characteristic difficulty in rhythmic movement with aging and its relation to parkinson's disease," *Experimental Aging Research*, vol. 14, no. 4, pp. 171–176, 2007. [Online]. Available: https://doi.org/10.1080/03610738808259744

[100] R. Okuno, M. Yokoe *et al.*, "Finger taps movement acceleration measurement system for quantitative diagnosis of Parkinson's disease," in *2006 International Conference of the IEEE Engineering in Medicine and Biology Society.* IEEE, 2006, pp. 6623–6626. [Online]. Available: https://doi.org/10.1109/IEMBS.2006.260904

[101] Á. Jobbágy, P. Harcos *et al.*, "Analysis of finger-tapping movement," *Journal of Neuroscience Methods*, vol. 141, no. 1, pp. 29–39, jan 2005. [Online]. Available: https://doi.org/10.1016/j.jneumeth.2004.05.009

[102] I. Q. Whishaw, O. Suchowersky *et al.*, "Impairment of pronation, supination, and body co-ordination in reach-to-grasp tasks in human Parkinson's disease (PD) reveals homology to deficits in animal models," *Behavioural Brain Research*, vol. 133, no. 2, pp. 165–176, jul 2002. [Online]. Available: https://doi.org/10.1016/S0166-4328(01)00479-X

[103] B. Hellwig, P. Mund *et al.*, "A longitudinal study of tremor frequencies in Parkinson's disease and essential tremor," *Clinical Neurophysiology*, vol. 120, no. 2, pp. 431–435, feb 2009. [Online]. Available: http://dx.doi.org/10.1016/j.clinph.2008.11.002

[104] F. Bergquist and M. Horne, "Can Objective Measurements Improve Treatment Outcomes in Parkinson's Disease?" *European Neurological Review*, vol. 9, no. 1, p. 27, 2014. [Online]. Available: http://doi.org/10.17925/ENR.2014.09.01.27

[105] K. Bunte, M. Biehl, and B. Hammer, "A General Framework for Dimensionality-Reducing Data Visualization Mapping," *Neural Computation*, vol. 24, no. 3, pp. 771–804, 2012. [Online]. Available: https://doi.org/10.1162/NECO_a_00250

[106] F. H. M. Oliveira, A. R. P. Machado, and A. O. Andrade, "Hand motion quantification using non-contact capacitive sensors," in *XXV Brazilian Congress on Biomedical Engineering*, Foz do Iguaçu, 2016, pp. 1829–1832.

[107] F. H. M. Oliveira, T. F. Zaruz *et al.*, "t-SNE Applied to Discriminate Healthy Individuals from Those with Parkinson's Disease Executing Motor Tasks Detected by Non-contact Capacitive Sensors," in *IFMBE Proceedings*, 2019, vol. 68, no. 1, pp. 421–425. [Online]. Available: https://doi.org/10.1007/978-981-10-9035-6_78

[108] F. H. M. Oliveira, T. F. Zaruz, and A. O. Andrade, "Use of Non-contact Capacitive Sensors to Detect Hand Gestures," in *XXVI Brazilian Congress on Biomedical Engineering*, ser. IFMBE Proceedings, R. Costa-Felix, J. C. Machado, and A. V. Alvarenga, Eds. Singapore: Springer Singapore, 2019, vol. 70/2, pp. 517–522. [Online]. Available: http://dx.doi.org/10.1007/978-981-13-2517-5_78

[109] F. H. M. Oliveira, A. G. Rabelo *et al.*, "On the Use of Non-Contact Capacitive Sensors for the Assessment of Postural Hand Tremor of Individuals with Parkinson's Disease*," in *2019 41st Annual International Conference of the IEEE Engineering in Medicine and Biology Society (EMBC)*. Berlin, Germany: IEEE, jul 2019, pp. 6591–6594. [Online]. Available: https://doi.org/10.1109/EMBC.2019.8856746

[110] F. H. M. Oliveira, D. F. Cunha *et al.*, "A Non-Contact System for the Assessment of Hand Motor Tasks in People with Parkinson ' s Disease," 2019, preprint on webpage at https://www.researchgate.net/publication/337935520_A_Non-Contact_System_for_the_Assessment_of_Hand_Motor_Tasks_in_People_with_Parkinson's_Disease.

[111] B. Winter, "Linear models and linear mixed effects models in R with linguistic applications," no. Tutorial 2, pp. 1–22, aug 2013. [Online]. Available: http://arxiv.org/abs/1308.5499

[112] A. G. Rabelo, L. P. Neves *et al.*, "Objective Assessment of Bradykinesia Estimated from the Wrist Extension in Older Adults and Patients with Parkinson's Disease," *Annals of Biomedical Engineering*, vol. 45, no. 11, pp. 2614–2625, nov 2017. [Online]. Available: https://doi.org/10.1007/s10439-017-1908-3

[113] S. Beardsmore-Rust, P. Watson *et al.*, "Detecting electric field disturbances for passive through-wall movement and proximity sensing," in *Proc. of SPIE*, B. M. Cullum and D. M. Porterfield, Eds., vol. 7313, may 2009, pp. 73 130P–73 130P–8. [Online]. Available: https://doi.org/10.1117/12.817919

[114] A. Aydin, P. B. Stiffell *et al.*, "A high sensitivity calibrated electric field meter based on the electric potential sensor," *Measurement Science and Technology*, vol. 21, no. 12, p. 125901, 2010. [Online]. Available: https://doi.org/10.1088/0957-0233/21/12/125901

[115] S. Spasojević, T. V. Ilić *et al.*, "Quantitative Assessment of the Arm/Hand Movements in Parkinson's Disease Using a Wireless Armband Device," *Frontiers in Neurology*, vol. 8, no. AUG, aug 2017. [Online]. Available: https://doi.org/10.3389/fneur.2017.00388

[116] J. Jankovic, "The Evolution of Diagnosis in Early Parkinson Disease," *Archives of Neurology*, vol. 57, no. 3, p. 369, mar 2000. [Online]. Available: https://doi.org/10.1001/archneur.57.3.369

[117] A. Rajput, B. Rozdilsky, and A. Rajput, "Accuracy of Clinical Diagnosis in Parkinsonism — A Prospective Study," *Canadian Journal of Neurological Sciences / Journal Canadien des Sciences Neurologiques*, vol. 18, no. 03, pp. 275–278, aug 1991. [Online]. Available: https://doi.org/10.1017/s0317167100031814

[118] A. J. Hughes, S. E. Daniel *et al.*, "Accuracy of clinical diagnosis of idiopathic Parkinson's disease: a clinico-pathological study of 100 cases." *Journal of Neurology, Neurosurgery & Psychiatry*, vol. 55, no. 3, pp. 181–184, mar 1992. [Online]. Available: http://dx.doi.org/10.1136/jnnp.55.3.181

[119] G. Rizzo, M. Copetti *et al.*, "Accuracy of clinical diagnosis of Parkinson disease," *Neurology*, vol. 86, no. 6, pp. 566–576, feb 2016. [Online]. Available: https://doi.org/10.1212/wnl.0000000000002350

"Show me the money."

- Jerry Maguire

A

List of scientific publications

Papers in the reviewed scientific journals

F. H. M. Oliveira, A. R. P. Machado, and A. O. Andrade, "On the Use of t -Distributed Stochastic Neighbor Embedding for Data Visualization and Classification of Individuals with Parkinson's Disease," Comput. Math. Methods Med., vol. 2018, pp. 1–17, Nov. 2018. https://doi.org/10.1155/2018/8019232

Submitted for publication

F. H. M. Oliveira, D. F. da Cunha, A. G. Rabelo, L. M. D. Luiz, M. F. Vieira, A. A. Pereira and A. O. Andrade, "A non-contact system for the assessment of hand motor tasks in people with Parkinson's disease," pp. 1-8, 2020. Manuscript submitted for publication.

Patent

ANDRADE, A. O. ; OLIVEIRA, F. H. M. ; ZARUZ, T. F. . Sistema para avaliação de sinais motores da doença de Parkinson. 2018, Brasil. Patente: Privilégio de Inovação.

Número do registro: BR1020180698648, título: “Sistema para avaliação de sinais motores da doença de Parkinson” , Instituição de registro: INPI - Instituto Nacional da Propriedade Industrial. Depósito PCT: 27/09/2018.

Registered computer program

OLIVEIRA, F. H. M.; ANDRADE, A. O. ; BARBOSA JR, J. A. F. ; MACHADO, A. R. P. ; PAIXAO, A. P. S. ; CAVALEIRO, G. L. . Leap Tremor Detection. 2014. Patente: Programa de Computador. Número do registro: BR512015000133-7, data de registro: 18/08/2014, título: ”Leap Tremor Detection” , Instituição de registro: INPI - Instituto Nacional da Propriedade Industrial.

Conference papers

F. H. M. Oliveira, J. A. F. B. Júnior, A. R. P. Machado, and A. O. Andrade, “Quantificação de tremor de punho utilizando o sensor Leap Motion,” in Anais do XXIV Congresso Brasileiro de Engenharia Biomédica, 2014, pp. 2762–2765.

F. H. M. Oliveira and A. O. Andrade, “Estratégia para detecção de tremor de punho utilizando o sensor Leap Motion,” in Anais do VII Simpósio em Engenharia Biomédica, 2014, pp. 143–148.

F. H. M. Oliveira and A. O. Andrade, “Preliminary evaluation of Leap Motion Controller as a human tremor record device,” in Anais do VIII Simpósio em Engenharia Biomédica, 2015, pp. 241–245.

F. H. M. Oliveira, A. R. P. Machado, and A. O. Andrade, “Hand motion quantification using non-contact capacitive sensors,” in XXV Brazilian Congress on Biomedical Engineering, 2016, pp. 1829–1832.

F. H. M. Oliveira, T. F. Zaruz, M. F. Vieira, and A. O. Andrade, “t-SNE Applied to Discriminate Healthy Individuals from Those with Parkinson’s Disease Executing Motor Tasks Detected by Non-contact Capacitive Sensors,” in IFMBE Proceedings, vol. 68, no. 1, 2019, pp. 421–425. https://doi.org/10.1007/978-981-10-9035-6_78

F. H. M. Oliveira, T. F. Zaruz, and A. O. Andrade, “Use of Non-contact Capacitive Sensors to Detect Hand Gestures,” in XXVI Brazilian Congress on Biomedical Engineering, vol. 70/2, R. Costa-Felix, J. C. Machado, and A. V. Alvarenga, Eds. Armação de Búzios: Springer Singapore, 2019, pp. 517–522. http://doi.org/10.1007/978-981-13-2517-5_78

F. H. M. Oliveira, A. G. Rabelo, L. M. D. Luiz, A. A. Pereira, M. F. Vieira, and A. O. Andrade, "On the Use of Non-Contact Capacitive Sensors for the Assessment of Postural Hand Tremor of Individuals with Parkinson's Disease*," in 2019 41st Annual International Conference of the IEEE Engineering in Medicine and Biology Society (EMBC), 2019, pp. 6591–6594. https://doi.org/10.1109/EMBC.2019.8856746

"That's all folks!"

- Looney Tunes

B

Supplementary materials

This appendix aggregates the supplementary materials (e.g., software, datasets and videos) produced during the development of this thesis.

The developed softwares and scripts are hosted in GitHub platform, follow the links:

- `https://github.com/oliveirafhm`
- `https://github.com/NIATS-UFU`

Chapter 5

The following link contains a supplementary material file that includes 12 text files containing various hand data collected with LMC for each trial of each setup, as described in Section 5.2 of Chapter 5.

Link: `http://dx.doi.org/10.13140/RG.2.2.22888.01287`.

Chapter 6

The following link contains a supplementary material file that includes three tables containing features estimated from signals of the executed tasks. Each table includes features extracted from filtered signals, instantaneous frequency, and instantaneous amplitude, respectively.

Link: `http://dx.doi.org/10.13140/RG.2.2.24985.16489`.

Chapter 7

The following link contains a supplementary material video file that shows an experiment trial of a subject with PD.

Link: `https://photos.app.goo.gl/FebrUd31ifuZMtos9`.